ABSTRACT

Title of Document: THEORETICAL AND EXPERIMENTAL STUDY ON FULLY-DEVELOPED COMPARTMENT FIRES

Yunyong Utiskul, Doctor of Philosophy, 2006

Directed By: Professor James G. Quintiere, Department of Fire Protection Engineering

To predict the effect of fire on the structures, one needs to understand physics of the fire growth in a compartment as to how the fuel interacts with the flame and its surroundings. This study explores these effects and applies them to the common fuel configurations such as pool and crib fires. The focus on the study is on the fully-developed fires where all available fuel becomes involved to the maximum extent and can potentially yield the severest damage to the structural elements. A single-zone compartment fire model is developed along with a fuel mass loss rate model that accounts for the thermal enhancement, oxygen-limiting feedback, and the fuel type and configuration. A criterion for a one-zone, fully-developed fire is established and validated with experiments. An empirical correlation for mixing of oxygen into the lower floor layer essential for the modeling is also developed. An experimental program for single-wall-vent compartment using wood crib and heptane pool as fuels is carried out to validate the mathematical model and explore a full range of phenomena associated with

fully developed fires: extinction, oscillation, fire area shrinkage, and response of fuel to thermal and oxygen effects. The simulation from the model is able to capture these phenomena and shows good agreement with the experiments. Some generalities of the fuel mass loss rate and compartment gas temperature are presented using the experimental results and the model simulations. The developed model has a potential to give burning time and temperature in a fire for any fuel, scale and ventilation.

THEORETICAL AND EXPERIMENTAL STUDY ON FULLY-DEVELOPED COMPARTMENT FIRES

By

Yunyong Utiskul

Dissertation submitted to the Faculty of the Graduate School of the
University of Maryland, College Park, in partial fulfillment
of the requirements for the degree of
Doctor of Philosophy
2006

Advisory Committee:
Professor James G. Quintiere, Chair
Professor Marino di Marzo
Associate Professor Arnaud Trouvé
Assistant Professor Andre Marshall
Associate Professor Peter C. Chang

Dedications

To My Parents

Acknowledgements

First and foremost I would like to thank Prof. James Quintiere, my mentor, teacher and friend, for guiding me through this process with his great knowledge and patience. Dr. Quintiere, I would not have come this far without your tremendous help and support. There were times when things did not go too well, but your encouragement held me up and kept me going. Dr. Quintiere, thank you again for believing in me. I, among the other students who have worked under your supervision, always know that we are very lucky to be your students.

I would like to also give my appreciation to the dissertation committee members, Dr. Marino di Marzo, Dr. Arnoud Trouvé, Dr. Andre Marshall and Dr. Peter Chang as well as the department of Fire Protection Engineering and Mechanical Engineering. I especially thank Dr. Marshall and Dr. Trouvé for their invaluable suggestions and comments. The discussion in our group meeting has given me a broad view of both experimental and numerical technique in fire research.

This dissertation would not be possible without the support from the National Institute of Standards and Technology and the John L. Bryan Chair Fund.

I would like to thank my friends Tensei Mizukami, Ming Wang, Nicolas Diné, Mekyoung Kim (Monique), Xin Liu, Joseph Panagiotou, Jonathan Perricone, and Peter Veloo for their tireless help and support. The time we shared in classes and the Potomac lab is priceless to me and I will not forget all the fun we have.

I would like to especially thank Alongkorn Kamson and Songchon Siripongchai for their help in formatting the dissertation and the drawing for experimental apparatus. Last but not least, I would like to thank my family for their support and encouragement.

Table of Contents

List of Tables

List of Figures

Nomenclature

A_e	=	Effective entrainment area
A_F	=	Total fuel exposed area
A_g	=	Bounding surface area
A_w	=	Wall total surface area
A_{Fp}	=	Total projected fuel surface area
$A_{C,o}$	=	Cross-sectional area of the vertical crib shafts
$A_{F,b}$	=	Burning fuel flux exposed area.
$A_{Fp,b}$	=	Projected flaming fuel surface area
b	=	Thickness of wood stick, side dimension of the square stick
B	=	B Number
c_p	=	Specific heat at constant pressure
c_v	=	Specific heat at constant volume
C	=	Constant
C_d	=	Flow coefficient
C_w	=	Empirical wood crib coefficient
C_{plume}	=	Plume entrainment coefficient
C_{mix}	=	Coefficient for mixing correlation
c_{pw}	=	Wall specific heat
D	=	Diameter
D_b	=	Burning diameter
D^*	=	Dimensionless fire diameter to opening height
$\hat{D}$	=	Dimensionless fire diameter to opening width
F_g	=	Shape factor from fuel to the compartment gas
F_w	=	Shape factor from fuel to the walls
g	=	Gravitational acceleration
h	=	Vertical coordinate
h_c	=	Convective heat transfer coefficient
$h_{c,ambient}$	=	Convective heat transfer coefficient outside of compartment
$h_{f,conv}$	=	Flame convective heat transfer coefficient
H_o	=	Height of the opening
k_w	=	Thermal conductivity of the wall
l	=	Length scale
L	=	Heat of gasification
L_f	=	Mean beam length of flame

L_i	=	Length of stick i
L_j	=	Length of stick j
L_s	=	Stick length
L_{mf}	=	Characteristic length scale for the flame volume
L_{mg}	=	Mean beam length for an entire uniform isothermal gas volume
L_{eff}	=	Effective heat of gasification
$L_{s,b}$	=	Stick burning length
$\dot{m}$	=	Mass outflow rate
$\dot{m}_b$	=	Burning rate
$\dot{m}_e$	=	Entrainment rate
$\dot{m}_F$	=	Fuel mass loss rate
$\dot{m}_o$	=	Incoming air flow rate
$\dot{m}_u$	=	Rate of unburned fuel gases and soot
$\dot{m}_{o,u}$	=	Incoming air flow rate between neutral plane and layer interface
$\dot{m}''_{F,\max}$	=	Asymptotic value for fuel mass loss rate
$\dot{m}''_{F,o}$	=	Free burning rate or fuel mass loss rate
$\dot{m}_{e,plume}$	=	Near-field entrainment rate for axisymmetric plume
$\dot{m}_{o,plume}$	=	Incoming flow
m_e^*	=	Dimensionless entrainment rate
m_o^*	=	Dimensionless inflow rate
n	=	Number of stick per layer
N	=	Neutral plane height, number of stick layers
N^*	=	Dimensionless neutral plane height
p_o	=	Pressure outside compartment
P	=	Differential pressure at the floor
$\dot{q}_{net}$	=	Net heat to the fuel surface
$\dot{q}''_f$	=	Flame heat flux
$\dot{q}_{External}$	=	Total external heat feedback
$\dot{q}_{Ext}$	=	Net radiation feedback to the non-flaming fuel area
$\dot{q}_{Ext,b}$	=	Net radiation feedback to the flaming fuel area
$\dot{q}_{wall}$	=	Heat transfer to the boundaries
$\dot{q}_{vent}$	=	Heat loss through the opening via radiation
$\dot{q}_{conv}$	=	Convection
$\dot{q}''_{rad}$	=	Radiative heat flux
$\dot{q}''_{wall}$	=	Heat flux to the wall

$\dot{q}''_{conv}$	=	Convective heat flux
$\dot{q}_{Ext,b}$	=	Net external heat transfer to the burning area
$\dot{q}''_{f,rad}$	=	Flame radiative heat flux
$\dot{q}''_{f,conv}$	=	Flame convective heat flux
$\dot{q}''_{f,net}$	=	Net flame heat flux
$\dot{q}''_{f,net,o}$	=	Net flame heat flux without compartment
$\dot{Q}$	=	Energy release rate or fire power
$\dot{Q}_{loss}$	=	Total heat loss
Q^*_{plume}	=	Dimensionless driving force for the plume
r	=	Stoichiometric mass of oxygen to fuel ratio
R	=	Gas constant
s	=	Stoichiometric mass of air to fuel ratio
S	=	Window sill height
S^*	=	Window sill dimensionless height
T	=	Compartment gas temperature, upper gas temperature
T_v	=	Fuel temperature or the gasifying temperature
T_f	=	Flame temperature
T_o	=	Ambient temperature
T_l	=	Lower layer gas temperature
T_u	=	Upper layer gas temperature
T_v	=	Fuel vaporization temperature
T_w	=	Wall surface temperature
T_∞	=	Surrounding temperature near fuel
v_e	=	Entrainment velocity
v^*	=	Characteristic velocity of incoming air
V	=	Compartment volume
V_g	=	Volume of the gray gas body
W_o	=	Width of the opening
X_s	=	Soot volume fraction
$X_{s,f}$	=	Soot volume fraction in flame
y_s	=	Mass yield of soot per mass of fuel burn
Y_s	=	Soot mass fraction
Y_{ox}	=	Oxygen mass fraction
$Y_{ox,\infty}$	=	Oxygen mass fraction near fuel
$Y_{ox,l}$	=	Lower layer oxygen mass fraction, oxygen mass fraction feeding the flame
$Y_{ox,u}$	=	Upper layer oxygen mass fraction

$Y_{ox,o}$	=	Oxygen mass fraction in free burning, ambient oxygen
z	=	Vertical coordinate
Z	=	Layer interface, smoke layer height, thermal discontinuity
z^*	=	Dimensionless smoke layer height
z_{ref}	=	Reference height
Z^*	=	Dimensionless smoke layer height with sill adjustment
χ_r	=	Radiation loss fraction
ε_g	=	Gas emissivity
ε_f	=	Flame emissivity
ε_w	=	Emissivity of the wall
ϕ	=	Equivalence ratio
κ_g	=	Absorption coefficient of the gas
κ_f	=	Absorption coefficient of the flame
ρ	=	Compartment gas density
ρ_f	=	Flame density
ρ_o	=	Gas density outside of the room
ρ_s	=	Soot density
ρ_w	=	Density of the wall
σ	=	Stefan-Boltzmann constant
$\dot{\omega}_{ox}$	=	Rate of oxygen reacted within the control volume
ψ	=	Combustion parameter
Δh_c	=	Heat of combustion per unit mass of fuel
Δh_{ox}	=	Heat of combustion per unit mass of oxygen
Δp	=	Pressure difference at any height
Δp_B	=	Pressure difference at the bottom edge of the opening
Δp_T	=	Pressure difference at the top edge of the opening

Chapter 1

Introduction

1.1 Background

A *fully-developed fire* is defined as the stage of fire where all available fuels become involved and the fire burns at its maximum potential according to the limit amount of the available fuel (*fuel-controlled fire*) or the available air supply (*ventilation-controlled fire*). At this stage, the heat flux conditions in the room can reach as high as 150 kW/m^2 [1] and a highest gas temperature can achieved in the range of 700 to 1200 ºC [2] which can possibly cause severe damage to the structure. Hence, the fully-developed stage is the greatest concern to the design for the structural stability and the safety of the firefighters.

In most buildings, fires in common residential spaces and offices become ventilation-controlled when the fully-developed stage is reached. In ventilation-controlled fires, all of available fuel gases are not consumed by the flames and these gases can burn as they pass through the openings causing the flames to emerge windows and doors. For a large fire at the fully-developed stage, the compartment is often filled with the smoke and the layer interface is close to the floor. Such a condition can be termed the *well-mixed* stage where the gas is assumed to have uniform properties throughout the compartment. A *single-zone* model assumption is usually suitable for this type of fires.

In a structural fire protection design, the information of the maximum temperature and fire duration is necessary to obtain a proper fire protection system for a given room with ventilation and fuel load configurations. To achieve such a requirement the *burning rate* and the *fuel mass loss rate* must be correctly calculated by taking into account for the fuel response to the thermal feedback enhancement from the enclosure and the vitiated oxygen effects. Current design tools including correlations and mathematical fire models do not address the fuel response; hence the burning time and temperature may not be properly predicted.

This dissertation presents a study that may fulfill the incompleteness of the current design tools by establishing a single-zone fire model that addresses the fuel response to the thermal feedback and limited oxygen effect and potentially gives the burning time and temperature for any fuel, scale, and ventilation.

1.2 Literature Review

A large number of studies in enclosure fire have been carried out through the last four decades. Experimental data obtained from those studies are significant for understanding the physics of fully-developed compartment fires as well as developing theoretical models which could effectively predict useful results such as the burning rate and gas temperature. However, it may not be possible to reference all available sources, but a concise review of relevant work is presented here in two categories: (1) experimental studies and (2) correlations and models.

1.2.1 Experimental Studies

Since the early work by Ingburg [3], many experimental data has been obtained for fully-developed compartment fire. Kawagoe [4, 5], one the pioneer researchers, studied the roles of ventilation and he was the first to introduce the relationship of the burning rate and the ventilation parameter, $A_o\sqrt{H_o}$, in fully developed compartment fires with small openings.

Gross [6] examined the burning rate of a combustible-fiberboard crib in enclosure of three different sizes and found that the mass loss rate was proportional to the ventilation parameter, $A_o\sqrt{H_o}$, although there were shifts in the data that resulted from different scales. He then employed a scale factor which represented the ratio of linear dimensions relative to the reference enclosure size to normalize the burning rate and ventilation parameter.

A comprehensive analysis on the results of the well-known C.I.B. test (a co-operative test program on fully developed fires in single compartment performed by eight laboratories in 1958) was given by Thomas and Heselden [7, 8]. In these tests the burning of wood cribs under a wide range of compartment shapes was measured. Various relationships between the mean burning rate, mean intensity of radiation and the mean gas temperature and parameters of the compartment and fuel were introduced empirically, and some by a theoretical consideration of the heat balance. The effects of scale were found to be minor which justified the use of small the scale compartments. The fuel mass loss rate was presented in the form of $\dot{m}_F / A_o\sqrt{H_o}$ which had an averaged value of about 5-6 kg/min-m$^{5/2}$. Heselden et al. [9] reviewed the constant k in the

expression $\dot{m}_F = kA_o\sqrt{H_o}$ for ventilation controlled fire in various experiments, both in small and full scale, and it was found to be approximately 6 kg/min-m$^{5/2}$. This was under the condition of a minimum 150 kg of fuel/m^2 of ventilation opening area. The constant *k* value was also in an agreement with work done by Kawagoe and Sekine [5]. It was noted that the averaged value of the term $\dot{m}_F / A_o\sqrt{H_o}$ from C.I.B test was found to be correlated with the geometry of the compartment and ventilation; the burning rate, therefore, was also normalized in the form of $\dot{m}_F / A_o\sqrt{H_o}(D/W)^{1/2}$ and presented as a function of $A_T / A_o\sqrt{H_o}$.

Tewarson [10, 11] published an experimental study on enclosure fires using both crib fire (cellulosic materials) and pool fire (ethyl alcohol and paraffin oil). Four burning regions were categorized based upon the characteristic variations of the ventilation parameter, burning rate, gaseous product mole fraction, and temperature. An empirical expression to estimate the ventilation parameter required for the interface of regions which corresponded to extreme danger i.e. producing the most toxic gas concentration were also given.

Takeda and Akita [12] found that as the ventilation or opening area of the compartment window increased, the burning of methanol changed from regimes of (I) extinction, (II) stable laminar burning, (III) *unstable oscillations*, and finally (IV) steady burning, including the possibility of *oscillations*. Tewarson [11] and Kim et al.[13] also found similar behavior. *Ghosting flame*, type of unstable flame that drifting away from the fuel surface was observed in the methanol pool fire experiment by Sugawa et al. [14]. In a full-scale test, the ghosting behavior was also observed by Audouin et al [15]. The

more recent study by Bertin et al. presented some diagnostics of the ghosting flame for a small-scale wall-fire experiment.

Harmathy [16, 17] published an extensive review of compartment wood crib fires. He claimed [18] that the conventional concept of fully developed ventilation-controlled fires, according to which the shortage of air in a compartment limiting the rate of burning was somewhat untenable based on the observation of a multitude of compartment experiments. He introduced a different form of ventilation parameter as $\rho\sqrt{g}A_o\sqrt{H_o}$ which was then normalized by with the fuel area, A_F, to represent the ratio of air flow rate available to the fuel flow. By using experimental data from various sources, Harmathy showed that there were two distinct regimes of the burning rate. These two regimes were known before as fuel bed controlled regime and ventilation controlled regime. A critical value of $\rho\sqrt{g}A_o\sqrt{H_o}/A_F$ and a linear relationship of the burning rate and the ventilation parameter were defined empirically. He also pointed out clearly that for the ventilation controlled regime the burning depended on both the shape and size of the compartment. In addition to his previous work, Harmathy found that [19] the burning of non-charring fuels was virtually unaffected by the ventilation level, whereas charring material burned faster up to a maximum as the flow rate of air increases. Bullen and Thomas [20] presented burning rates per unit area of pool and crib fires in terms of $\rho\sqrt{g}A_o\sqrt{H_o}/A_F$ and found a distinction between the two fuel types.

Propane pool fire experiments by Santo and Delichatsios [21] showed that the vitiated air supply considerably affected flame radiation to decrease. They also suggested this can be due to the reduction on soot formation causing a lower adiabatic flame

temperature. Tewarson et al. [22] also found for plastic and liquid pool fires that the flame radiative heat flux increased as the oxygen concentration increased.

Peatross and Beyler [23] performed an experimental study on full-scale compartment fires with natural and overhead forced ventilation to access the effect of the ventilation on the compartment fire behavior. The fuels included diesel fuel, wood cribs, and polyurethane slabs. A *well-mixed* condition for oxygen concentration was found for all forced ventilation tests. They also found that the reduced oxygen concentration at the flame base caused the reduction in the fuel mass loss rate, and a linear relationship between them was observed. Thermal enhancement was not included in their analysis. Such an effect, however, could be relatively low in their wood crib experiments and the large diesel pool fires due to the scale effect on flame emissivity.

Fleischmann and Parkes [24]conducted pool fire experiments using heptane pool fire with 20 cm diameter. The ventilation was varied by adjusting the opening width and height. They reported the mass loss rate to be nearly 7 times higher than the free burning due to the thermal feedback enhancement. The experiments were compared with the prediction using a closed form approximation of COMPF2 [25], a single-zone model in which the effect of vitiated oxygen was not included. The prediction showed a lower gas temperature for most cases than the experiments. The discrepancy can be due to the oxygen vitiation effect that was not accounted for by the model.

Delichatsios et al.[26, 27] analyzed the experiments by Ohmiya et al. [28] and demonstrated the effects of fuel type, area and geometry on the mass loss rate. Their analysis showed the mass loss rate in the ventilation-controlled regime followed the trend

of the mass inflow rate and the dependence of the mass loss rate on the inflow rate varied as the temperature distribution in the enclosure changed from uniform to stratified. They also found that not all the exposed fuel area was involved in burning. However, a clear explanation for the reason of the mass loss rate dependence on the inflow rate was not given.

Experiments for two ventilation openings have been conducted by Kumar et al.[29] to study the effect of cross ventilation on the gas temperature and the fuel mass loss rate. They found that the temperatures in cross ventilation condition are higher than those in single ventilation for a large fire size.

In recent studies carried out at the University of Maryland, experiments were conducted using a 40 cm cube compartment burning heptane in varying diameter pans. Wakatsuki [30] studied single ceiling vents, Ringwelski [31] studied equal area vents at the top and bottom of a wall, and Rangwala [32] examined a one-zone model of the wall vent case. In addition, Utiskul et al [33] focused on the ventilation effects and in particular the region of low ventilation burning of heptane pool fires and examined the wall case with additional instrumentation. Hu et al.[34, 35] have simulated the experiment by Utiskul using FDS by to characterize the dynamics of the compartment fires under poorly ventilated. Fundamental experiments used to characterize the local flame response to vitiated air conditions have been conducted by Williamson et al. [36] with the emphasis on to local effects to serve as a basis for the flame dynamics within a single FDS computational grid cell.

Some current full-scale experimental programs have been conducted as part of an international collaborative fire model project (ICFMP) to use as the benchmark exercise series for fire modeling. 4 full-scale test series [37-40] were completed and available to the public.

1.2.2 Correlations and Models

Kawago and Sekine [5] have computed temperature-time curves by integrating the energy balance of compartment fires with the time. This method was limited to ventilation controlled fire with a constant rate of heat release. Lie[41] has proposed a parametrical expression that that fitted Kawagoe's computed temperature-time curves. McCaffrey et al [42] have proposed a method for predicting the upper layer gas temperature of a pre-flashover compartment. This later called MQH correlations and was based on a simplified energy balance and some simple assumptions to estimate the loss of energy to the wall and vents. Several parametric methods and temperature correlations were developed from many sources and researchers: Eurocode [43], Tanaka[44], Magnusson and Thelandersson[45], Harmathy[16], Babrauskas[25], Law [46], and etc. A comprehensive review for these correlations are found in the SFPE's engineering guide to fire exposures [47]. Nevertheless, these correlations have not include the fuel response to thermal feedback and the vitiated oxygen.

One-zone models were first developed in the sixties and aimed at modeling the post-flashover fire phase. Two-zone models for application in solving compartment fires originated in the mid-1970s. Several groups: Harvard, IITRI, NIST, BRI (Japan), CSTB (France) pursued their development. In nearly all cases these codes could describe the

fire phenomena in broad strokes of a homogeneous upper and lower layer of room gases, penetrated by a fire plume. Models of individual physics and chemistry make up the subroutine strung together by conservation of mass, species and energy for each of the layers, and orifice flow through wall vents based upon models to describe the primary transport of gases. Plume entrainment studies gave empirical correlations to describe the uptake of lower layer gases into the hotter upper layer. Many phenomenological aspects were brushed over or only slightly included. The most sophisticated models used to simulate compartment fires are CFD models also called field models. The CFD modeling technique is used in a wide range of engineering disciplines and is based on a complete time-dependent, three-dimensional solution of the fundamental conservation laws [2]. CFD models are now considered to be mature in fire applications and give the most complete prediction; however, the drawback of CFD technique is that it is computational and time demanding. Also CFD model cannot adequately resolve on scales and therefore need special models for turbulence and combustion.

A comprehensive report for the computer fire models has been presented by Friedman [48] and recently updated by Olenick and Carpenter [49]. Friedman also provided some discussion on specifying the fire in the models and emphasized that for a more realistic fire that includes fuel response to the vitiated oxygen and thermal feedback are needed

1.3 Problem Statement and Scope of the study

Current theoretical models do not include fuel response to vitiated oxygen and the burning enhancement from the hot gas and enclosure (from literature review [48-59]). Hence, the temperature and the fire duration may not be correctly predicted. Existing experimental data are presented for different scales and described in different variables, but usually in terms of a ventilation factor. These data at different scales, however, have not been fully organized such that their generality may become acceptable to use in the design.

This study will address the problem within the scope of the fully-developed compartment fires. Only a single-wall vent configuration, doorway or window, is considered. A uniform property assumption is employed in the development of a theoretical model and its validity is given by a criterion of the fire size and the opening configuration presented later in the dissertation.

1.4 Objective and Methodology

The objective of the dissertation is to establish a fully-developed compartment fire model to predict the fuel mass loss rate and the average temperature for fully-developed compartment fires as a function of fuel type and configuration, compartment size, ventilation, wall properties and physical scale. To achieve our goal, the following steps are pursued.

1.) A single-zone model that addresses the fuel response, scale effect, and flame extinction is formulated. The compartment heat transfer is properly treated and the burning area in ventilation limited fire is also addressed.

2.) A near-vent mixing correlation characterizing the mixing between the smoke layer and the incoming air flow is developed based on controlled experiments to estimate the near-flame oxygen concentration necessary to predict the compartment fuel mass loss rate.

3.) A criterion for a single-zone model justification in compartment fires is examined and used as the scope of the study.

4.) Key experiments for single-wall-vents are carried out to validate the single-zone model and explore the phenomena associated with the fully-developed fires through a range of ventilation.

1.5 Contents

The contents of this dissertation are as follows:

Chapter 2: A theory of the compartment burning rate and the fuel response to the thermal feedback and ventilation effect are described in detailed with the application to the pool and crib fire. Discussions on ventilation-controlled burning area, flame and smoke emissivities, and flame extinction theory are included. A validation of the theory for the fuel mass loss rate is presented.

Chapter 3: A review of the part studies on mixing phenomena is given and a new mixing correlation based on experimental data is proposed. The experimental description

and the measurement method are presented. The mixing correlation from the past studies is evaluated with the current experimental results.

Chapter 4: A justification the use of a single-zone model based on the smoke layer height is discussed. A simplified method to determine the smoke layer height is presented and validated with the experimental results. A criterion for the single-zone model to be valid as a function of fire size and the opening configuration is given.

Chapter 5: A formulation of the single-zone model is presented in details. A summary for the conservation relationships, compartment heat transfers, fuel mass loss rate model and criteria for energy release essential to zone modeling are given. The description for the numerical solver and time integration method is also presented.

Chapter 6: Description of the key experiments is provided. Observations are described on a full range of fire phenomena found in experiments: response of fuel to thermal and oxygen feedback, oscillations, and fire area shrinkage. The experimental results are presented along with the model simulations to validate the performance of the model and show some generalities. The fuel type and scale effects are examined.

Chapter 7: Concluding remarks of the study are drawn. Limitation and potential of the single zone model is discussed. Recommendations for the future works are given.

Chapter 2

Burning Rate and Fuel Behavior in Compartment Fires

2.1 Introduction

To predict the effect of fire on the structures, one needs to understand physics of the fire growth in a compartment as to how the fuel interacts with the flame and its surroundings. More specifically, the fuel burning rate which mainly controls the temperature rise can be predicted by studying the effects of ventilation and thermal enhancement on the fuel. This chapter explores these effects and applies them to the common fuel configurations such as pool and crib fires. Some important discussions on ventilation-controlled burning area, flame and smoke emissivities, and flame extinction theory are also included in this chapter.

2.2 Compartment Burning Rate

The burning rate is defined as the rate at which the fuel, usually but not exclusively in the gas-phase, is consumed by the chemical reaction within the enclosure. The burning rate plays a significant role in compartment fire because it represents how much energy is released into the system. The energy release rate or fire power, $\dot{Q}$, within the enclosure is given as

$$\dot{Q} = \Delta h_c \dot{m}_b , \tag{2.1}$$

where $\dot{m}_b$ is the burning rate and Δh_c is the heat of combustion per unit mass of fuel. In some literature, however, the term burning rate was used to describe the fuel mass loss rate. While these two rates may arguably follow the same trend; they have completely different meaning. The fuel mass loss rate refers to the rate at which a condensed-phase fuel is decomposed to gases due to the energy transferred from its surrounding heat sources such as flames, hot gas, and enclosure walls. We can describe the relationship for the mass loss rate and the burning rate assuming there are no inerts in the evolved fuel as follow:

[Fuel mass loss rate] = [Burning rate] + [Rate of unburned fuel gases and soot]

or

$$\dot{m}_F = \dot{m}_b + \dot{m}_u \,. \tag{2.2}$$

In a situation where there is no unburned fuel gas, the value of burning rate and fuel mass loss rate are identical. A parameter that is generally used to describe the burning and mass loss rate relationship is known as the global equivalence ratio which is given as

$$\phi = \frac{\dot{m}_F}{\dot{m}_o} \cdot s \,, \tag{2.3}$$

where $\dot{m}_o$ is the incoming air flow rate and s is the stoichiometric mass of air to fuel ratio. When $\phi < 1$, a compartment fire is termed *over-ventilated* and no unburned fuel exists. As for $\phi \geq 1$, the amount of fuel mass is more than what is needed stoichiometrically and all of the available oxygen is consumed by the chemical reaction, thus the burning is governed by the amount of incoming air. The latter case is called *under-ventilated*

condition. This leads us to another way of presenting the burning rate and fuel mass loss rate as follows:

$$\begin{aligned} \dot{m}_b &= \dot{m}_F \quad ; \phi < 1 \\ \dot{m}_b &= \frac{\dot{m}_o}{s} \quad ; \phi \geq 1 \end{aligned} \tag{2.4}$$

In compartment fire experiments the fuel mass loss rate can be directly measured using weighing cells to track the weight of the fuel over time; however, measurement for the burning rate may not be done directly especially in the under-ventilated condition. The detection of burning may require other special methods such as unburned hydrocarbon measurements or calorimetry for the compartment fire system. The latter still faces some difficulties as there is the potential for flames to burn outside of the compartment where there is plenty of air supply.

In order to predict the burning rate, the fuel mass loss rate must be accurately known as appears in Eq (2.4). This is always true even for the under-ventilated condition, where burning depends on available air, because the fuel mass loss rate also determines the burning state as shown in Eq (2.3). The following sections describe our methodology in predicting the fuel mass loss rate.

2.3 Compartment Effect on Fuel Mass Loss Rate

From the definition provided previously, the fuel mass loss rate can be simply expressed by

$$\dot{m}_F = \frac{\dot{q}_{net}}{L}, \tag{2.5}$$

where $\dot{q}_{net}$ is the net heat to the fuel surface and L is the heat of gasification depending on the fuel type. It shall be noted that this expression is based upon a quasi-steady assumption; although, it is suitable to describe the expenditure of the fuel mass loss with or without the presence of compartments giving that the fuel responses fast to the changes of the net heat transfer. Let us first consider the burning in an open environment case (*free burning*). Without an enclosure, the heat to gasify the condensed fuel in Eq. (2.5) only comes from the flame. Assuming the fuel surfaces are blackbody, the net heat is given as

$$\dot{q}_{net} = \dot{q}''_f A_{F,b} - \sigma A_{F,b} T_v^4 , \tag{2.6}$$

where $\dot{q}''_f$ is the flame heat flux, $A_{F,b}$ is the burning fuel area (exposed to or covered by flames), and T_v is the fuel surface temperature or the gasifying temperature. As for burning in the compartment where the smoke is enclosed and the wall is hot, the net heat to the fuel is then given as

$$\dot{q}_{net} = \dot{q}''_f A_{F,b} - \sigma A_{F,b} T_v^4 + \dot{q}_{External} , \tag{2.7}$$

where $\dot{q}_{External}$ is the total external heat feedback from smoke and compartment wall surfaces. It is obvious that the external heat is one of the main differences between the free burning and the compartment burning; however, the flame heat flux in the compartment may differ from that in free burning as described by Tewarson [22] and Santo and Delichatsios [21]. The flame heat flux depends on the local oxygen concentration and in a compartment that will be reduced due to mixing between smoke and incoming air when the opening size decreases. Thus, there are two effects on the compartment fuel mass loss rate we shall discuss further, ventilation and thermal effects.

2.3.1 Ventilation Effects

To examine the effects of the ventilation on the fuel mass loss rate, we first look at the flame heat flux which is composed of radiation and convection parts as follow:

$$\dot{q}''_f = \dot{q}''_{f,rad} + \dot{q}''_{f,conv} \tag{2.8}$$

From the stagnant layer solution [60], the flame convective heat flux can be written as

$$\dot{q}''_{f,conv} = \frac{h_{f,conv}}{c_p}\left(\frac{\ln(1+\mathrm{B})}{\mathrm{B}}\right)\left(\frac{Y_{ox,\infty}\Delta h_c}{r} - c_p\left(T_v - T_\infty\right)\right), \tag{2.9}$$

where $\mathrm{B} = \dfrac{Y_{ox,\infty}\,\Delta h_c / r - c_p\left(T_v - T_\infty\right)}{L}$,

T_∞ is the surrounding temperature near fuel,

$Y_{ox,\infty}$ is the oxygen mass fraction near fuel, and

$h_{f,conv}$ is the convective heat transfer coefficient.

By assuming small B number, the blocking factor, $\ln(1+\mathrm{B})/\mathrm{B}$, converges to 1, hence Eq. (2.9) reduces to

$$\dot{q}''_{f,conv} = \frac{h_{f,conv}}{c_p}\left(\frac{Y_{ox,\infty}\Delta h_c}{r} - c_p\left(T_v - T_\infty\right)\right). \tag{2.10}$$

As for the radiative component,

$$\dot{q}''_{f,rad} = \varepsilon_f \sigma T_f^4, \tag{2.11}$$

where ε_f is the flame emissivity, and T_f is the flame temperature. Rewrite the flame heat flux to the fuel as follow:

$$\dot{q}''_f = \frac{h_{f,conv}}{c_p}\left(\frac{Y_{ox,\infty}\Delta h_c}{r} - c_p\left(T_v - T_\infty\right)\right) + \varepsilon_f \sigma T_f^4 \text{, or} \tag{2.12}$$

$$\dot{q}''_f = \frac{h_{f,conv} Y_{ox,\infty}\Delta h_c}{c_p r} - h_{f,conv}\left(T_v - T_\infty\right) + \varepsilon_f \sigma T_f^4 \tag{2.13}$$

By neglecting the second term in the right hand side of the Eq (2.13) for its small contribution and based on Tewarson [22] that the flame radiation, $\varepsilon_f \sigma T_f^4$, decreases as the oxygen concentration is decreased, we may see that the flame heat flux only depends on the local oxygen concentration. Hence, as a first order approximation,

$$\dot{q}''_f \sim Y_{ox,l}, \tag{2.14}$$

where $Y_{ox,l}$ is the oxygen mass fraction feeding the flame. We also expect the net flame heat flux, $\dot{q}''_{f,net} = \dot{q}''_f - \sigma T_v^4$, to follow the same behavior.

$$\dot{q}''_{f,net} \sim Y_{ox,l}, \tag{2.15}$$

In free burning case, the flame heat flux is also

$$\dot{q}''_{f,net,o} \sim Y_{ox,o}, \tag{2.16}$$

where $Y_{ox,o}$ is the oxygen fraction in the free burning generally equals to 0.233. Thus, from (2.15) and (2.16),

$$\frac{\dot{q}''_{f,net}}{\dot{q}''_{f,net,o}} = \frac{Y_{ox,l}}{Y_{ox,o}} \text{, or} \tag{2.17}$$

$$\dot{q}''_{f,net} = \dot{q}''_{f,net,o}\frac{Y_{ox,l}}{Y_{ox,o}}. \tag{2.18}$$

Recall the expression for the fuel mass loss rate.

$$\dot{q}''_{f,net,o} = \dot{m}''_{F,o} L \,, \tag{2.19}$$

where $\dot{m}''_{F,o}$ is the free burning rate or fuel mass loss rate in opened environment per unit area. We have,

$$\dot{q}''_{f,net} = \dot{m}''_{F,o} L \frac{Y_{ox,l}}{Y_{ox,o}} \,. \tag{2.20}$$

We obtain the fuel mass loss rate in the compartment from Eq. (2.5) as

$$\dot{m}_F = \frac{\dot{q}''_{f,net} A_{F,b} + \dot{q}_{External}}{L} \text{, or} \tag{2.21}$$

$$\dot{m}_F = \dot{m}''_{F,o} A_{F,b} \frac{Y_{ox,l}}{Y_{ox,o}} + \frac{\dot{q}_{External}}{L} \,, \tag{2.22}$$

where $A_{F,b}$ is the burning fuel exposed area. For over ventilated fire, $\phi < 1$, $A_{F,b}$ equals to the total fuel exposed area, A_F; however, $A_{F,b}$ for under ventilated case needs a more detailed description which will be discussed further in the section 2.5.

As the opening size is reduced, the mixing between the smoke and the incoming air will increase and the oxygen feeding the fire will be reduced, and the fuel mass loss rate will correspondingly be reduced as described by the first term on the right hand side of Eq (2.22), which here will be called the ventilation effect from this point on. This phenomenon has been observed in many experimental studies and represents the ventilation-controlled burning [9, 16, 18, 33]. The ventilation effect in Eq (2.22), although simple, has a very useful form because it is based on the free burning

rates, $\dot{m}''_{F,o}$, which are either available in the literatures for various fuel types and configurations or possible to obtain experimentally.

A common correlation for the free burning rate per unit area of large liquid pool fires ($D > 2$ m) is given as [61]

$$\dot{m}''_{F,o} = \dot{m}''_{F,\max}\left(1 - e^{-\kappa_f L_f}\right), \tag{2.23}$$

where $\dot{m}''_{F,\max}$ is the asymptotic value for fuel mass loss rate, κ_f is the flame absorption coefficient depending on the fuel type, and L_f is the mean beam length. For a cylindrical shape flame with a diameter (D), $L_f = 0.66D$ [2]. For a heptane pool (C_7H_{16}) the asymptotic fuel mass loss rate is 0.101 kg/m^{2}s and the flame absorption coefficient is 1.66 m^{-1} [62].

A dimensionless correlation describing the time-average free burning rate per unit exposed area for wood cribs was established by Heskestad [63] as follow:

$$\frac{\dot{m}''_{F,o}}{C_w b^{-1/2}} = 0.968\left(1 - \exp\left(-\frac{(sb)^{1/2} A_{C,o}}{0.02 A_F}\right)\right), \tag{2.24}$$

where b is thickness dimension of a stick, s is the spacing between sticks, $A_{C,o}$ is the cross-sectional area of the vertical crib shafts, and C_w is the empirical wood crib coefficient given by Block [64] for some species of wood as 1.03 mg/cm$^{1.5}$ for Ponderosa pine, 1.33 for Oak, and 0.88 for Sugar pine. The exposed fuel surface area, A_F, for wood cribs can be determined by the following expressions:

For a square footprint crib,

$$A_F = nb^2\left[(1-n+2m)2N+2n-m\right], \tag{2.25}$$

where N is the number of stick layers, n is the number of stick per layer, b is the side dimension of square stick, L_s is the stick length, and $m = L_s / b$.

For a rectangular footprint crib,

$$A_F = b^2\left[m_i n_i(2N-1)+N\left(n_i+n_j+2m_j n_j-2n_i n_j\right)+n_j\left(3n_i-n_j\right)\right] \text{ ; for even } N, \tag{2.26}$$

$$A_F = b^2\left[(N-1)\left(2m_j+1\right)n_j+n_i\left(1+m_i+2n_j+N+2N\left(m_i-n_j\right)\right)\right]; \text{ for odd } N, \tag{2.27}$$

where n_i and n_j are the number of stick i and j per layer respectively, L_i and L_j are the length of stick i and j respectively, $m_i = L_i / b$, and $m_j = L_j / b$. The derivation for Eq. (2.25) to (2.27) is provided in the Appendix.

In addition to the free burning rate, another variable needed to estimate the effect of the ventilation is the concentration of the oxygen feeding the flame ($Y_{ox,l}$). In room fires when the vent is small and the smoke layer descends close to the floor, the entering cold fresh air stream can be contaminated by the smoke due to the buoyancy and shear mixing [65] occurring near the vent. This phenomenon, called vent mixing, leads to the reduction in oxygen feeding the flame and it is therefore an important factor to explain the effect of ventilation on the fuel mass loss rate in the compartment fires. The phenomenon of vent mixing is discussed in more details in Chapter 3.

2.3.2 Thermal Effect

From the previous section we see that the effect of ventilation on fire is the reduction in burning due to the oxygen deficiency. The thermal effect however plays the enhancement part of the burning [66]. It is the external radiation feedback that leads the room fire from the growth phase to the flashover and fully-involved stage. In general, the external radiation can be given as:

$$\dot{q}_{External} = \begin{pmatrix} \text{Net radiation feedback} \\ \text{to the flaming fuel area} \end{pmatrix} + \begin{pmatrix} \text{Net radiation feedback to} \\ \text{the non - flaming fuel area} \end{pmatrix} \quad \text{, or}$$

$$\dot{q}_{External} = \dot{q}_{Ext,b} + \dot{q}_{Ext} \tag{2.27}$$

It is necessary to distinguish between the flaming and non-flaming fuel surface areas for the net radiation feedback due to the fact that (1) in ventilation-limited burning the flame only burns at the available amount of supplied air and may not pyrolyze or cover the entire fuel surface area [67], and (2) for a thick flame which has a large emissivity, the radiation feedback may not be so significant in the flaming area since it may not penetrate through the thick sooty flame. Figure 2.1 illustrates the flaming and non-flaming surface area of a pool fire with the radiation heat feedback.

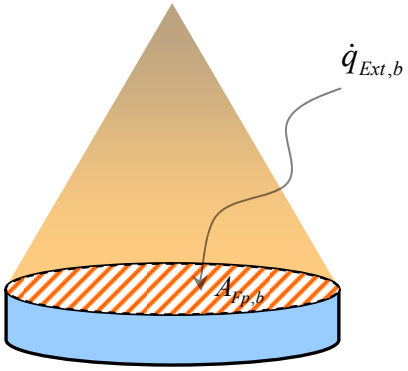

Figure 2.1a

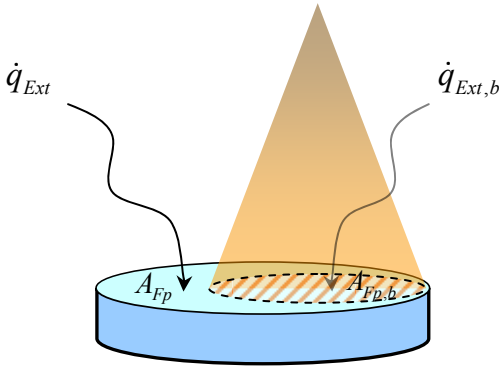

Figure 2.1b

Figure 2.1 External radiation feedback on flaming and non-flaming surface area for a pool fire. 2.1a is for over ventilated and 2.1b is for under ventilated case.

The net radiation feedback to the flaming and non-flaming fuel area can be given respectively as following:

$$\dot{q}_{Ext,b} = F_g\left(1-\varepsilon_f\right)\varepsilon_g A_{Fp,b}\left(T^4 - T_o^4\right) + F_w\left(1-\varepsilon_f\right)\left(1-\varepsilon_g\right)A_{Fp,b}\left(T_w^4 - T_o^4\right), \text{ and} \qquad (2.28)$$

$$\dot{q}_{Ext} = F_g\varepsilon_g\left(A_{Fp} - A_{Fp,b}\right)\left(T^4 - T_v^4\right) + F_w\left(1-\varepsilon_g\right)\left(A_{Fp} - A_{Fp,b}\right)\left(T_w^4 - T_v^4\right), \qquad (2.29)$$

where T is the compartment gas temperature, T_o is the ambient temperature, T_w is the wall temperature, T_v is the fuel vaporization temperature or the fuel surface temperature, F_g is the shape factor from the fuel to the compartment gas, F_w is the shape factor from the fuel to the walls, $A_{Fp,b}$ is the projected flaming fuel surface area, and A_{Fp} is the total projected fuel surface area. The emissivity of the flame, ε_f, and the smoke, ε_g, will be addressed in more detail in section 2.4.

For a pool fire, the projected area, A_{Fp}, is identical to the exposed area A_F, but for a crib fire the projected area is given as

$$A_{Fp} = L_s^2 + 4L_s bN; \qquad \text{for a square footprint crib, or}$$

$$A_{Fp} = L_i L_j + 2\left(L_i + L_j\right)bN; \qquad \text{for a rectangular footprint crib.} \qquad (2.30)$$

The above expressions are only intended to approximate the crib area affected by the radiation feedback. This is because the external heat transfer mostly radiates to the outer sticks surface but moderately to the internal sticks. As for the flaming projected fuel area, $A_{Fp,b} = A_{Fp}$ when $\phi < 1$. Similarly to the exposed area, when $\phi \geq 1$, $A_{Fp,b}$ needs to be approximated based on how much the fuel is actually burned and will be discussed further in section 2.5.

It should be noted that while the enhancement by radiation feedback can be significant for pool fires or the case where flame spread on a horizontal surface as seen in some literatures [12, 20, 24, 33], it may appear to be minimal for crib fires or some furniture items [68]. This small effect for cribs is due to the following reasons: (1) the intensity of flaming and pyrolysis of the crib primarily comes from the internal sticks which is due to its internal radiation among sticks; relatively small amount comes from the outer sticks surface, (2) the wood crib flame can be very sooty and hence prevents the external radiation to penetrate through the thick flame and reach the crib outer surface, and (3) the crib outer surface area is a small fraction of the total wood exposed surface area in a crib.

2.4 Smoke and Flame Emissivities

To estimate the radiation feedback the emissivity of the smoke or the upper gas layer and the flame are needed. Based on a gray gas assumption the emissivity of the flame, composed of soot uniformly distributed, can be given as [69]

$$\varepsilon_f = 1 - \exp\left(-\kappa_f L_{mf}\right), \tag{2.31}$$

where κ_f is an absorption coefficient of the flame which depends on soot volume fraction, and L_{mf} is a characteristic length for the flame volume or a mean beam length which depends on the volumetric configuration and on the orientation of the flux direction[2]. Some effective absorption coefficients have been given from literature as 0.5 - 0.8 m^{-1} for wood cribs [70, 71], and 1.6 m^{-1} for large heptane pool [62]. For the cylindrical shape flame of height equal two diameters, D, radiating to the plane end

surface, the corrected (for finite optical thickness) mean beam length [72] is given as follow:

$$L_{mf} = 0.6D\,. \tag{2.32}$$

The mean beam length given above is suitable for common fuel configurations such as circular pool fires and square crib fires; however, it may be different for a fire with the short-width and long-length base. That being said, we shall use Eq. (2.32) to approximate the emissivity of the flame for all fuel configurations in this study. For pool fires, *D* is the diameter of the fuel pan; for crib fires, *D* refers to the shortest edge of the crib footprint.

The emissivity of the upper gas layer can be fundamentally estimated by the calculation code developed by Modak [73] provided the gas compositions are known. However, Quintiere and McCaffrey [68] showed that a simpler empirical approach could also give reasonable predictions for the upper gas emissivity which had a good agreement with the result from Modak's code. In this study we will employ the simpler approach for computational convenience. The gas emissivity of the upper is given as

$$\varepsilon_g = 1 - \exp\left(-\kappa_g L_{mg}\right). \tag{2.33}$$

The mean beam length, L_{mg}, for an entire uniform isothermal gas volume radiating to its entire boundary can be approximated by [72]

$$L_{mg} = \frac{0.36V_g}{A_g}, \tag{2.34}$$

where the V_g is the volume of the gray gas body and A_g is the bounding surface area. The following analysis is provided to obtain the absorption coefficient, κ_g.

The volume fraction of the soot in gas can be written as

$$X_s = \frac{\rho Y_s}{\rho_s}, \tag{2.35}$$

where ρ_s is the soot density and Y_s is the soot mass fraction. Assuming a stoichiometric condition in the flame, the volume fraction of soot in the flame can be given as

$$X_{s,f} = y_s \left[\frac{\dot{m}_F}{\dot{m}_F + \dot{m}_o} \right]_{sto} \cdot \frac{\rho_f}{\rho_s}, \text{ or} \tag{2.36}$$

$$X_{s,f} = \frac{y_s}{1+s} \cdot \frac{\rho_f}{\rho_s}, \tag{2.37}$$

where y_s is the mass yield of soot per mass of fuel burn, s is the stoichiometric mass of air to fuel ratio and ρ_f is the flame density. Consider a control volume of a compartment in Figure 2.2, we can write a conservation equation for soot mass fraction as

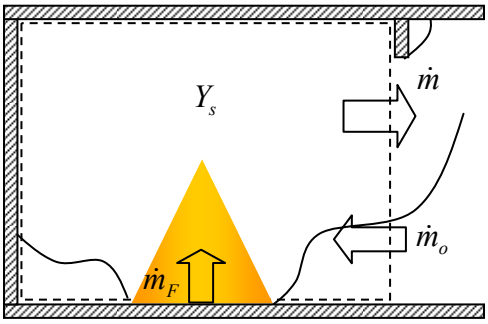

Figure 2.2 Control volume diagram for soot mass fraction in a compartment fire.

$$V \frac{d}{dt}(\rho Y_s) + \dot{m} Y_s = y_s \dot{m}_b, \tag{2.38}$$

where $\dot{m}_b$ is the burning rate. Dividing Eq. (2.33) by ($\dot{m}\rho_s$) yields

$$\frac{V}{\dot{m}} \frac{d}{dt}\left(\frac{\rho Y_s}{\rho_s} \right) + \frac{Y_s}{\rho_s} = \frac{y_s \dot{m}_b}{\dot{m}\rho_s}, \tag{2.39}$$

We wish to write from Eq. (2.39)

$$\frac{V}{\dot{m}}\frac{d}{dt}\left(\frac{\rho Y_s}{\rho_s}\right)+\frac{Y_s}{\rho_s}=\frac{y_s}{\dot{m}/\dot{m}_b\,\rho_s}\cdot\frac{1+s}{1+s}\cdot\frac{\rho_f}{\rho_f}, \tag{2.40}$$

Substituting Eq. (2.35) and (2.37) yields

$$\frac{V}{\dot{m}}\frac{d}{dt}\left(X_s\right)+\frac{X_s}{\rho}=\frac{X_{s,f}}{\rho_f}\cdot\frac{1+s}{\dot{m}/\dot{m}_b}. \tag{2.41}$$

Rearranging

$$\rho\frac{V}{\dot{m}}\frac{d}{dt}\left(X_s\right)+X_s=X_{s,f}\left(\frac{1+s}{\dot{m}/\dot{m}_b}\right)\frac{\rho}{\rho_f} \tag{2.42}$$

Assuming ideal gas and constant pressure, $\rho T=\rho_o T_o$ and $\rho T=\rho_f T_f$. We have

$$\frac{\rho_o T_o V}{T\dot{m}}\frac{d}{dt}\left(X_s\right)+X_s=X_{s,f}\left(\frac{1+s}{\dot{m}/\dot{m}_b}\right)\frac{T_f}{T}. \tag{2.43}$$

Since the spectral absorption coefficient is proportional to soot volume fraction [72] , $\kappa=CX$; we obtain

$$\frac{\rho_o T_o V}{T\dot{m}}\frac{d}{dt}\left(\kappa_g\right)+\kappa_g=\kappa_f\left(\frac{1+s}{\dot{m}/\dot{m}_b}\right)\frac{T_f}{T}. \tag{2.44}$$

For steady state, the above equation reduces to

$$\kappa_g=\kappa_f\left(\frac{1+s}{\dot{m}/\dot{m}_b}\cdot\frac{T_f}{T}\right). \tag{2.45}$$

From conservation of mass in steady state, $\dot{m} = \dot{m}_F + \dot{m}_o$, Eq. (2.3), and (2.4) we have

$$\begin{aligned} \frac{\dot{m}}{\dot{m}_b} &= \frac{s}{\phi} + 1 \qquad \text{for } \phi < 1 \\ \frac{\dot{m}}{\dot{m}_b} &= s + \phi \qquad \text{for } \phi \geq 1 \end{aligned} \tag{2.46}$$

Hence,

$$\begin{aligned} \kappa_g &= \kappa_f \frac{T_f}{T}\left(\frac{1+s}{\phi+s}\right)\phi \qquad \text{for } \phi < 1 \\ \kappa_g &= \kappa_f \frac{T_f}{T}\left(\frac{1+s}{\phi+s}\right) \qquad \text{for } \phi \geq 1 \end{aligned} \tag{2.47}$$

This gives an approximation for the quasi-steady emissivity of the upper layer gas or the smoke in the compartment fires.

2.5 Burning Area in Ventilation Limited Fires

Thomas and Bennetts [67] observed flames partially burning over a series of liquid fuel trays in their experimental study on long and wide enclosures. They reported that after ignition the flame formed itself at the front of the fuel tray closest to the vent. Later, when the fuel in the front tray was exhausted, the flame moved towards the rear of the enclosure (away from vent) to the next adjacent tray. This behavior takes place because the compartment reaches the ventilation-limited condition where the burning is controlled by the amount of supplied air. We also experienced the same phenomena in our experiment programs (Chapter 6) with distributed fuel packages all over the floor. Motivated by such observations, we offer a reason why only a certain amount of fuel area will react with the limited amount of air supply. The flame therefore burns only on this

certain area to match its needed fuel, and then "moves" when the local fuel is exhausted. The following analysis is put forth to estimate the burning area in ventilation-limited fire [74]. From Eq. (2.22) and (2.28), the expression for the fuel burning rate can be given as

$$\dot{m}_b = \dot{m}''_{F,o} A_{F,b} \frac{Y_{ox,l}}{Y_{ox,o}} + \frac{\dot{q}''_{Ext,b} A_{Fp,b}}{L}. \tag{2.48}$$

Recall Eq. (2.4) for the under ventilated condition and substitute into Eq. (2.48) we have,

$$\frac{\dot{m}_o}{s} = \dot{m}''_{F,o} A_{F,b} \frac{Y_{ox,l}}{Y_{ox,o}} + \frac{\dot{q}''_{Ext,b} A_{Fp,b}}{L}. \tag{2.49}$$

For pool fires, the exposed area is identical to the projected area ($A_{F,b} = A_{Fp,b}$), hence upon rearranging we have

$$A_{F,b} = \frac{\dot{m}_o}{s} \Bigg/ \left(\dot{m}''_{F,o} \frac{Y_{ox,l}}{Y_{ox,o}} + \frac{\dot{q}''_{Ext,b}}{L} \right). \tag{2.50}$$

If we assume that the fuel burns in a circular shape i.e. $A_{F,b} = \pi D_b^2 / 4$, we have

$$\frac{\pi D_b^2}{4} = \frac{\dot{m}_o}{s} \Bigg/ \left(\dot{m}''_{F,o} \frac{Y_{ox,l}}{Y_{ox,o}} + \frac{\dot{q}''_{Ext,b}}{L} \right). \tag{2.51}$$

Substituting the emissivities of the smoke and the flame discussed in section 2.4 with $D = D_b$ into the $\dot{q}''_{Ext,b}$ term (given by Eq. (2.28)), we can iteratively solve for the burning diameter, D_b, and hence obtain the fuel burning area for pool fires.

As for crib fires, to estimate the burning area when $\phi \geq 1$ the following assumptions are required: (1) the crib burns in a square shape footprint, (2) the number of layers, *N*, does

not change, and (3) the ratio of n/L_s is kept constant. Substituting Eq. (2.25) and (2.30) to Eq. (2.32) yields,

$$\frac{\dot{m}_o}{s} = \dot{m}''_{F,o}\left(\frac{nb^2 L_{s,b}}{L_s}\left[(1-\frac{nL_{s,b}}{L_s} + 2\frac{L_{s,b}}{b})2N + 2\frac{nL_{s,b}}{L_s} - \frac{L_{s,b}}{b} \right] \right)\frac{Y_{ox,l}}{Y_{ox,o}} + \frac{\left(L_{s,b}^2 + 4L_{s,b}bN\right)\dot{q}''_{Ext,b}}{L} \quad (2.52)$$

By substituting the emissivities with $D = L_{s,b}$ and iterating Eq. (2.52), we can obtain the stick burning length, $L_{s,b}$, which provides the fuel exposed area and flaming projected area for crib fires.

2.6 Flame Extinction Behavior

It has been shown in previous studies [33, 75] that the flame extinction behavior in compartment fires may not be sufficiently defined by a single point of one limiting parameter but by a flammability line that is based upon a critical flame temperature below which the extinction occurs. The flame temperature can be determined by the level of supplying oxygen and the temperature of the incoming air stream and hence shows the dependency of flame extinction on oxygen level and temperature in the immediate surroundings. This flame temperature is what would occur at the flame sheet by theory. The flame temperature can be given as [75]

$$c_p\left(T_f - T_l\right) = \frac{\Delta h_c - L + c_p\left(T_v - T_l\right) + \dfrac{\dot{q}_{Ext,b}}{\dot{m}_b}}{1 + \left(r/Y_{ox,l}\right)}, \quad (2.55)$$

where T_f is the flame temperature, T_l is the lower layer gas temperature, $Y_{ox,l}$ is the lower layer oxygen mass fraction, r is the stoichiometric mass of oxygen to fuel ratio, $\dot{q}_{Ext,b}$ is the net external heat feedback in the flaming area given in Eq. (2.28) and $\dot{m}_b$ is the burning rate given in Eq. (2.4). It should be noted that the subscript l in the temperature and oxygen mass fraction also denotes the near flame or locally feeding the flame condition. This equation assumes negligible flame radiation at extinction and applies generally to diffusion flame due to condensed phase burning. Given $Y_{ox,l}$ and T_l are known, the flame temperature T_f can be solved for. If T_f is less than a critical flame temperature of 1300 ºC [76], we have extinction, otherwise the flame will sustain its burning.

2.7 Experimental Evaluation for Fuel Mass Loss Rate Theory

In the previous section, a theory for describing fuel mass loss rate based on the free burning with the effect of the oxygen reduction and thermal feedback has been carefully elaborated; however, an evaluation of the theory is needed to ensure its usefulness. This concept, in fact, is not entirely new and some assessments have been done before. Quintiere and McCaffrey [68] predicted the mass loss rate of wood and plastic cribs using the same theory and the comparison with measured value showed a good agreement. Ringwelski [31] also calculated the mass loss rate of heptane pool in small-scale compartment with some success. In this section, some evaluations of the compartment mass loss rate model will be provided for the common fuel configurations, crib and pool fires. Five cases were selected to cover from over to under ventilated conditions.

The fuel mass loss rates were calculated as described in the previous sections and compared to the measured value. The calculation was based on the measured value of the local oxygen level ($Y_{ox,l}$), upper gas temperature (T), the compartment wall temperature (T_w), and the free burning rate ($\dot{m}_{F,o}$). The calculation assumed the shape factors, F_g and F_w, were unity, and the flame temperature, T_f, was 1300 ºC for estimating the absorption coefficient of the upper gas layer (Eq. (2.47)). It is convenient to also introduce now some notation used in the comparison. The dash lines represent the "flame effect" ($\dot{m}''_{F,o} A_{F,b} Y_{ox,l} / Y_{ox,o}$) and the "thermal feedback effect" ($\dot{q}_{External} / L$) which are the first and second term on the right hand side of Eq. (2.22) respectively. The dark solid line is the calculated fuel mass loss rate which is the summation of the dash lines. The free burning rate is also shown for every case.

2.7.1 Heptane Pool Fire

Experimental data for heptane pool burning in a small-scale compartment with a two-slit-wall-vent by Utiskul et al. [33] was used here. For more detail description of the experimental program, the reader is directed to the cited source. To calculate the heptane mass loss rate, the effective heat of gasification, L_{eff} = 1.4 kJ/g, was used instead of its thermodynamic value due to the presence of heat loss to the fuel container (See Appendix D)

Figure 2.3 and 2.4 show the over ventilated case and Figure 2.5 shows the under-ventilated for the pool fire. We can see that in general the calculations for heptane mass loss rate show a good agreement with the measured values. In Figure 2.3, $\phi \approx 0.12$ and

the vent is relatively large. The ventilation effect is almost at the free burning value which indicates the small reduction of the oxygen level, and the thermal feedback is also minimal because of a large amount of heat loss through vent flow. On the other hand, in Figure 2.4, $\phi \approx 0.28$; we see more effect of the ventilation (the value is relative lower than the free burning), and a more significant thermal effect due to the higher gas temperature. In Figure 2.5, the mass loss rate is less than the free burning value and the calculation also shows the same behavior. In this case, $\phi \approx 1.6$, the ventilation has a strong effect since the oxygen concentration decreased due to small amount of incoming fresh air through the small vents and the filling of the smoke; eventually the flame in this case became weak and went to complete extinction.

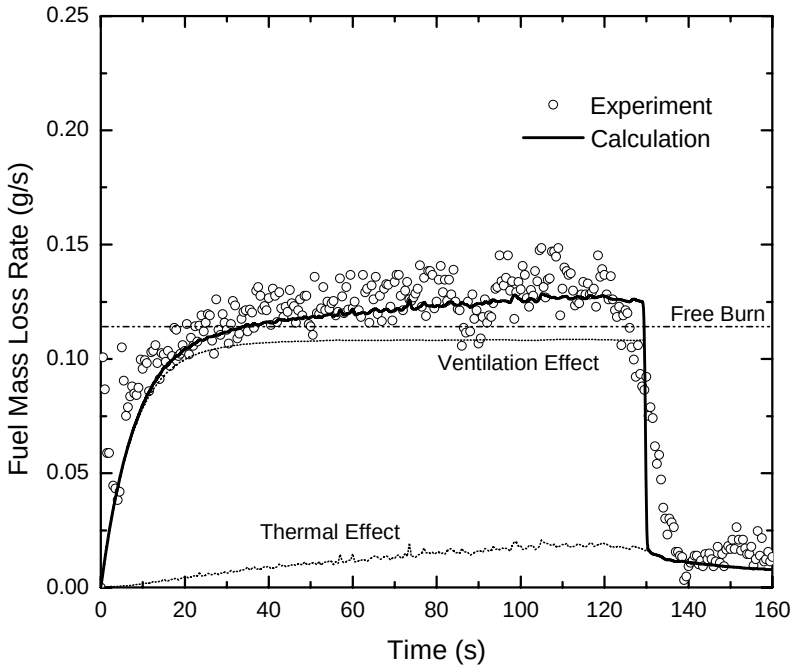

Figure 2.3 Calculated vs. measured mass loss rate for 12 cm diameter heptane pool fire with 2-slid-vent of 3 cm x 40 cm (height x width); $\phi \approx 0.12$, Free burning = 0.114 g/s.

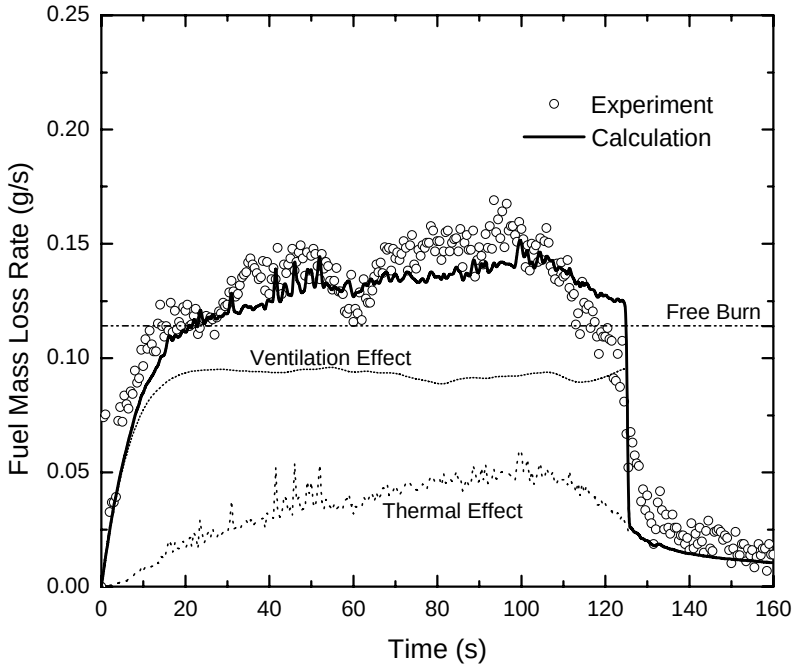

Figure 2.4 Calculated vs. measured mass loss rate for 12 cm diameter heptane pool fire with 2-slid-vent of 3 cm x 20 cm (height x width); $\phi \approx 0.28$, Free burning = 0.114 g/s.

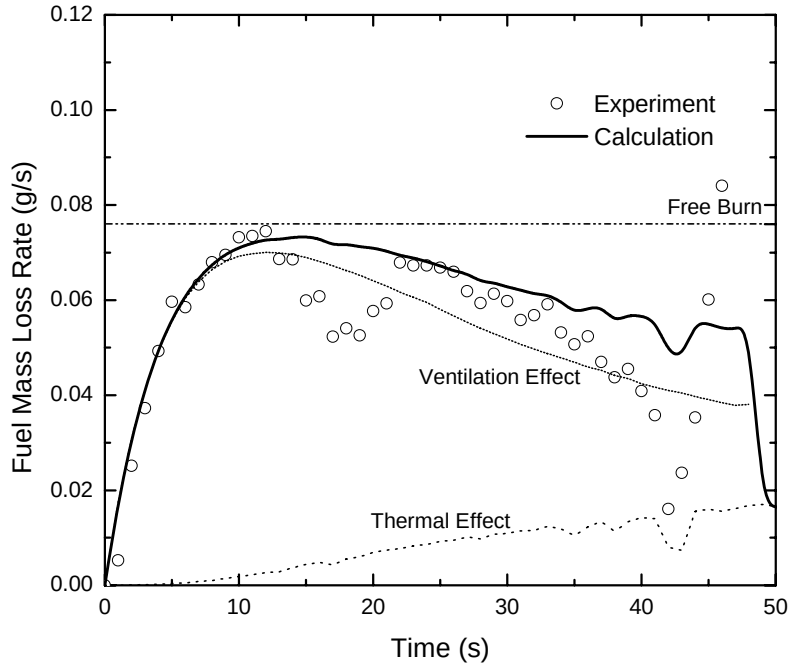

Figure 2.5 Calculated vs. measured mass loss rate for 9.5 cm diameter heptane pool fire with 2-slid-vent of 1 cm x 6 cm (height x width) ; $\phi \approx 1.6$, Free burning = 0.078 g/s.

2.7.2 Wood Crib Fire

For a wood crib fire, we used the data taken in this study. The wood cribs were burned in a small-scale compartment with a doorway-like opening. The compartment and crib configuration (referred to Crib#2) can be found in Chapter 6. The heat of gasification for wood was 2.8 kJ/g [69], and the flame absorption coefficient of wood crib used here was 0.51 m^{-1} [71]. The comparisons in Figure 2.6 and 2.7 show a good agreement with the experiment. In general the radiation feedback is believed to not contribute much on enhancing the crib mass loss rate; nevertheless, it is evident from Figure 2.6 and 2.7 that the thermal effect can be significant and should not be ignored in the prediction.

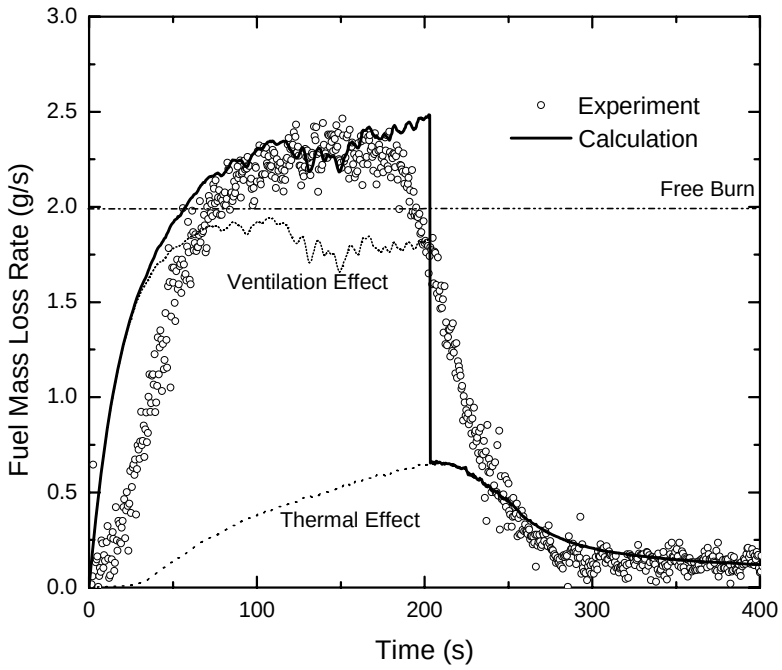

Figure 2.6 Calculated vs. measured mass loss rate for wood crib #2 with a doorway vent of 28 cm x 30 cm (width x height); $\phi \approx 0.41$, Free burning = 2.0 g/s.

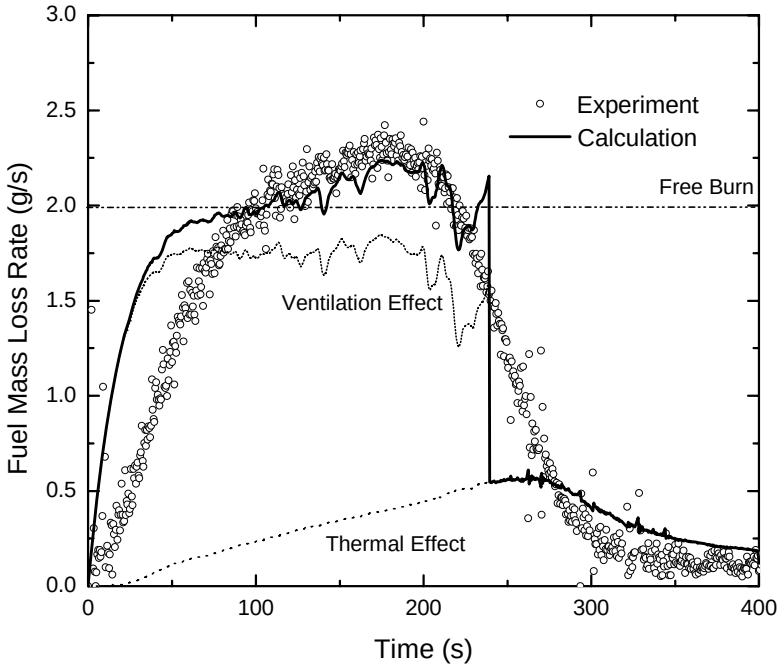

Figure 2.7 Calculated vs. measured mass loss rate for wood crib #2 with a doorway vent of 28 cm x 15 cm (width x height); $\phi \approx 0.82$, Free burning = 2.0 g/s.

2.8 Summary

This section is to summarize all the previously discussed expressions that are necessary to estimate the compartment burning rate and fuel mass loss rate.

The compartment burning rate:

$$\begin{aligned} \dot{m}_b &= \dot{m}_F \quad ;\phi < 1 \\ \dot{m}_b &= \frac{\dot{m}_o}{s} \quad ;\phi \geq 1 \end{aligned} \qquad \text{where } \phi = \frac{\dot{m}_F}{\dot{m}_o} \cdot s \tag{2.56}$$

The fuel mass loss rate:

$$\dot{m}_F = \dot{m}''_{F,o} A_{F,b} \frac{Y_{ox,l}}{Y_{ox,o}} + \frac{\dot{q}_{External}}{L} \tag{2.57}$$

$$\dot{q}_{External} = \dot{q}_{Ext,b} + \dot{q}_{Ext} \tag{2.58}$$

$$\dot{q}_{Ext,b} = F_g\left(1-\varepsilon_f\right)\varepsilon_g A_{Fp,b}\left(T^4 - T_o^4\right) + F_w\left(1-\varepsilon_f\right)\left(1-\varepsilon_g\right)A_{Fp,b}\left(T_w^4 - T_o^4\right) \tag{2.59}$$

$$\dot{q}_{Ext} = F_g\varepsilon_g\left(A_{Fp} - A_{Fp,b}\right)\left(T^4 - T_v^4\right) + F_w\left(1-\varepsilon_g\right)\left(A_{Fp} - A_{Fp,b}\right)\left(T_w^4 - T_v^4\right) \tag{2.60}$$

Free Burning Rate per unit area of fuel:

$$\dot{m}''_{F,o} = \dot{m}''_{F,\max}\left(1 - e^{-\kappa_f L_f}\right) \qquad \text{for Pool Fire} \tag{2.61}$$

$$\frac{\dot{m}''_{F,o}}{C_w b^{-1/2}} = 0.968\left(1 - \exp\left(-\frac{(sb)^{1/2} A_{C,o}}{0.02 A_F}\right)\right) \qquad \text{for Crib Fire} \tag{2.62}$$

Flame and Smoke Emissivity:

$$\varepsilon_f = 1 - \exp\left(-\kappa_f L_{mf}\right) \tag{2.63}$$

$$\varepsilon_g = 1 - \exp\left(-\kappa_g L_{mg}\right) \tag{2.64}$$

Smoke absorption coefficient:

$$\frac{\rho_o T_o V}{T\dot{m}}\frac{d}{dt}\left(\kappa_g\right) + \kappa_g = \kappa_f\left(\frac{1+s}{\dot{m}/\dot{m}_b}\right)\frac{T_f}{T} \qquad \text{for transient} \tag{3.65}$$

$$\kappa_g = \kappa_f \frac{T_f}{T}\left(\frac{1+s}{\phi+s}\right)\phi \qquad \text{for } \phi < 1$$

$$\kappa_g = \kappa_f \frac{T_f}{T}\left(\frac{1+s}{\phi+s}\right) \qquad \text{for } \phi \geq 1 \qquad \text{for quasi-steady} \tag{3.66}$$

2.9 Conclusion

The distinctive descriptions for the compartment burning rate and the fuel mass loss rate and their relationship have been provided in this chapter. The effect of

enclosures on burning has been discussed in terms of the enhancement by the thermal feedback as well as the diminishment by the reduction of oxygen level in the incoming stream. We have also addressed the applications of the fuel mass loss rate model and the burning area in ventilation-limited on pool and crib fires. A convenient approach to estimate the smoke emissivity as a function of the global equivalence ratio has been provided. A global flame extinction criterion has also been presented. Finally, the fuel mass loss rate model has been evaluated with small-scale heptane and wood crib experiments in over and under ventilated condition, and the comparison shows a very good agreement.

Chapter 3

Near Vent Mixing Phenomenon in Compartment Fires

3.1 Introduction

In compartment fires generally there is a distinct interface between the upper layer (hot gases or smoke) and the lower layer (cold gas or incoming air feeding the flame) because of buoyancy. This interface can be very close to the floor depending mainly on the fire size and the opening size. However, the mass transport or *mixing* between the two layers does occur [65]. The fire plume that entrains cold gas in the lower layer due to buoyant effects is a primary mass transport from the lower layer to the upper layer. Secondary, but still significant, mixing processes can occur in compartment fires due to 1) a cold flow injected into the smoke layer that is basically the inverse of the hot fire plume penetrating the upper layer, 2) wall flows [77] caused by local buoyant effects, and 3) near opening mixing associated with the cold incoming air flow entraining the hot gas in the smoke layer and diffuses downward into the lower layer. These mixing phenomena can affect the sharp distinction between stratified compartment layers and even force a well-mixed gas condition in the compartment. Similar mixing also occurs as a hot jet emerges from an opening into another room impinging upon its ceiling. These near vent mixing phenomena are illustrated in Figure 3.1.

Since there is some mass entrained from the upper layer, the lower layer gas can be contaminated by the combustion products which will increase the lower gas

temperature and decrease the oxygen concentration to be less than that of the ambient air (21% by volume). The reduction in oxygen level then causes the ventilation effect on the fuel mass loss rate as described in Chapter 2. This chapter will provide some review of the past studies regarding mixing phenomena as well, and will propose a new mixing correlation based on experimental data. Our study will be restricted to the mixing near vent that associates with the incoming flow only; the wall flow and forced injected cold flow in the upper layer are not considered here.

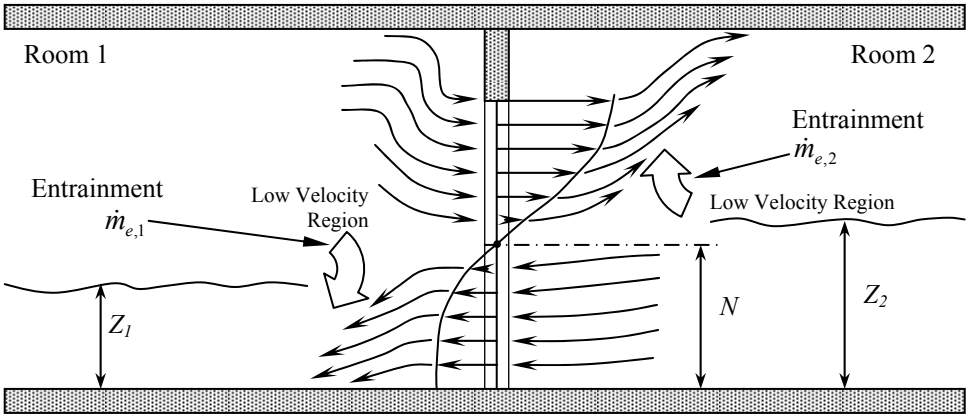

Figure 3.1 Schematic of Near Vent Mixing

3.2 Past works for near opening mixing phenomenon

A method of characterizing the near vent mixing behavior has not been well established; however, some investigations have been carried out. Quintiere et al [78] showed a visualization for mixing near a vent using a smoke trace technique (Figure 3.2). They also observed in their experiment mixing occurred as the cold air jet entered the doorway, expanded horizontally and descended towards the floor. McCaffrey and Quintiere [79] suggested that the flow rate of the mixed stream can be significant relative to the vent flow rate.

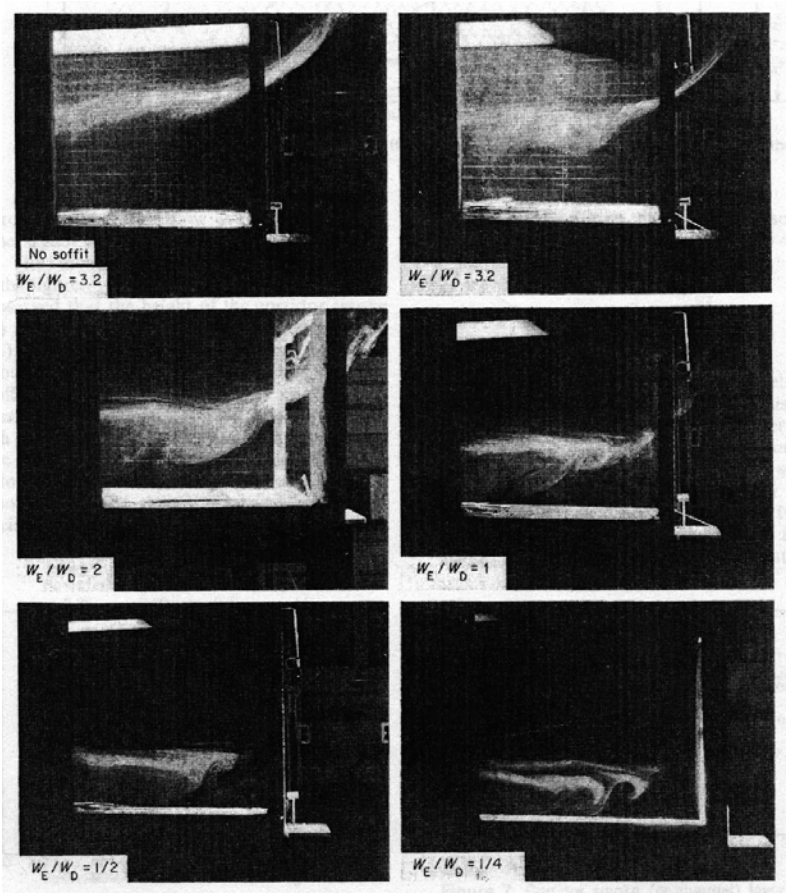

Figure 3.2 Smoke traces displaying the mixing region between cold entering air and hot combustion products

Zukoski et al. [80, 81] developed a correlation for the mixing rate based on saltwater simulation experiments. The hot gas flow was simulated by the salt water flow, and the cold air counter flow by the fresh water. By this technique they were able to control the mass flow through the opening and measure precisely the mixing or mass entrained rate in doorway flow. Zukoski's correlation was based on an assumption that the cold incoming flow through the opening would behave like a point source buoyant plume entraining the hot gas in the upper layer and then descending downward to the lower layer. A similar assumption was made for the outflow emerging from an opening

into another room impinging upon its ceiling. This is shown in Figure 3.3. BRI2002 [53], a two-zone model capable to predicting smoke transport in multi-compartments, also uses the point source plume approach with an adjusted virtual origin to describe the penetration of a cold gas through the hot layer.

From point source plume theory, the entrainment is given as

$$\dot{m}_e = \mathrm{C}_{\mathrm{plume}} \cdot \rho \sqrt{g} h^{5/2} \left(Q^*_{plume} \right)^{1/3}, \tag{3.1}$$

where h is the vertical coordinate, ρ is the density of the surrounding hot gas (entrained gas), and $\mathrm{C}_{\mathrm{plume}}$ is a constant for the plume. Q^*_{plume} is the dimensionless driving force for the plume which in this case can be given as

$$Q^*_{plume} = \left(\frac{\rho_o - \rho}{\rho} \right) \frac{\dot{m}_{o,plume}}{\rho \sqrt{g} h^{5/2}}, \tag{3.2}$$

where $\dot{m}_{o,plume}$ iss the incoming flow, and ρ_o is the density of the incoming flow. Rearranging Eq. (3.1) and (3.2), Zukoski proposed the ratio of the entrained flow rate to the incoming door flow in the upper layer as

$$\frac{\dot{m}_e}{\dot{m}_{o,plume}} = \mathrm{C}_{\mathrm{mix}} \left(\frac{\rho_o - \rho}{\rho} \right) \left(Q^*_{plume} \right)^{-2/3}. \tag{3.3}$$

The correlation of the salt water experimental data was reasonably good for a $\mathrm{C}_{\mathrm{mix}} = 0.3$; however, Zukoski pointed out for the point source plume approach that it was illogical for two reasons. First, the plume theory was developed to describe the far field of a weakly buoyant, axisymmetric plume while the doorway plume is not axisymmetric. Secondly, the doorway incoming flow has initial momentum which is not always negligible. Despite the good correlated salt water data and the comments by Zukoski, the

point source approach also appears to be challenging to apply to the data from real compartment fire experiments. This is due to the fact that $\dot{m}_{o,plume}$ in Eq. (3.2) and (3.3) is not the total incoming flow but only the part that emerges into the hot gas layer, and may not be easily measured in a real compartment fire experiment. We shall discuss more about the point source plume approach when discussing our experimental results in section 3.4.

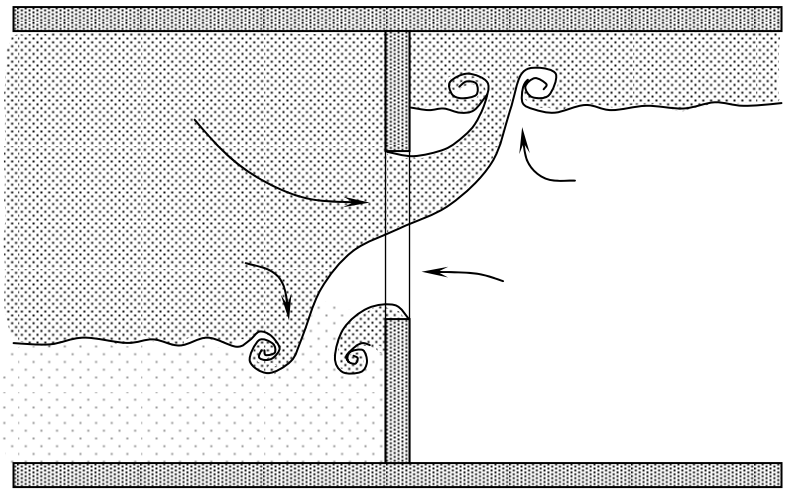

Figure 3.3 Schematic illustrating doorway/window mixing flow

Quintiere and McCaffrey [68] also developed a mixing model for their compartment crib fire experiments with some success. They treated the mixing differently from the point source plume approach by Zukoski. The concept was that the incoming cold air behaved like a jet entering the doorway with a characteristic velocity, expanding horizontally, and diffusing downward because of buoyancy. While the cold air descended, the surrounding hot gas was entrained with a velocity that is proportional to the incoming flow characteristic velocity. In this study, we also use the same basic concept of a cold air jet entering the doorway for our proposed mixing model, but we

ignore the air jet expansion effect i.e. the width of the jet approximately equals to the opening width.

3.3 Proposed Mixing Correlation

In a room fire, the mass flows through the vents are driven by the pressure difference between inside and outside of the room. The cool incoming fresh air is separated from the hot outflowing combustion product by the horizontal plane called the *neutral plane* where the pressure difference across the vent is zero and the flow reverses direction at that height. Since the layer interface or the thermal discontinuity inside the compartment is usually lower than the neutral plane for a vent with bidirectional flows, some part of the incoming fresh air will emerge into the hot gas layer as illustrated in Figure 3.4 and entrains hot gas while it diffuses downward to the lower layer. This process causes the mixing to take place, and we shall use it as a basis for the following approach.

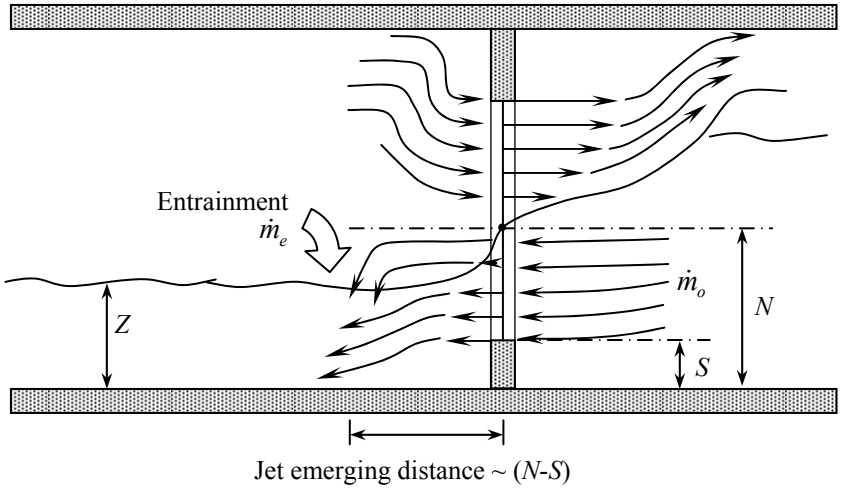

Figure 3.4 Schematic showing mixing with entering air jet approach

Considering the doorway flows in Figure 3.4, a mean velocity of the incoming air flow can be given as

$$v^* = \frac{\dot{m}_o}{\rho_o W_o (N - S)}, \tag{3.4}$$

where $\dot{m}_o$ is the total incoming air flow rate, ρ_o is the density of the incoming air, W_o is the opening width, and N is the neutral plane height. The entrainment velocity is assumed proportional to a characteristic velocity (here taken as the mean doorway velocity) v^*:

$$v_e = \mathrm{C} \cdot v^* \tag{3.5}$$

Hence we can write the net rate of mass entrained as

$$\dot{m}_e = \rho A_e v_e, \tag{3.6}$$

where ρ is the density of the gas entrained, and A_e is an effective entrainment area. As illustrated in Figure 3.4 we assume that there is some characteristic length scale by which the air jet can emerge into the hot layer; here we pick the distance between the opening sill to the neutral plane $(N - S)$ as our length scale (for a doorway which has no sill, the length scale is only the neutral plane height). A 3-D schematic to determine the effective entrainment area is shown in Figure 3.5.

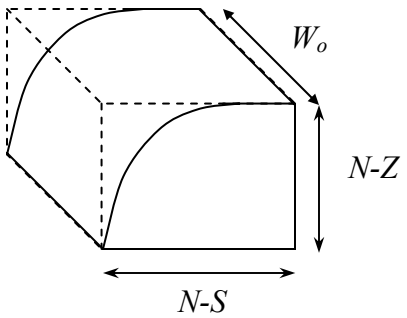

Figure 3.5 Schematic showing effective entrainment area

We write

$$A_e \approx 2\left[\left(N-S\right)+W_o\right]\cdot\left(N-Z\right), \tag{3.7}$$

where Z is the layer interface or the thermal discontinuity and S is the widow sill height. Hence, from Eq (3.4) to (3.7) we have the ratio of the mass entrained and the total incoming mass flow or the *mixing ratio* as

$$\frac{\dot{m}_e}{\dot{m}_o} \sim \frac{\rho 2v^*\left[\left(N-S\right)+W_o\right]\left(N-Z\right)}{\rho_o W_o (N-S)v^*}. \tag{3.8}$$

For constant pressure, $\rho T = \rho_o T_o$; we have

$$\frac{\dot{m}_e}{\dot{m}_o} \sim \left(\frac{T_o}{T}\right)\left(1+\frac{N-S}{W_o}\right)\left(\frac{N-Z}{N-S}\right), \tag{3.9}$$

where T and T_o are the temperature of the hot gas in the upper layer and the incoming air flow respectively. Hence, we wish to obtain a correlation for the mixing ratio empirically in the form of Eq. (3.9).

3.4 Experiments for Mixing Correlation

An experimental program was arranged to establish the correlation for the mixing ratio at the quasi-steady state. A brief description on experimental setup and measurement methods will be provided here; however, the reader is directed to Chapter 6 for a more detail discussion on instrumentation and measurement techniques.

3.4.1 Experimental Setup and Measurements

The compartment size was 40x40x120 cm (height x width x depth). The opening was a single wall vent, as a doorway or window. To be able to better define the fuel mass supply rate, a propane gas burner was used instead of the real fuels such as liquid pools or wood crib. The burner with the diameter of 17 cm was filled with gravel to uniformly distribute the propane gas and can provide the energy release rate of up to 11 kW. By adjusting the width of the opening, the ventilation conditions ranged between over to under ventilated. The effect of the fire location on the mixing was also considered. This is done by placing the burner either near or far from the opening. Figure 3.6 shows the layouts of the compartment and measurement apparatus.

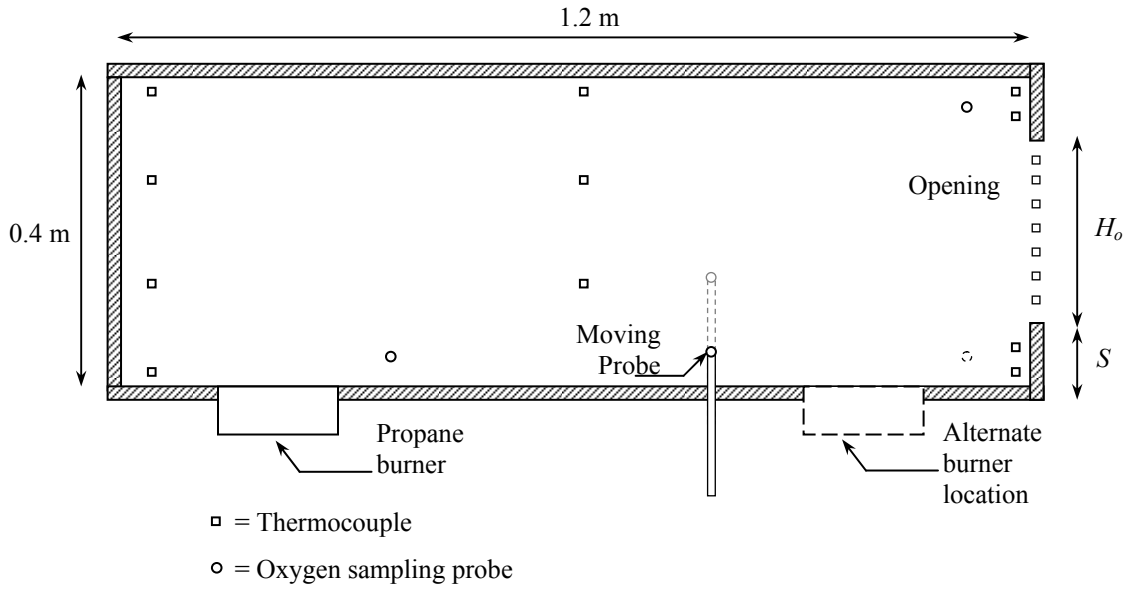

Figure 3.6 Compartment configuration and measurement layout

The gas temperatures were measured using K-type thermocouples located across the opening, the center of the compartment and near the back wall. Two stationary gas sampling probes for measuring oxygen mole fraction were located in the lower layer and

the upper layer. However, the vertical profiles for oxygen and temperature could also be determined by using a movable probe attached to a traverse which traveled vertically to collect the gas for oxygen concentration and temperature measurements at the selected elevations. Usually the moving probe remained at each location for 20 – 30 sec, and the time was recorded whenever the probe was moved. To ensure the measurements were perform at a steady state with consistency in every test, before we started to use the moving probe, we waited at least 5 minutes after a new fire setting, or until the oxygen levels read at a fixed point became steady. The experiment ended when we had collected enough data for the profile (usually from the floor to 2 cm below ceiling).

The neutral plan height was determined for each test by observing the flow reversal of a smoke trace produced by incense sticks when moved vertically at the opening. The layer interface was also determined by the same smoke trace method. Here, the incense smoke was released in side the compartment and the flow reversed was observed. The temperature and oxygen profiles were also used to support the observed measurement for the layer interface.

3.4.2 Results

Shown in Figure 3.7, an image was captured near the opening to portray the mixing phenomena in our experiment. Titanium tetrachloride was used to seed the incoming flow near the neutral plane together with a illuminated light source to produce the flow pattern images.

The experimental results from a typical test are shown in Figure 3.8. The gas temperatures and oxygen concentrations from stationary probes are presented with their time history. The vertical profiles for oxygen and temperature are also shown. Each plot on these profiles is the mean value obtained by averaging the readings over time at each selected elevation. Generally the oxygen profile showed a more noticeable location of the layer interface than the temperature profile did.

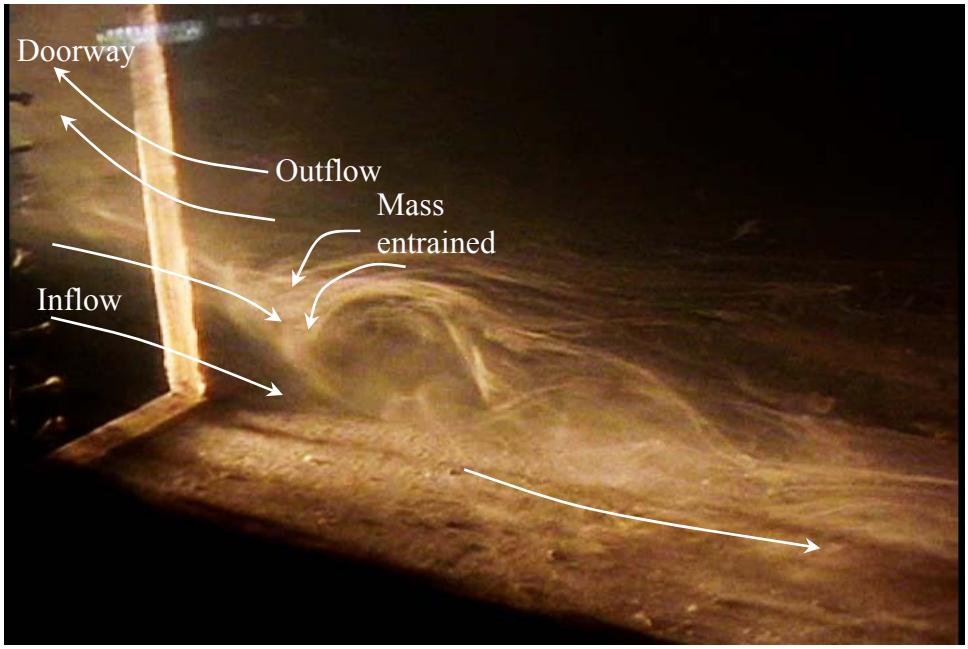

Figure 3.7 Image capturing doorway mixing phenomena

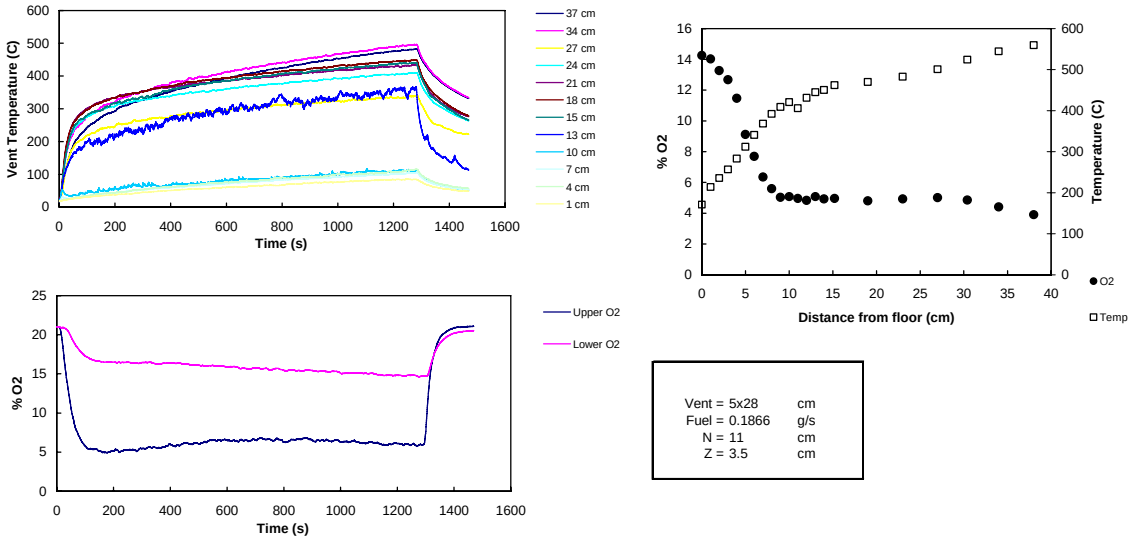

Figure 3.8 Typical experimental results

Since our interest was the quasi-steady results, a mean value to represent the oxygen concentrations in lower and upper and the hot gas temperature must be determined. For consistency purposes, a method to define the mean value for oxygen was used in every test as follows:

As observed from the oxygen concentration results, the profiles along the vertical direction were relatively linear, although the oxygen in the lower layer was typically less uniform than that in the upper layer. Two linear curve fits were superimposed on the oxygen profile plots in the upper and lower layer. For the lower layer, the oxygen data measured between the observed layer interface to the floor were used for linear fit, while for the upper layer the data between the observed neutral plan and the ceiling were considered. The mean value to represent the oxygen level in the corresponding layer was picked at the middle of each linear curve fit (arithmetic average). This is shown in Figure 3.9. It should be noted that the oxygen readings from the stationary probes were not used

to determined the mean value; however, they were used to confirm the measurement from the moving probe at the same particular height, and to ensure the experiment had reached a nearly steady state.

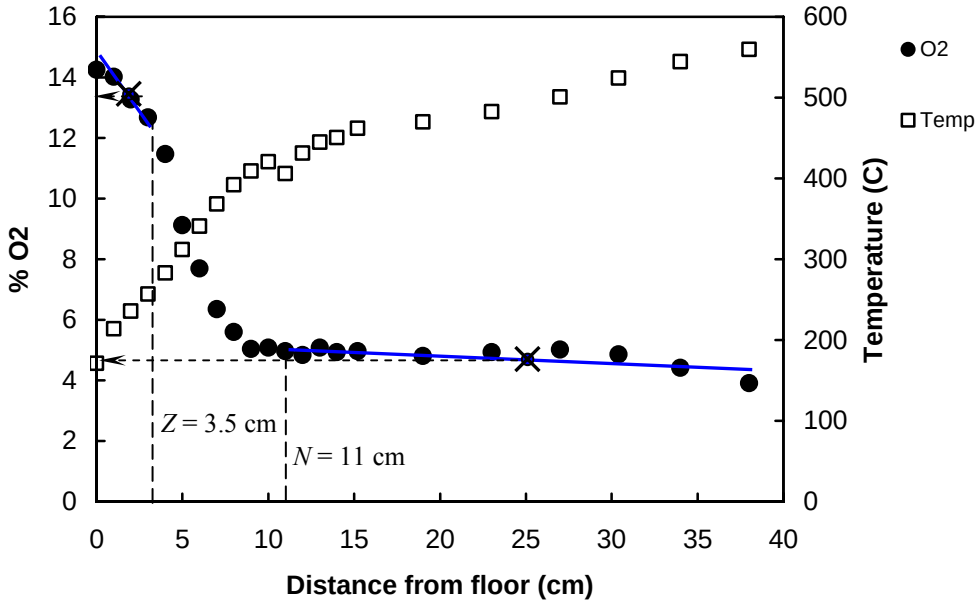

Figure 3.9 Defining the spatial-mean value for oxygen concentration in upper and lower layer

As for the gas temperature, the mean value was the average of the readings from the thermocouple trees positioned at the vent and center of the box. Only the thermocouples located above the layer interface were considered. We picked the readings to average at 10 minutes after starting the fire. This time was usually in the middle of the moving probe measurement (half way between the compartment floor and ceiling).

Last but not least, the mass entrainment rate ratio ($\dot{m}_e/\dot{m}_o$) needed to be determined. It was not measured directly, but it could be accurately estimated from the oxygen concentration measurements as follow:

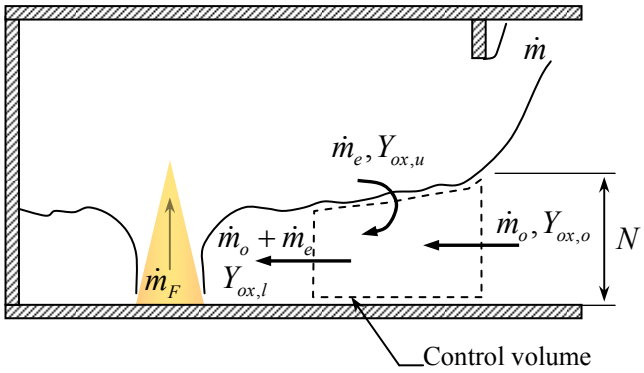

Figure 3.10 Schematic illustrating control volume to determine $\dot{m}_e/\dot{m}_o$

From the control volume shown in Figure 3.10 we can write a steady state conservation of oxygen as

$$\dot{m}_o Y_{ox,o} + \dot{m}_e Y_{ox,u} = (\dot{m}_e + \dot{m}_o) Y_{ox,l}, \tag{3.10}$$

where $Y_{ox,u}$, $Y_{ox,l}$, and $Y_{ox,o}$ are the oxygen mass fraction measured in the upper layer, the lower layer, and the ambient air (0.233) respectively. Upon rearranging, we have

$$Y_{ox,l} = \frac{Y_{ox,o} + (\dot{m}_e/\dot{m}_o) Y_{ox,u}}{1 + (\dot{m}_e/\dot{m}_o)}, \text{ or} \tag{3.11}$$

$$\frac{\dot{m}_e}{\dot{m}_o} = \frac{Y_{ox,o} - Y_{ox,l}}{Y_{ox,l} - Y_{ox,u}}. \tag{3.12}$$

Hence, based on the measurement for oxygen concentration in the upper and the lower layers we could now determine the mixing ratio. It should be noted that the mixing ratio can also be determined from the conservation of energy equation (using the temperature in the lower and upper layer); however, we chose not to do so since the temperature profile was less distinct and not as uniform through out the height. Hence, using the temperature would result in less accuracy than using the oxygen concentration.

The data from every test in our experimental program were processed the same way as described previously. In total there are 37 tests and the summary of the results was shown in Table 3.1.

Table 3.1 Result summary for mixing experimental program

Test	Vent Geometry [m]			$\dot{m}_F$ [g/s] Fuel supplied rate	Measurement				
	W_o Opening width	H_o Opening height	S Sill height		N [m] Neutral plane height	Z [m] Smoke Layer height	T [K] Average Gas temperature	$X_{ox,u}$ Average upper layer O_2 conc.	$X_{ox,l}$ Average lower layer O_2 conc.
1	0.10	0.28	0	0.2488	0.110	0.100	713	0.0870	0.1788
2	0.15	0.28	0	0.1244	0.140	0.120	574	0.1583	0.1987
3	0.15	0.28	0	0.1866	0.125	0.100	664	0.1412	0.1969
4	0.15	0.28	0	0.0746	0.150	0.120	479	0.1760	0.2025
5	0.10	0.28	0	0.1866	0.135	0.100	674	0.1190	0.1888
6	0.15	0.28	0	0.2488	0.125	0.090	672	0.1190	0.1978
7	0.15	0.28	0	0.1244	0.150	0.100	567	0.1666	0.1994
8	0.05	0.28	0	0.0746	0.120	0.080	583	0.1455	0.1852
9	0.10	0.28	0	0.1244	0.135	0.090	613	0.1486	0.1889
10	0.15	0.28	0	0.2488	0.135	0.090	711	0.1442	0.1995
11	0.15	0.28	0	0.1866	0.135	0.085	644	0.1521	0.1943
12	0.10	0.28	0	0.0746	0.135	0.085	504	0.1694	0.1984
13	0.15	0.20	0	0.1866	0.100	0.060	617	0.1258	0.1967
14	0.05	0.28	0	0.0746	0.120	0.060	527	0.1365	0.1722
15	0.05	0.28	0	0.1244	0.120	0.050	672	0.0955	0.1547
16	0.05	0.28	0	0.1866	0.115	0.045	807	0.0045	0.1220
17	0.05	0.28	0	0.1244	0.120	0.045	606	0.1082	0.1506
18	0.03	0.28	0	0.1244	0.115	0.040	674	0.0844	0.1435
19	0.03	0.28	0	0.1866	0.115	0.040	725	0.0349	0.1164
20	0.05	0.28	0	0.1866	0.110	0.035	681	0.0652	0.1402
21	0.03	0.28	0	0.1244	0.100	0.030	636	0.0470	0.1189
22	0.03	0.28	0	0.1866	0.100	0.030	619	0.0240	0.1111
23	0.03	0.28	0	0.2488	0.100	0.030	719	0.0101	0.107
24	0.05	0.28	0	0.2488	0.105	0.025	825	0.0327	0.133
25	0.03	0.28	0	0.2488	0.090	0.020	643	0.0247	0.1133
26	0.05	0.28	0	0.2488	0.115	0.025	697	0.0043	0.0982
27	0.15	0.21	0.07	0.1244	0.170	0.090	609	0.1522	0.1858
28	0.15	0.21	0.07	0.2488	0.160	0.085	777	0.1158	0.1781
29	0.10	0.21	0.07	0.1866	0.150	0.070	745	0.1038	0.1650
30	0.10	0.21	0.07	0.2488	0.150	0.070	827	0.0803	0.1512
31	0.10	0.21	0.07	0.1244	0.160	0.070	644	0.1294	0.1709
32	0.15	0.21	0.07	0.1866	0.160	0.070	699	0.1324	0.1780
33	0.12	0.14	0.14	0.1866	0.190	0.090	777	0.0634	0.1272
34	0.12	0.14	0.14	0.2488	0.180	0.100	838	0.0171	0.1019
35	0.09	0.14	0.14	0.1244	0.190	0.085	713	0.0586	0.1238
36	0.08	0.14	0.14	0.1866	0.180	0.090	872	0.0159	0.0954
37	0.12	0.14	0.14	0.1244	0.190	0.070	683	0.1013	0.1486

3.5 Analysis and Discussion on Experimental Results

Having obtained the experimental data as described in the previous section, we present here the application of those data to our proposed mixing correlation, referred as the *entering jet* approach, as well as the correlation given by Zukoski [80], the *point source plume* approach.

3.5.1 Oxygen Depletion in Compartment Fires

Evidence to show the significance of mixing phenomena is that the oxygen level in the lower layer can actually be less than that in the ambient air. To show this, in Figure 3.11, the mean values of the lower layer oxygen concentration were plotted against the ventilation factor, a dimensionless variable representing the ratio of air to fuel mass flow[33] or the inverse equivalence ratio. It can be seen that the lower layer oxygen indeed decreases from its ambient value as the ventilation factor is decreased. This, therefore, confirms the existence of the mixing phenomena.

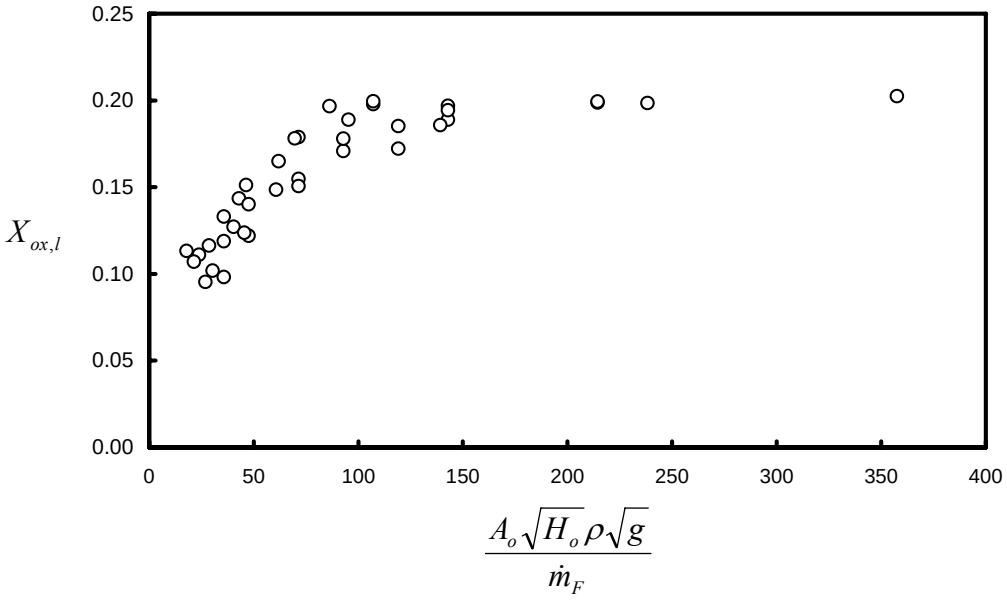

Figure 3.11 Measured oxygen fraction in the controlled-fuel-mass-supply experiments

3.5.2 Mixing Correlation: Entering Air Jet Approach

We now proceed with our discussion on the analysis on the *entering-jet* correlation. Shown in Figure 3.12, the mixing ratio, calculated from Eq. (3.12) using the mean oxygen concentrations in the lower and upper layer, was plotted with the parameter presented in the right hand side of Eq. (3.9). The data were shown for doorways (open symbols) and windows (filled symbols). It appears that the mixing ratios are surprisingly well correlated with Eq. (3.9) despite the questionable assumptions on the distance the cold air flow through the hot layer and the effective entrainment area. The correlation exhibits a linear relationship up to an apparent asymptote for the mixing ratio of 1.28. This can be put into an expression for the mixing ratio as follow:

$$\begin{aligned} \frac{\dot{m}_e}{\dot{m}_o} &= 1.14\left(\frac{T_o}{T}\right)\left(1+\frac{N-S}{W_o}\right)\left(\frac{N-Z}{N-S}\right) \quad \text{for } \left(\frac{T_o}{T}\right)\left(1+\frac{N-S}{W_o}\right)\left(\frac{N-Z}{N-S}\right) < 1.1 \\ \frac{\dot{m}_e}{\dot{m}_o} &= 1.28 \qquad\qquad\qquad\qquad\qquad\qquad \text{for } \left(\frac{T_o}{T}\right)\left(1+\frac{N-S}{W_o}\right)\left(\frac{N-Z}{N-S}\right) \geq 1.1 \end{aligned} \tag{3.13}$$

Eq. (3.13) is reasonable because we would expect more mixing when the layer interface is low and the opening is small (small value of Z and W_o). But it is not obvious to directly see the buoyancy effect ($\Delta T / T_o$). As the layer interface and the neutral height depends on the gas temperature (described later in Chapter 4), it was possible to express Z and N in terms of T_o / T. This suggests that the correlation proposed here shows the effect of opening geometry, while the effect of buoyancy is embedded in the layer interface and the neutral plane.

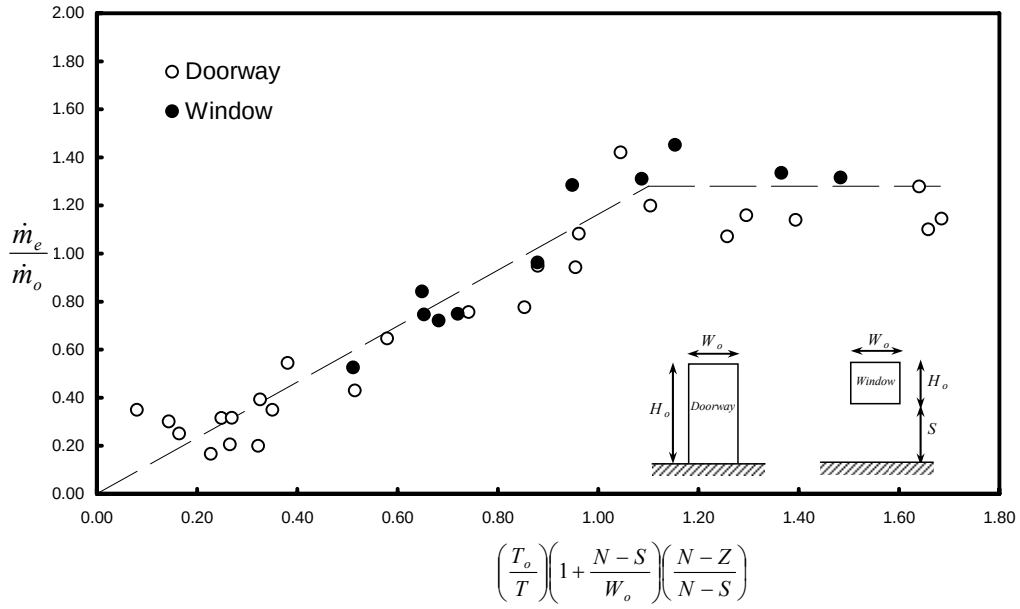

Figure 3.12 Near vent mixing correlation: Entering-jet approach

3.5.3 Mixing Correlation: Plume Approach

In order to apply the *plume approach* mixing model in Eq. (3.2) and (3.3) to our experimental data, the estimation for some parameters based on the available measurements was needed.

As mentioned previously,

$$\dot{m}_{o,plume} = \dot{m}_{o,u} \tag{3.14}$$

where $\dot{m}_{o,u}$ is the incoming air flow that emerges into the hot gas layer. From Karlsson and Quintiere [2] we have

$$\dot{m}_{o,u} = \frac{2}{3} C_d W_o \sqrt{2g}\left(\frac{T-T_o}{T}\right)^{1/2} (N-y)^{3/2}, \tag{3.15}$$

where $y = Z$ for $Z > S$, $y = S$ for $Z \le S$, and C_d is the flow coefficient.

Using the measured neutral plane height, layer interface and upper layer gas temperature, $\dot{m}_{o,u}$ can be estimated. Next, mixing ratio on the left hand side of Eq (3.3), $\dot{m}_e/\dot{m}_{o,u}$, can be determined from

$$\frac{\dot{m}_e}{\dot{m}_{o,u}} = \frac{\dot{m}_e}{\dot{m}_o} \cdot \frac{\dot{m}_o}{\dot{m}_{o,u}}, \tag{3.18}$$

where $\dot{m}_e/\dot{m}_o$ was calculated from Eq. (3.12) using the oxygen measurement and the total incoming air flow rate ($\dot{m}_o$) is given from mass conservation as

$$\dot{m}_o = \dot{m} - \dot{m}_F, \tag{3.19}$$

where $\dot{m}$ is the total outflow from the compartment and $\dot{m}_F$ is the fuel (propane) supply rate. Substituting the outflow expression from Karlsson and Quintiere [2] yields

$$\dot{m}_o = \left(\frac{2}{3} \mathrm{C_d} W_o \sqrt{2g} \left(\frac{T - T_o}{T} \right)^{1/2} \left(H_o + S - N \right)^{3/2} \right) - \dot{m}_F, \tag{3.20}$$

where H_o is the height of the opening. Rewrite Eq. (3.2) and (3.3) as

$$Q^*_{plume} = \left(\frac{T - T_o}{T_o} \right) \frac{\dot{m}_{o,u}}{\rho \sqrt{g} h^{5/2}}, \tag{3.21}$$

$$\frac{\dot{m}_e}{\dot{m}_{o,u}} = \mathrm{C_{mix}} \left(\frac{T - T_o}{T_o} \right) \left(Q^*_{plume} \right)^{-2/3}. \tag{3.22}$$

In Figure 3.13, the ratio of $\dot{m}_e/\dot{m}_{o,u}$ from measurement is plotted against $(\Delta T)/T_o \left(Q^*_{plume} \right)^{-2/3}$. The mixing correlation from salt-water modeling suggested by Zukoski [80, 81] and used in BRI2002 by Tanaka [53] are also shown. The data seemed to be scattered and did not correlate well in this manner. Also the data shows the higher

mixing ratio than the correlation used by Zukoski and Tanaka. This may be due to that the estimation for $\dot{m}_e/\dot{m}_{o,u}$ was not accurate enough since only 5% error in the measure neutral plane (*N*) or layer interface (*Z*) would cause almost 25% change in $\dot{m}_e/\dot{m}_{o,u}$.

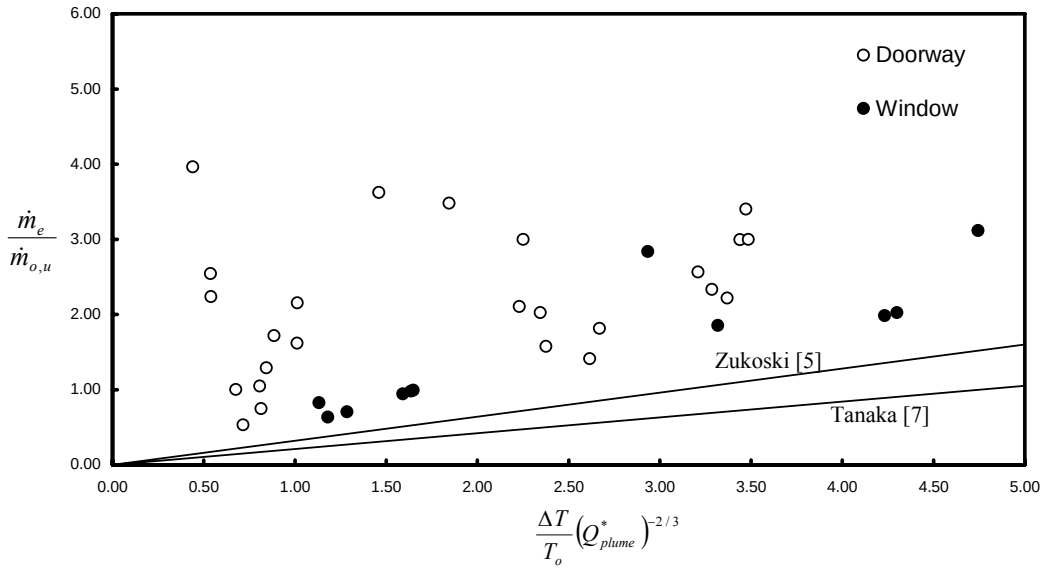

Figure 3.13 Mixing correlation: Plume approach

Therefore, we attempted to plot $\dot{m}_e/\dot{m}_o$ with $(\Delta T)/T_o\left(Q^*_{plume}\right)^{-2/3}$ instead and this is shown in Figure 3.14 where the data appeared to correlate better. Perhaps, had we been able to accurately measure $\dot{m}_e/\dot{m}_{o,u}$, the data might have correlated better. From Figure 3.14, linear coefficient, C_{mix}, for our data was found to be 0.46. The data seemed to correlate well for small $(\Delta T)/T_o\left(Q^*_{plume}\right)^{-2/3}$, while became slightly scattered for larger $(\Delta T)/T_o\left(Q^*_{plume}\right)^{-2/3}$. The mixing also reached a constant value when the layer interface was closed to the floor as seen in the entering-jet approach. Hence, the expression for the mixing ratio for the point source approach can be written as

$$\frac{\dot{m}_e}{\dot{m}_o} = 0.46\left(\frac{T - T_o}{T_o}\right)\left(Q^*_{plume}\right)^{-2/3}, \quad \text{for } \left(\frac{T - T_o}{T_o}\right)\left(Q^*_{plume}\right)^{-2/3} < 2.75$$
$$\frac{\dot{m}_e}{\dot{m}_o} = 1.28 \quad , \quad \text{for } \left(\frac{T - T_o}{T_o}\right)\left(Q^*_{plume}\right)^{-2/3} \geq 2.75 \tag{3.23}$$

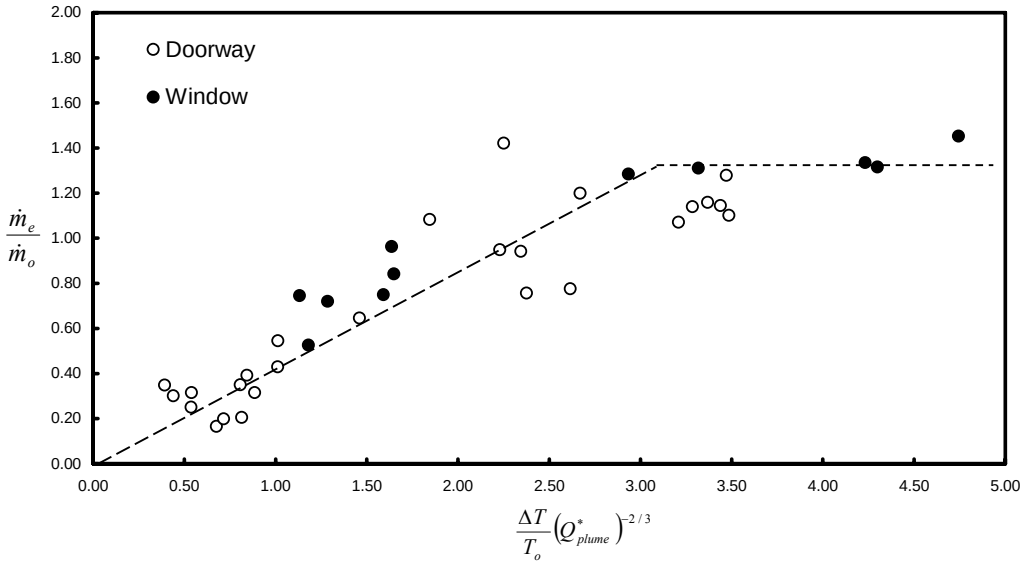

Figure 3.14 Alternative mixing correlation: Plume approach based on total flow

3.5.4 Mixing for Well-mixed Compartment Fires: Application to a Single Zone Model

A well-mixed condition in the compartment fire is defined when the layer interface or the smoke is close to the floor. The opening geometry and fire size plays an important role on the location of the layer interface as described later in Chapter 4 where some criteria for the well-mixed condition will be given. When this condition prevails, the properties of the gas in the compartment are said to be uniform and a single zone model can be effectively used to predict the gas temperature and species in the compartment. Nevertheless, in reality a sharp gradient of the oxygen concentration still exists near the floor. In other words, the oxygen that is feeding the flame is not the same as in the bulk smoke layer even though the smoke layer is close to the floor. In order to

overcome this, the mixing can be used as a mechanism to help defining the local oxygen feeding the flame in a single zone model.

We choose to use a constant maximum value of 1.28 for the mixing ratio as suggested by Eq. (3.13) for the well-mixed compartment fires with a single-wall-vent configuration. This limit would apply when the layer is close to the floor. For comparative purposes, although not the same case, an empirical mixing for a small-scale compartment with a two-slid-vents was given by Utiskul and Quintiere [74]. This case has a thin slit neat the floor for inlet air. The maximum constant value of $\dot{m}_e/\dot{m}_o$ was found to be 3.2 in their low-ventilation experimental study. The higher value is likely due to the slit having a higher velocity than a door or window.

3.5 Conclusion

An experimental study on near vent mixing phenomena has been presented. Two approaches for the mixing correlations, *entering-jet* approach and *point-source plume* approach, were described and applied to the current experimental data. The data correlated reasonably well by both methods, although the entering-jet method is in better agreement with the experimental data. The entering-jet method is also more practical to apply into a design tool such as a two zone model. A constant maximum value for the mixing in well-mixed compartment fires has been suggested for use in a single zone model. Last but not least, it is worth mentioning again that the mixing phenomena presented here are based on quasi-steady data and limited to a single-wall-vent configuration.

Chapter 4

Justification the Use of Single Zone Model

4.1 Introduction

A concept of the zone model has been around since the sixties and still be a very powerful tool to model the behavior of the room fire. There are generally two kinds of the zone models: a single-zone model and a two-zone model. Each has its own merits when applied properly. The single zone model assumes homogeneous gas with uniform properties through out the compartment. The two zone model separates the compartment gas into the upper layer where the combustion products and fire plume reside and the lower layer for the remainder gas region in which the air enters. At the early state of fire growth or the fire plume by itself contains the combustion, but is treated as a negligible volume. For the developing fire where the smoke is stratified, the two zone model is a better representation of the processes. However, a single zone model can be a suitable choice for the following conditions: 1) flashover takes place and the fire reaches its fully-developed state with a maximum involvement of the available fuel in the room, the gas temperature could be extremely high and becomes almost uniform through out the entire room. 2) The fuel area is large compared to the room floor area. The fire is therefore not localized and the model of homogeneous gas is a good representation. 3) The smoke layer is close to the floor.

In this study, we aim at examining the fully-developed fire with a major consideration on the fuel responses to the heat feedback and the oxygen reduction. The fire that of our interest is not a room with a small localized fire, but a room with fuel load such as furniture distributed all over the floor. Hence, a single zone model is our choice mainly due to the scope of our study for large fully-developed fires.

Nevertheless, criteria that can justify the validity of a single zone approach should be presented with a rational background in order to show a range of fire scenarios that fits its assumption. As mentioned before, the hypothesis for the homogeneous gas is good when the fuel area is large compared to floor and the smoke layer height is low. Cadorin [50] uses the fuel area at 25% of the total floor and the smoke layer height at 20% of the compartment height as the criteria for switching from two-zone to one-zone. However, for our purpose, that is to justify the use of the single zone model, specifying a level of smoke layer height alone may not be enough. This is because, unlike the fuel area, the smoke layer height is not an input or initial condition for fire scenario. Hence, we shall examine the smoke layer height and its controlling parameter to use as our criteria that will determine the validity of single zone approximation. A method of calculating the layer height will be presented and validated with experimental results in this chapter.

4.2 Compartment Layer Interface

An analytical model developed by Rocket [82] described the classical method of predicting the fire induced flows in a room and the *thermal discontinuity height* (here called the *smoke layer height* or the *layer interface height*) where a steep thermal gradient

separates the hot smoke layer and the lower cooler layer. As the plume is generally assumed to be a principal mechanism for transfer of mass from the lower layer to the upper layer, in his analysis the discontinuity height adjusts itself to a location where the mass rate entrained by the plume as it passes up to upper layer, equals the mass rate flowing out from the room. From the model, the effect of the plume size, the plume base location, and the sill height (in case of the window flow) to the discontinuity height has been illustrated.

In this section we shall follow the same concept as described by Rocket to examine the parameters that control the smoke layer height (Z) in dimensionless form and consequently attempt to show some generality from our result. A model to estimate the layer height is now formulated and will be validated with experimental results.

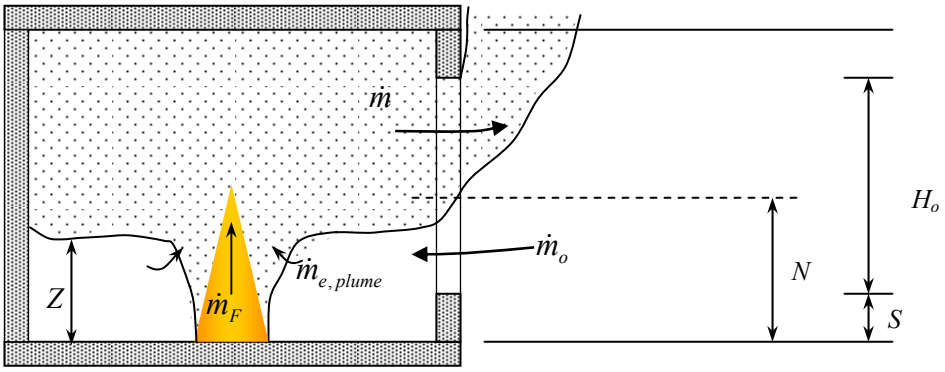

Figure 4.1 Schematic for the plume entrainment in a compartment fire

4.2.1 Smoke Layer Height Estimation

Consider a compartment with a stratified smoke layer in Figure 4.1. By assuming the fuel flow rate is small relatively to the vent flow rate and thus can be neglected, from

the conservation of mass in the compartment we have $\dot{m} = \dot{m}_o$. Hence, the concept of estimating the smoke layer height could also be based on that the total mass *inflow* through the vent is equal to the plume mass entrainment rate at the smoke layer height ($\dot{m}_o = \dot{m}_{e,plume}$). For an axisymmetric plume, the near-field entrainment rate (applicable to the flame), $\dot{m}_{e,plume}$, is given by Quintiere and Grove [83] as

$$\frac{\dot{m}_{e,plume}}{\rho_o \sqrt{gD} D^2} = 0.0565\sqrt{\Psi}\left(\frac{Z}{D}\right)^{1/2}\left(1+0.357\frac{Z}{D}\right)^2, \tag{4.1}$$

where $\Psi = \dfrac{(1-\chi_r)(\Delta h_c / s)}{c_p T_o}$,

Z is the smoke layer height, D is the diameter of the fire (the base diameter of the plume), χ_r is the radiation loss fraction, Δh_c is the heat of combustion per unit mass of fuel, s is the stoichiometric air-to-fuel mass ratio. Except for variations in χ_r, the combustion parameter, Ψ, is nearly a constant for most cases since $\Delta h_c / s = \Delta h_{ox} / 0.233$, where Δh_{ox} is the heat of combustion per unit mass of oxygen (~13 kJ/g for most fuel). Upon dividing Eq. (4.1) by $A_o\sqrt{H_o}$ where A_o is the opening area and H_o is the opening height, we have

$$\frac{\dot{m}_{e,plume}}{A_o\sqrt{H_o}\rho_o\sqrt{g}} = 0.0565\sqrt{\Psi}\left(\frac{Z}{D}\right)^{1/2}\left(1+0.357\frac{Z}{D}\right)^2\frac{D^2}{A_o}\left(\frac{D}{H_o}\right)^{1/2}.$$

We wish to write this as

$$\frac{\dot{m}_{e,plume}}{A_o\sqrt{H_o}\rho_o\sqrt{g}} = 0.0565\sqrt{\Psi}\left(\frac{Z/H_o}{D/H_o}\right)^{1/2}\left(1+0.357\frac{Z/H_o}{D/H_o}\right)^2\left(\frac{D^2}{W_o H_o}\right)\left(\frac{D}{H_o}\right)^{1/2}.$$

Upon defining

$$z^* = \frac{Z}{H_o},\ D^* = \frac{D}{H_o},\ \hat{D} = \frac{D}{W_o}, \text{ and } m_e^* = \frac{\dot{m}_{e,plume}}{A_o\sqrt{H_o}\rho_o\sqrt{g}},$$

we have the dimensionless plume entrainment rate as

$$\dot{m}_e^* = 0.0565\sqrt{\Psi}\left(\frac{z^*}{D^*}\right)^{1/2}\left(1+0.357\frac{z^*}{D^*}\right)^2\left(D^*\right)^{3/2}\hat{D} \tag{4.2}$$

Consider now the mass flow rate through the vent in a compartment with the stratified smoke layer. From Karlsson [2] the total mass inflow can be written as

$$\begin{aligned}
\dot{m}_o &= \frac{2}{3}\mathrm{C_d}W_o\rho_o\sqrt{2g\left(1-\frac{T_o}{T}\right)}\left(N-Z\right)^{1/2}\left(N+\frac{Z-S}{2}\right) \quad ;\text{for } Z > S \\
\dot{m}_o &= \frac{2}{3}\mathrm{C_d}W_o\rho_o\sqrt{2g\left(1-\frac{T_o}{T}\right)}\left(N-S\right)^{3/2} \qquad\qquad ;\text{for } Z \le S
\end{aligned} \tag{4.3}$$

where S is the window sill height and C_d is the flow coefficient taking value of 0.65. Dividing Eq. (4.3) by $A_o\sqrt{H_o}\rho_o\sqrt{g}$ yields

$$\frac{\dot{m}_o}{A_o\sqrt{H_o}\rho\sqrt{g}} = \frac{2\sqrt{2}}{3}\mathrm{C_d}\sqrt{\left(1-\frac{T_o}{T}\right)}\left(\frac{N-Z}{H_o}\right)^{1/2}\left(\frac{N}{H_o}+\frac{Z-S}{2H_o}\right);\ \text{for } \frac{Z}{H_o} > \frac{S}{H_o}$$

$$\frac{\dot{m}_o}{A_o\sqrt{H_o}\rho\sqrt{g}} = \frac{2\sqrt{2}}{3}\mathrm{C_d}\sqrt{\left(1-\frac{T_o}{T}\right)}\left(\frac{N-S}{H_o}\right)^{3/2} \qquad ;\text{for } \frac{Z}{H_o} \le \frac{S}{H_o}$$

Upon defining

$m_o^* = \dfrac{\dot{m}_o}{A_o\sqrt{H_o}\rho_o\sqrt{g}}$, $\theta = \dfrac{T_o}{T}$, and $S^* = \dfrac{S}{H_o}$, we have the dimensionless vent flow rate as

$$m_o^* = \frac{2\sqrt{2}}{3} C_d (1-\theta)^{1/2} \left(N^* - z^*\right)^{1/2} \left(N^* + \frac{z^* - S^*}{2}\right) \quad ; \text{ for } \; z^* > S^*$$
$$m_o^* = \frac{2\sqrt{2}}{3} C_d (1-\theta)^{1/2} \left(N^* - S^*\right)^{3/2} \quad ; \text{ for } \; z^* \le S^* \tag{4.4}$$

Now let the total mass inflow rate equal to the entrainment rate, $m_e^* = m_o^*$, we have

$$z^* = f(D^*, N^*, S^*, \hat{D}, \text{and } \theta) \tag{4.5}$$

Hence, for a given size of fire (D) and the opening (H_o, W_o and S), one can iteratively solve for the smoke layer height (z^*) from Eq. (4.5) if θ and N^* are known. Notice that statement in Eq. (4.5) is not completely correct since in reality the plume entrainment rate should equal to the sum of the total mass inflow rate *and* the near vent mixing (discussed in Chapter 3). However, the mixing was neglected here for simplification.

From Eq. (4.5), it can be seen accordingly that the smoke layer height does not depend on one variable but is coupled with a few parameters such as the temperature rise, neutral plane height, and opening configuration. Thus, to completely generalize and present the smoke layer height with all governing parameters may not be easy; however, with proper estimations of the temperature rise (θ) and the neutral height (N^*) some generalities may be revealed.

4.2.2 Experimental Validation

In this section the calculation of the smoke layer height is compared with the measurements taken from our compartment fire experiments with a propane gas burner. It is the same test program conducted to study the mixing behavior presented in Chapter 3.

In these tests, the propane gas burner has a constant diameter but supplied different fuel mass flow rates. The tests can be categorized into three groups based on their D^* and S^* values as follows:

Group 1: Doorway with $D^* = 0.61$ and $S^* = 0$,

Group 2: Window with $D^* = 0.81$ and $S^* = 0.333$, and

Group 3: Window with $D^* = 1.21$ and $S^* = 1$.

The gas temperature measured from the experiment ranges from 480 K to 840 K which corresponds to the dimensionless temperature (θ) of 0.35 to 0.6. As for the neutral plane, we shall assume that the neutral plan is located at the middle of the opening (see figure 4.2). This is a reasonable assumption as the measurement showed approximately the same value. Hence, the dimensionless neutral plane height is given as $N^* = S^* + 0.5$. Note for large fires we except a minimum for θ of about 0.25 and for N^* of about 0.5.

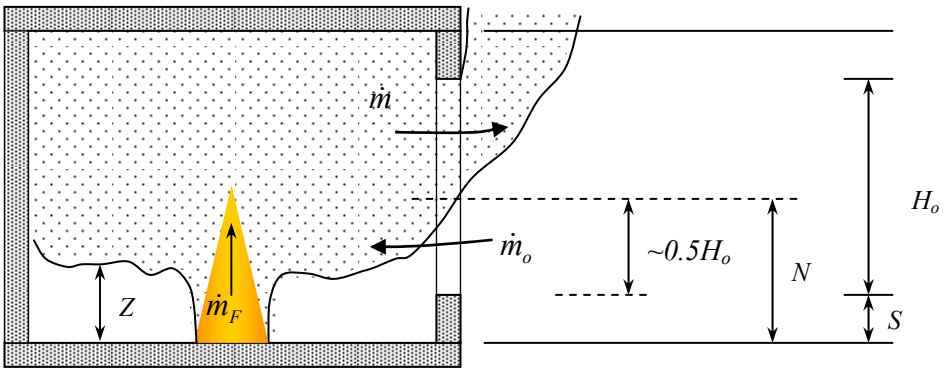

Figure 4.2 Approximation of the neutral plane location at the middle of the opening

Based on the given value of D^*, N^*, S^* and θ, the dimensionless smoke layer height (z^*) can be shown as a function of $\hat{D}$ or D/W_o. This was done by using a built-in function in Mathematica called **FindRoot** which uses the Newton-Raphson method to

numerically search for the solution of the nonlinear equation with a specified starting point.

Our interest in this chapter is to examine the location of the layer interface, z^* defined previously as Z/H_o. But it may not be the best parameter to show the relative location of the layer, especially when comparing the doorway case to the window case. This is because H_o is the opening height and is not measured from the same reference level (floor) as the smoke layer. (See Figure 4.1) Hence, we shall present our smoke layer height results in terms of Z^* which is defined as

$$Z^* = \frac{Z}{H_o + S} = \frac{z^*}{1 + S^*}. \tag{4.6}$$

Figure 4.3 shows the measured and calculated smoke layer heights from *Group 1* ($D^* = 0.61$ and $S^* = 0$) in dimensionless form, $Z^* = Z/(H_o + S)$, as a function of $\hat{D}$ or D/W_o. The dark solid line is the calculation based on a value of $\theta = 0.5$, and the dash lines show the variation of the calculation based on the range of the measured temperatures ($\theta \sim$ 0.35 to 0.6).

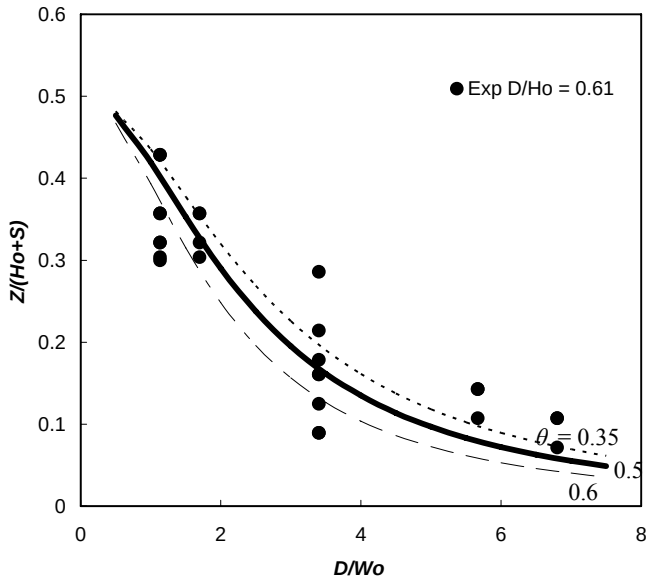

Figure 4.3 Dimensionless smoke layer height from measurement and calculation
(*Group 1*; $D/H_o = 0.61,\ S/H_o = 0$)

It can be seen from Figure 4.3 that the calculation tracks the trend of the measured data reasonably well. However, the scatter of experimental data proves that there exist some other controlling parameters which were omitted here or roughly approximated such as the neutral plane height, temperature, heat loss, fuel mass supply, and vent mixing.

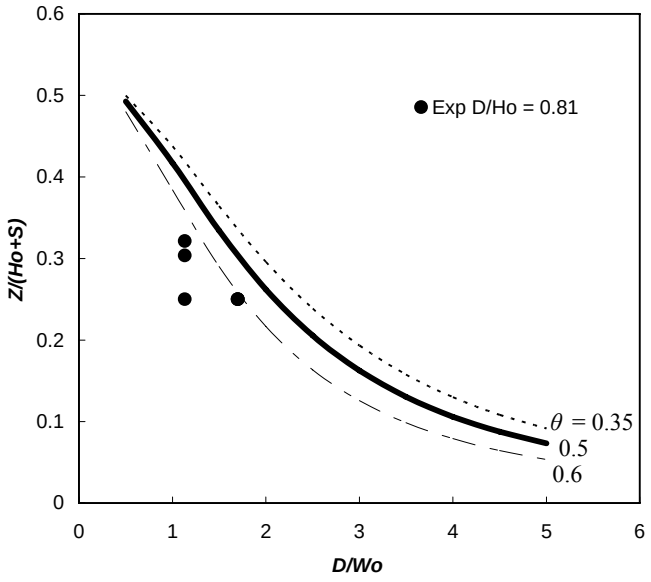

Figure 4.4 Dimensionless smoke layer height from measurement and calculation (*Group 2*; $D/H_o = 0.81,\ S/H_o = 0.33$)

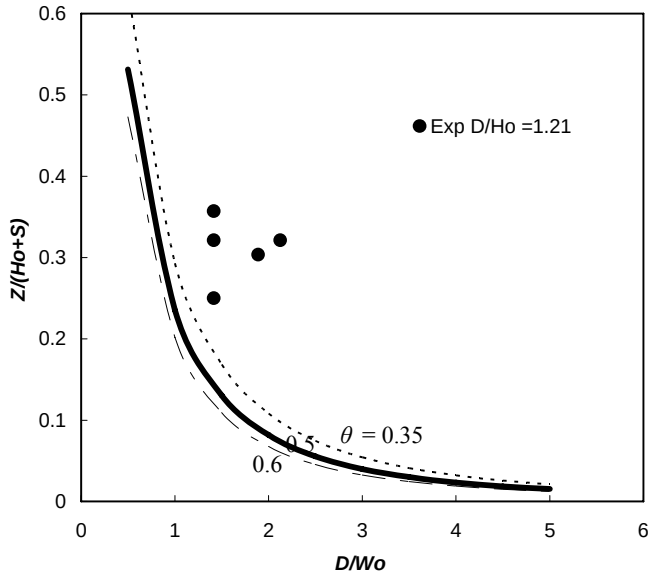

Figure 4.5 Dimensionless smoke layer height from measurement and calculation (*Group 3*; $D/H_o = 1.21,\ S/H_o = 1$)

Figure 4.4 and 4.5 show the measured value and the calculation of Z^* for *Group 2* ($D^* = 0.81$ and $S^* = 0.333$) and *Group 3* ($D^* = 1.21$ and $S^* = 1$) respectively. The

calculation seems to be overestimated but able to follow the tread of the data for *Group 2*, while for *Group 3* the calculation is underestimated. However, it is excessive to conclude that calculation fails to predict a good result since we have only limited experimental data points. In addition, a possible reason for the underestimated result in *Group 3* may be due to the fact that the mixing is neglected in the calculation. This could cause a significant effect since all the tests belonging to *Group 3* have the mixing ratio that reaches the maximum value of 1.28 (See Figure 3.12). Generally if the mixing or the inflow rate increases, the plume entrainment will balance that increment and thus result in higher level of the smoke layer. Had the mixing been included in the calculation, the prediction line would have shifted up and possibly matched the experimental data.

4.3 Layer Interface Generalization and Criteria for a Single Zone Model

We now proceed our discussion to the criteria for the smoke layer height that justify the use of a single zone model. From the previous section, we showed that it might not be possible to achieve a complete generalization for the smoke layer height but with a rational approximation for the temperature and the neutral plane height one could have a rough, but sensible, idea of where the smoke layer height would be given the size of fire and the opening. In this section we employ the method described in section 4.2 to show the layer height for a typical doorway and window.

It is worth mention here that some assumptions are made for all the prediction presented in this section as follows: 1) The neutral plan height is assumed to be at the middle of the opening height ($N^* = S^* + 0.5$), 2) the dimensionless temperature (θ) is

approximated to be 0.5, and 3) the window sill dimensionless height (S^*) is taken to range from 0.3 to 1. These assumptions are based on a typical window and doorway commonly seen in a building.

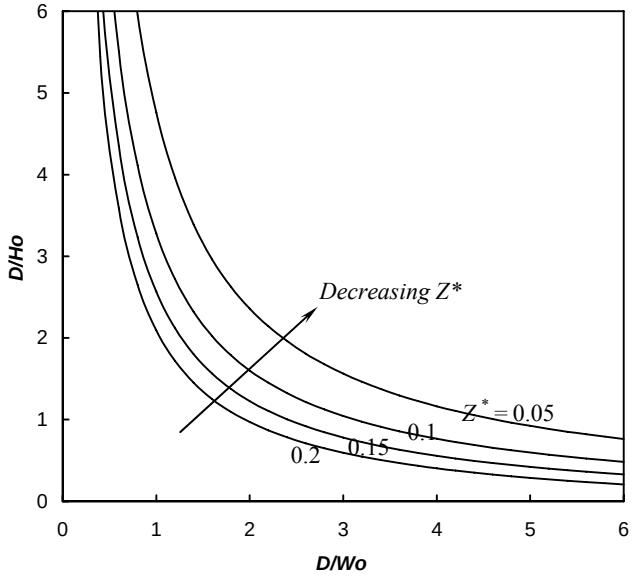

Figure 4.6 Contour of the dimensionless smoke layer height for a typical doorway.

In figure 4.6 the dimensionless smoke layer height $Z^* = Z/(H_o + S)$ is shown as a function of D/H_o and D/W_o for a typical doorway. Figure 4.7 and 4.8 show for typical windows with the sill height S^* of 0.3 and 1 respectively. From these contours we can see that for a given size of the opening the smoke layer height decreases as the fire size increases. On the other hand, for a given size of fire, the smoke layer height decreases as the width or the height of the opening decreases.

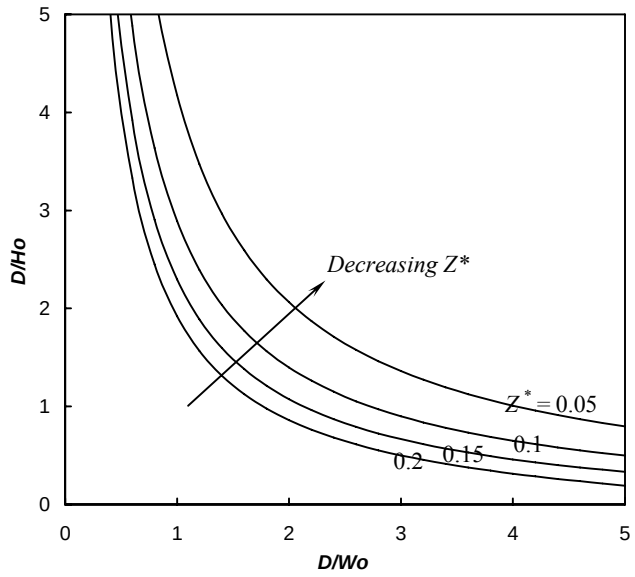

Figure 4.7 Contour of the dimensionless smoke layer height for a window with S^*=0.3

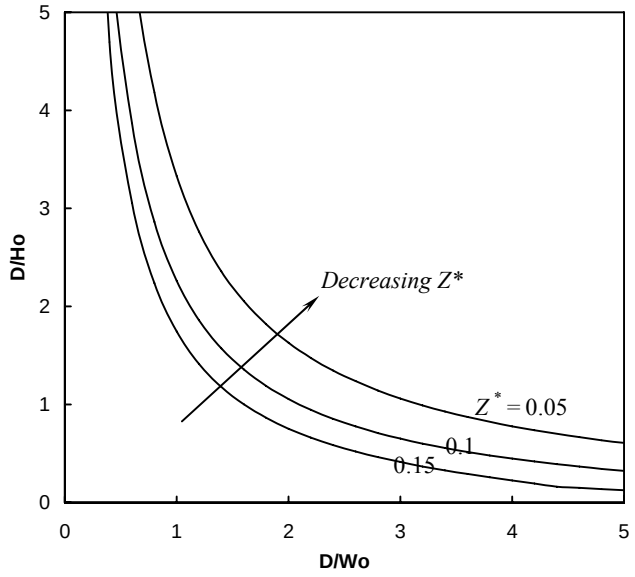

Figure 4.8 Contour of the dimensionless smoke layer height for a window with S^*=1

The effect of window sill (S^*) is shown in Figure 4.9 where the same smoke layer height contour (Z^* = 0.15) is plotted for different S^*. It is clear from both figures that for a given size of fire and opening, the doorway vent (S^* = 0) will have a higher smoke layer

height than that of the window ($S^* > 0$) with the same height and width. Figure 4.9 also shows the boundary for Z^* to be less or greater then 0.15 for a given opening and fire size.

Up to this point, some generalizations for the smoke layer height in the compartment have been presented; however, to complete our discussion on the criteria for a single zone model, we need to specify a level of the smoke layer height that would justify the condition of the compartment to be well-mixed. In Ozone, a two-zone model developed by Cadorin [50], the criterion for the layer interface height is set at 20% of the compartment height as a default value to switch from a two-zone model to a single-zone model. As for our study, we shall select $Z^* = 0.2$ to be our criterion. This selection although is arbitrary, it is only for informative purposes. Note that criterion used by Cadorin is based on the compartment height, while our criterion Z^* is based on the opening and the sill height. Generally Cadorin's criterion is the same as our criterion when the opening height extends to the ceiling. Using the vent height location to set the layer criterion leads to a lower layer height than a criterion on the room height.

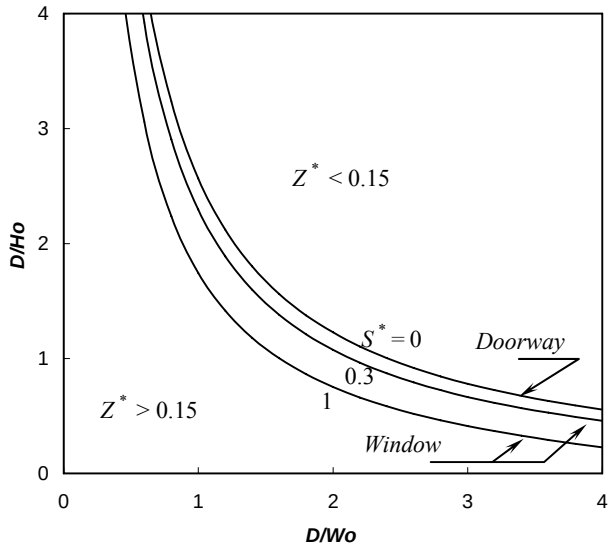

Figure 4.9 Contour of the dimensionless smoke layer height at $Z^* = 0.15$ for doorway ($S^* = 0$) and window ($S^* = 0.3$ and 1)

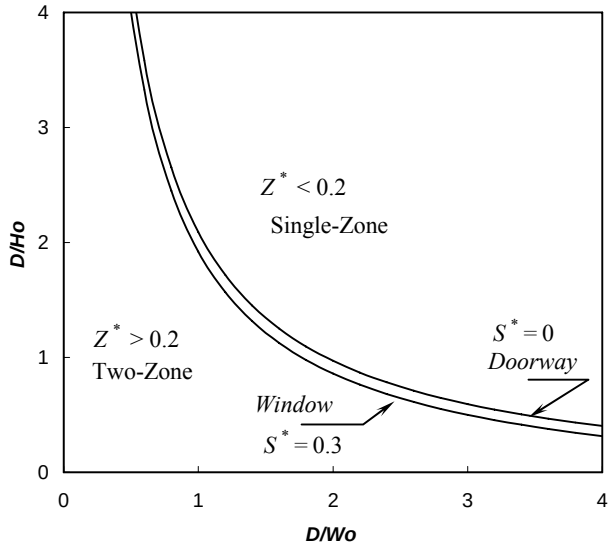

Figure 4.10 A single zone model criteria: Contour of the dimensionless smoke layer height at $Z^* = 0.2$ for doorway ($S^* = 0$) and window ($S^* = 0.3$)

Since we select $Z^* = 0.2$ as an indication of the well-mixed condition, we can use Figure 4.10, where the contours of the smoke layer height at $Z^* = 0.2$ are illustrated, to represent our criteria to justify the use of a single zone model. Based on this figure, one

can determine if a single zone model is appropriate for a compartment fire given the size of the opening and the size of the fire. In addition, from Figure 4.10, as $D^2/H_oW_o \approx (3/2)^2$, the smoke layer follow the criterion Z^*= 0.2 for the doorway case. Hence this generally says that any floor fire with diameter $D > 3/2\sqrt{A_o}$ yields a layer close to the floor less than 20% of the doorway height.

4.4 Conclusion

A method to determine the smoke layer height in the compartment has been presented in this chapter. The method has been validated and the calculated result is in good agreement with the experimental measurement especially for the doorway case. For the window case with a high sill, the calculation is overestimated. The reason is due to neglecting the near vent mixing flow which, in this case, is found experimentally to be significant. A general criterion on the smoke layer height for a single zone model to be valid is selected at 20% of the height of the opening (measured from the floor). Base on this criterion, a plot showing the boundary between the single zone and the two zones as a function of opening and fire size (D/H_o and D/W_o) has been presented. An approximation also shows that the criterion of the smoke layer height at 20% of the opening height will hold for a floor fire with diameter, $D > 3/2\sqrt{A_o}$.

Chapter 5

Formulation of a Single-Zone Mathematical Model

5.1 Introduction

To create a complex model that could provide an absolute prediction on every aspect of the compartment fire behavior may not be possible at this time. Nevertheless, a simple, yet beneficial model could be derived in order to demonstrate the important mechanisms. Some discussion on the theory of the compartment burning rate and fuel interaction on external feedback and ventilation have been provided in Chapter 2; however, in order to reveal the true benefit of the theory, a complete mathematical model that integrates the fuel response and the enclosure heat transfers via the conservation relationships is needed.

A single-zone model in which the compartment gas is assumed to be homogeneous is employed in this study to investigate the behavior of the quasi-steady but interactive fires. Generally a two-zone model, assuming two separate uniform-property zones representing the smoke layer and the lower layer, is probably more correct since in reality the gas properties are stratified. However, in some circumstances such as a post-flashover fire in a small room where everything gets involved in burning, or a fully-developed fire in a low ventilation condition where smoke layer is nearby the floor, a single-zone model can be reasonably used. Chapter 4 discusses a justification of using the single-zone model and criteria of fire scenario that the single-zone model satisfies. In this

chapter, we present a layout of the single-zone model that includes the conservation relationships, the fuel burning theory (Chapter 2), the mixing behavior (Chapter 3), and the flame extinction. A tool, Mathematica®, and methods to integrate the equations are also presented.

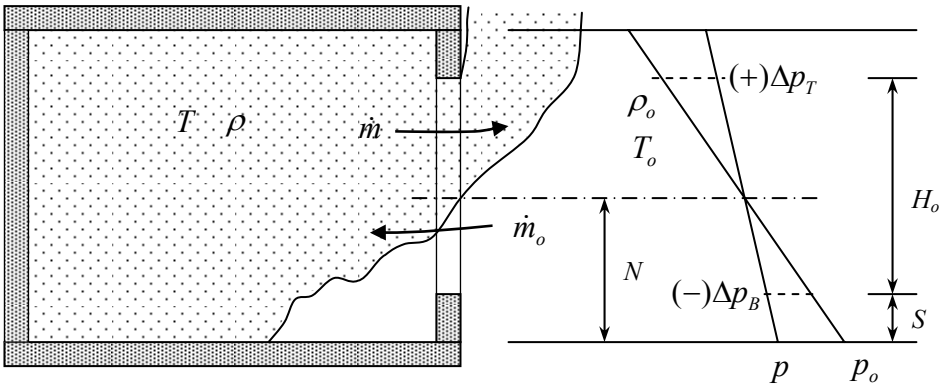

Figure 5.1 Schematic showing bidirectional vent flow

5.2 Flow Dynamics

In a room fire, the mass flows through the vents are driven by the hydrostatic pressure differences between inside and outside of the room. The pressure differences arise from the temperature differences due to fire itself or the forced ventilation system in the building. We only consider here the flow due to the temperature difference or the natural convection. Figure 5.1 shows the pressure profile inside and outside of the room for a single-zone model. Since the pressure is hydrostatic we have for the pressure in the room

$$p(z) = p(z_{ref}) - \rho g z \,, \tag{5.1}$$

and for the pressure outside of the room

$$p_o(z) = p_o(z_{ref}) - \rho_o g z \,, \tag{5.2}$$

where z_{ref} is the reference height, z is the vertical coordinate measured from z_{ref}, ρ_o gas density outside of the room and ρ is the density inside of the room. The pressure difference at any height is defined as $\Delta p(z) = p(z) - p_o(z)$. Hence,

$$\Delta p(z) = \Delta p(z_{ref}) + (\rho_o - \rho) g z \tag{5.3}$$

For a bidirectional flow at the vent, the point where the flow reverses direction is called the *neutral plane* (N) where $\Delta p(N) = 0$. Let z = 0 at the floor, the neutral plane height measured from the floor is given as

$$N = \frac{-\Delta p(0)}{(\rho_o - \rho) g}. \tag{5.4}$$

The mass flows through the wall vent over its height can be determined by Bernoulli's equation with a correction factor (known as an orifice flow coefficient) as

$$\dot{m}_i = \mathrm{C_d} \int W_o \rho_i \cdot v_i(z) dz, \tag{5.5}$$

where W_o is the width of the vent, $\mathrm{C_d}$ is the flow coefficient ($\approx$0.6-0.7) [84], and the subscript i represent where the flow comes from (inside or outside). The velocity at any height, $v(z)$, is given as

$$v_i(z) = \sqrt{\frac{2|\Delta p(z)|}{\rho_i}}. \tag{5.6}$$

Now letting the neutral plane be the reference level, mass flow through the vent between the height ($z_a < z < z_b$) is given as

$$\dot{m}_i = \mathrm{C_d} \int_{z_a}^{z_b} W_o \sqrt{2 g \rho_i (\rho_o - \rho) z}\, dz, \quad \text{or}$$

$$\dot{m}_i = \frac{2}{3} \mathrm{C_d} W_o \sqrt{2 g \rho_i (\rho_o - \rho)} \left(z_b^{3/2} - z_a^{3/2} \right), \tag{5.7}$$

where z_a and z_b are measured from the neutral plane (the reference height). Since there are three possible flow direction types that can occur at a wall vent: 1) *bidirectional flow*, a typical flow pattern occurring in most of stage of fire (Figure 3.1), 2) *out-flow only*, occurring in the filling stage (Figure 3.2a), and 3) *in-flow only*, usually taking place in small vent case and right after flame extinction or sudden drop in temperature (Figure 3.2b). The types depend on the sign of the pressure differences calculated at the bottom and top edges of the opening giving respectively as follow:

$$\Delta p_B = \Delta p(0) + (\rho_o - \rho) g S \text{, and} \tag{5.8}$$

$$\Delta p_T = \Delta p(0) + (\rho_o - \rho) g (H_o + S), \tag{5.9}$$

where H_o is the height of the vent, S is the sill height, and $\Delta p(0)$ is the pressure difference at the floor. Hence, in general the mass inflow through the vent is given as

$$\dot{m}_o = \frac{2}{3} \mathrm{C_d} W_o \sqrt{2 g \rho_o (\rho_o - \rho)} \left(z_2^{3/2} - z_1^{3/2} \right), \tag{5.11}$$

where $z_1 = \begin{cases} 0, & \text{for} \quad \Delta p_B < 0 \,\&\, \Delta p_T > 0 \\ N - (H_o + S), & \text{for} \quad \Delta p_B < 0 \,\&\, \Delta p_T \le 0 \\ 0, & \text{for} \quad \Delta p_B \ge 0 \,\&\, \Delta p_T > 0 \end{cases}$, and

$$z_2 = \begin{cases} N - S, & \text{for} \quad \Delta p_B < 0 \,\&\, \Delta p_T > 0 \\ N - S, & \text{for} \quad \Delta p_B < 0 \,\&\, \Delta p_T \le 0 \\ 0, & \text{for} \quad \Delta p_B \ge 0 \,\&\, \Delta p_T > 0 \end{cases}.$$

The mass outflow rate through the wall vent is given as follow:

$$\dot{m} = \frac{2}{3} \mathrm{C_d} W_o \sqrt{2 g \rho (\rho_o - \rho)} \left(z_4^{3/2} - z_3^{3/2} \right), \tag{5.12}$$

where $z_3 = \begin{cases} 0, & \text{for} \quad \Delta p_B < 0 \,\&\, \Delta p_T > 0 \\ 0, & \text{for} \quad \Delta p_B < 0 \,\&\, \Delta p_T \le 0 \\ S - N, & \text{for} \quad \Delta p_B \ge 0 \,\&\, \Delta p_T > 0 \end{cases}$, and

$$z_4 = \begin{cases} H_o + S - N, & \text{for} \quad \Delta p_B < 0 \;\&\; \Delta p_T > 0 \\ 0, & \text{for} \quad \Delta p_B < 0 \;\&\; \Delta p_T \le 0 \\ H_o + S - N, & \text{for} \quad \Delta p_B \ge 0 \;\&\; \Delta p_T > 0 \end{cases}.$$

Since the pressure in a room fire is basically at atmospheric level, assuming an ideal gas we have $\rho = \rho_o T_o / T$ which allows us to also write the mass flow expressions and the pressure difference in term of the compartment gas temperature (T) and outside gas temperature (T_o).

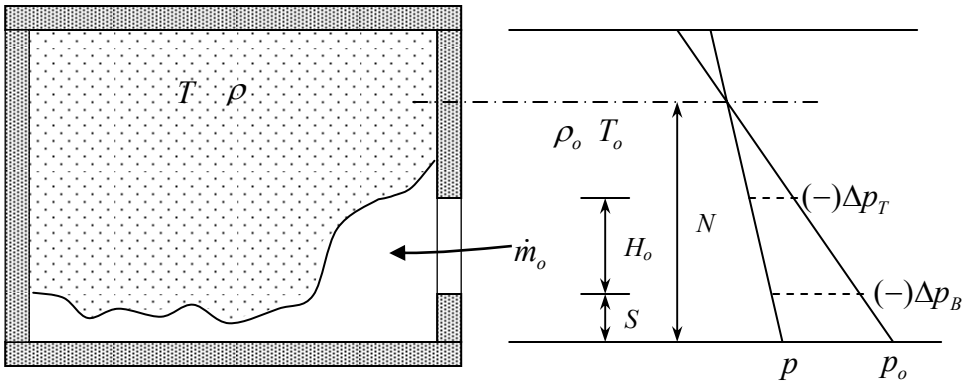

(a)

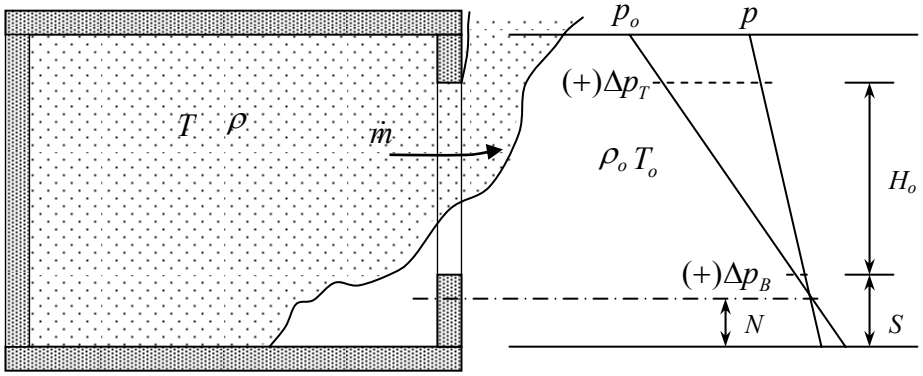

(b)

Figure 5.2 (a) Inflow-only (b) Outflow-only

5.3 Conservation Relationships

The conservation laws are probably the most fundamental equations describing transports for mass, energy, and species in a control volume. The conservation of energy for the compartment principally can be thought of as providing the governing relationship for $\Delta p(0)$; the conservation of mass – the relationship for T; and conservation of oxygen – for the oxygen concentration. The conservation equations are given in this section; however, a detailed derivation of the control volume analysis in integral form is not presented here and the reader is directed to a more fundamental text [85] or the cited source [60, 86]. Figure 5.3 shows a control volume for a single-zone model.

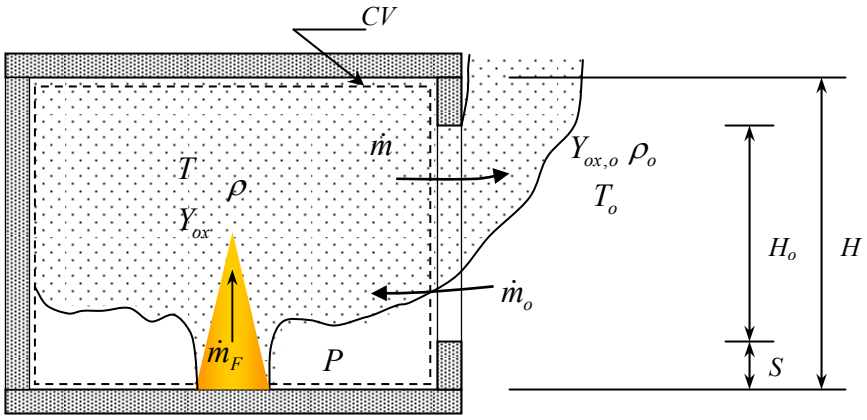

Figure 5.3Schematic showing a control volume for the single-zone model

5.3.1 Conservation of Mass

From a control volume shown in Figure 5.3, the mass conservation equation is

$$\frac{dm}{dt} + \sum_{\substack{j=1 \\ \text{net out}}}^{J} \dot{m}_j = 0 \tag{5.13}$$

Since the pressure in the compartment does not change much relative to the atmospheric one and assume ideal gas, we have for the gas density inside the enclosure as $\rho = \rho_o T_o / T$. Hence, from $m = \rho V$ we can write the mass equation as

$$\rho_o T_o V \frac{d}{dt}(1/T) + \dot{m} - \dot{m}_o - \dot{m}_F = 0\,, \tag{5.14}$$

where T is the gas temperature, $\dot{m}$ is the outflow rate, $\dot{m}_o$ is the inflow rate, $\dot{m}_F$ is the fuel mass loss rate, and V is the enclosure volume.

5.3.2 Conservation of Oxygen

The change of the species in the compartment occurs as a result of the combustion as well as the mass flow across the vent. Similarly from the mass equation, the oxygen conservation equation is defined as

$$\frac{d}{dt}(mY_{ox}) + \sum_{\substack{j=1 \\ \text{net out}}}^{J} \dot{m}_j Y_{ox,j} = -\dot{\omega}_{ox}\,, \tag{5.15}$$

where $\dot{\omega}_{ox}$ is the rate of oxygen reacted within the control volume. Since the energy release rate can be given as $\dot{Q} = \dot{\omega}_{ox}\Delta h_{ox}$, where Δh_{ox} is the heat of combustion per unit mass of oxygen. For $m = \rho_o T_o V / T$ we have,

$$\rho_o T_o V \frac{d}{dt}(Y_{ox}/T) + \dot{m}Y_{ox} - \dot{m}_o Y_{ox,o} = -\dot{Q}/\Delta h_{ox}\,. \tag{5.16}$$

5.3.3 Conservation of Energy

The energy equation is responsible for the thermal feedback to the fuel and can be shown in terms of the energy release due to combustion and the total loss by convection, conduction, and radiation. Without the considering the shaft work, the energy equation is

$$c_v \frac{d}{dt}(mT) + c_p \sum_{\substack{j=1 \\ \text{net out}}}^{J} \dot{m}_j T_j = \dot{Q} - \dot{Q}_{loss}\,, \tag{5.17}$$

where $\dot{Q}$ the energy release rate and $\dot{Q}_{loss}$ is the total heat loss. Consider the differential term

$$c_v \frac{d}{dt}(mT) = c_v V \frac{d}{dt}(\rho T) = c_v V \frac{d}{dt}\left(\frac{p}{R}\right).$$

For $R = c_p - c_v$ and $\gamma = c_p / c_v$, we have for the energy equation

$$\frac{V}{\gamma - 1}\frac{dp}{dt} + c_p \dot{m} T - c_p \dot{m}_o T_o - c_p \dot{m}_F T_F = \dot{Q} - \dot{Q}_{loss}. \tag{5.18}$$

From $p(z,t) = p_o(z) + \Delta p(z,t)$ and since $p(0,t) \approx p(z,t)$, then $\frac{dp}{dt} = \frac{d}{dt}[\Delta p(0,t)]$.

Let $P = \Delta p(0)$, we can also write

$$\frac{V}{\gamma - 1}\frac{dP}{dt} + c_p \dot{m} T - c_p \dot{m}_o T_o - c_p \dot{m}_F T_F = \dot{Q} - \dot{Q}_{loss}. \tag{5.19}$$

The total heat loss is given as

$$\dot{Q}_{loss} = \dot{q}_{wall} + \dot{q}_{vent}, \tag{5.20}$$

where $\dot{q}_{wall}$ is the heat transfer to the boundaries, and $\dot{q}_{vent}$ is the heat loss through the opening via radiation. These losses will be described in section 5.4.

5.4 Compartment Heat Transfer

In the compartment fire, convection and radiation are responsible for the heat transfer from the hot gas to the compartment boundary. Conduction is then responsible for the transfer through the solid boundary. The heat transfer path can be represented by an electric circuit analogy as shown in Figure 5.4. In a room fire, if the structural elements are protected with insulation, the conduction may dominate the heat transfer process since the gas temperature will be very close to the insulation surface temperature.

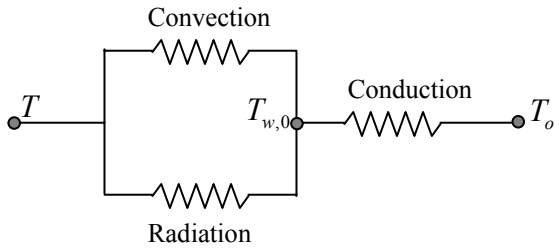

Figure 5.4 Electric circuit analogy for compartment heat transfer

5.4.1 Convection

Natural convection usually is more common than force convection in the compartment fire. In general, the range of the convective heat transfer in the compartment to be from 5 to 40 W/m^{2}K [87, 88] depending on the flow condition. An empirical correlation for the average convective heat transfer as a function of the dimensionless energy release has been presented by Tanaka and Yamada [88]. An alternate correlation for the convection was also proposed by Zukoski and Kubota [89]. Nevertheless, here for our model we will employ an empirical correlation for the convection, developed in a recent scale modeling study for compartment heat transfer by Veloo [90], as a function of the temperature rise in the compartment. This correlation is consistent with Tanaka and Yamada [88] and is developed for a higher range of temperature. It is given as

$$\frac{h_c}{\rho_o c_p (gl)^{1/2}} = \begin{cases} 3.5\times10^{-3} & ;\dfrac{T-T_o}{T_o} < 2.2 \\ 16\times10^{-3}\left(\dfrac{T-T_o}{T_o}\right) - 31.7\times10^{-3} & ;\dfrac{T-T_o}{T_o} \geq 2.2 \end{cases}, \tag{5.21}$$

where h_c is the convective heat transfer coefficient and l is the length scale taken here as the compartment height H. The convection heat transfer from gas to the wall is simply

$$\dot{q}_{conv} = h_c A_w (T - T_{w,0}), \tag{5.22}$$

where $T_{w,0}$ is the wall surface temperature and A_w is the wall total surface area.

5.4.2 Radiation

Radiation heat transfer is probably the most complex enclosure heat transfer mode since it depends on gas temperature and the soot distribution information. Nevertheless, a good approximation can be made with the homogeneous gray gas assumption for the flame and smoke. Following an analysis presented by Karlsson and Quintiere [2], we have the radiation exchange between gas and the compartment wall (assuming a grey uniform-temperature wall) as

$$\dot{q}_{rad} = \frac{A_w \sigma \left(T^4 - T_{w,0}^4\right)}{1/\varepsilon_g + 1/\varepsilon_w - 1}, \tag{5.23}$$

where σ is the Stefan-Boltzmann constant, 5.67×10^{-8} W/m^{2}K, ε_g and ε_w are the emissivity of the gas and wall respectively. Since the wall surface will become soot covered as the fire moves to the fully-developed stage, it might be reasonable to set ε_w to be unity.

The emissivity for gas and flame have been given in section 3.4 previously as

$$\varepsilon_g = 1 - \exp\left(-\kappa_g L_{mg}\right), \quad \text{and} \tag{5.24}$$

$$\varepsilon_f = 1 - \exp\left(-\kappa_f L_{mf}\right), \tag{5.25}$$

where κ_f and κ_g are absorption coefficients of the flame and the gas respectively, L_{mf} and L_{mg} mean beam length of the flame and gas volume (see detail in Chapter 2).

Assuming the flame temperature is about 1300 ºC, a differential equation describing the absorption coefficient of the gas can be written as

$$\frac{\rho_o T_o V}{T\dot{m}} \frac{d}{dt}\left(\kappa_g\right) + \kappa_g = \kappa_f \left(\frac{1 + r/Y_{ox}}{\dot{m}/\dot{m}_b} \right) \frac{1573}{T} . \tag{5.26}$$

5.4.3 Conduction

Two methods to determine the conduction through the compartment boundary are presented here. The first one is to solve a transient one-dimensional heat conduction using a finite difference numerical solution, and the second is to solve a convolution integral equation for a transient heat conduction assuming the wall is semi-infinite. The latter method is more practical since the equations are maintained only in time without spatial conduction computation; however, the finite difference method was chosen for the model due to some the inability to implement the integral equation into our differential equation solver (**NDSolve** in Mathematica®, discussed in section 5.8).

5.4.3.1 One-Dimensional Heat Conduction

Since the height and the width of the wall are generally much larger than its thickness, a one-dimensional conduction is appropriate. The transient heat equation is given as

$$\frac{\partial T_w}{\partial t} = \frac{1}{\rho_w c_{pw}} \frac{\partial}{\partial x}\left(k_w \frac{\partial T_w}{\partial x} \right), \tag{5.27}$$

where T_w is the wall temperature, c_{pw} is the specific heat of the wall, ρ_w the density of the wall, and k_w is the thermal conductivity of the wall. The boundary conditions are

$$-k_w \left.\frac{\partial T_w}{\partial x}\right|_{x=0} = \dot{q}''_{wall} = \dot{q}''_{conv} + \dot{q}''_{rad} = h_c\left(T - T_{w,0}\right) + \varepsilon_g \sigma\left(T^4 - T_{w,0}^4\right) \tag{5.28}$$

$$-k_w \left.\frac{\partial T_w}{\partial x}\right|_{x=tk} = h_{c,ambient}\left(T - T_{w,0}\right) \tag{5.29}$$

By spatially discretizing the Eq. (5.27) with the centered difference scheme into *n* elements, we have a system of algebraic ordinary differential equations as follows:

$$\left(\begin{array}{l} \dfrac{dT_{w,1}}{dt} = \dfrac{k_{w,2}\left(T_{w,2} - T_{w,1}\right) - k_{w,1}\left(T_{w,1} - T_{w,0}\right)}{\Delta x^2 \rho_w c_{pw,1}} \\ \dfrac{dT_{w,2}}{dt} = \dfrac{k_{w,3}\left(T_{w,3} - T_{w,2}\right) - k_{w,2}\left(T_{w,2} - T_{w,1}\right)}{\Delta x^2 \rho_w c_{pw,2}} \\ \qquad\qquad \vdots \\ \dfrac{dT_{w,n}}{dt} = \dfrac{k_{w,n+1}\left(T_{w,n+1} - T_{w,n}\right) - k_{w,n}\left(T_{w,n} - T_{w,n-1}\right)}{\Delta x^2 \rho_w c_{pw,n}} \end{array}\right) \tag{5.30}$$

Boundary conditions

$$\begin{array}{l} \dfrac{-k_{w,1}\left(T_{w,1} - T_{w,0}\right)}{2\Delta x} = h_c\left(T - T_{w,0}\right) + \varepsilon_g \sigma\left(T^4 - T_{w,0}^4\right) \\ \dfrac{-k_{w,n}\left(T_{w,n+1} - T_{w,n-1}\right)}{2\Delta x} = h_{c,ambient}\left(T_{w,n} - T_o\right) \end{array} \tag{5.31}$$

5.4.3.2 Integral Analysis

For a semi-infinite wall, transient conduction can be formulated in terms of surface temperature and a net heat flux, which is a function of time, as that

$$T_{w,0} - T_o = \frac{1}{\sqrt{\pi k_w \rho_w c_{pw}}} \int_0^t \frac{\dot{q}''_{wall}(\tau)}{\sqrt{t-\tau}} d\tau\,, \tag{5.32}$$

where $\dot{q}''_{wall} = \varepsilon_g \sigma\left(T^4 - T_{w,0}^4\right) + h_c\left(T - T_{w,0}\right)$, and $T_{w,0}$ is the wall surface temperature. A numerical integration, trapezoidal rule, can be performed to integrate Eq. (5.33). From Eq. (5.32) we write

$$T_{w,0}(n+1) = T_o + \frac{1}{\sqrt{\pi k_w \rho_w c_{pw}}}\left(\int_0^{t(n)} \frac{\dot{q}''_{wall}(\tau)}{\sqrt{t(n+1)-\tau}} d\tau + \int_{t(n)}^{t(n+1)} \frac{\dot{q}''_{wall}(\tau)}{\sqrt{t(n+1)-\tau}} d\tau \right), \tag{5.33}$$

where n is the time step and let δ is the time interval, $\delta = t(n+1) - t(n)$. It can be seen that the second integral involves singularity since $\tau = t(n+1)$ at the upper limit. This problem can be removed as follows: By Letting

$$u^2 = t(n+1) - \tau$$

we have

at $\tau = t(n)$, $u^2 = t(n+1) - t(n)$ or $u = \sqrt{\delta}$

at $\tau = t(n+1)$, $u^2 = 0$

Since $2udu = -d\tau$, we can write the second integral in Eq. (5.33) in the transformed variable, u, as

$$\int_{t(n)}^{t(n+1)} \frac{\dot{q}''_{wall}(\tau)}{\sqrt{t(n+1)-\tau}} d\tau = \int_{u(n)=\sqrt{\delta}}^{u(n+1)=0} \frac{\dot{q}''_{wall}\left(t(n+1)-u^2\right)}{u} \cdot (-2u) du = 2\int_0^{\sqrt{\delta}} \dot{q}''_{wall}(\tau) du$$

Hence, by trapezoidal rule,

$$\int_{t(n)}^{t(n+1)} \frac{\dot{q}''_{wall}(\tau)}{\sqrt{t(n+1)-\tau}} d\tau = \sqrt{\delta} \cdot \left[\dot{q}''_{wall}\left(t(n+1)\right) + \dot{q}''_{wall}\left(t(n)\right)\right] \tag{5.34}$$

Now consider the first integral

$$\int_0^{t(n)} \frac{\dot{q}''_{wall}(\tau)}{\sqrt{t(n+1)-\tau}} d\tau = \left[\begin{array}{l} \frac{1}{2} \frac{\dot{q}''_{wall}\left(t(1)\right)}{\sqrt{t(n+1)+t(1)}} + \frac{\dot{q}''_{wall}\left(t(2)\right)}{\sqrt{t(n+1)+t(2)}} + \cdots \\ \qquad \cdots + \frac{\dot{q}''_{wall}\left(t(n-1)\right)}{\sqrt{t(n+1)+t(n-1)}} + \frac{1}{2} \frac{\dot{q}''_{wall}\left(t(n)\right)}{\sqrt{t(n+1)+t(n)}} \end{array} \right], \text{ or}$$

$$\int_0^{t(n)} \frac{\dot{q}''_{wall}(\tau)}{\sqrt{t(n+1)-\tau}} d\tau = \frac{\delta}{2} \sum_{i=1}^{n-1} \left[\frac{\dot{q}''_{wall}\left(t(i)\right)}{\sqrt{t(n+1)+t(i)}} + \frac{\dot{q}''_{wall}\left(t(i+1)\right)}{\sqrt{t(n+1)+t(i+1)}} \right] \tag{5.35}$$

Hence from Eq. (5.33) to (5.35)

$$T_{w,0}(n+1) = T_o + \frac{1}{\sqrt{\pi k_w \rho_w c_{pw}}}\left(I_1 + I_2\right), \tag{5.36}$$

where $I_1 = \frac{\delta}{2}\sum_{i=1}^{n-1}\left[\frac{\dot{q}''_{wall}\left(t(i)\right)}{\sqrt{t(n+1)+t(i)}} + \frac{\dot{q}''_{wall}\left(t(i+1)\right)}{\sqrt{t(n+1)+t(i+1)}}\right]$,

$I_2 = \sqrt{\delta}\cdot\left[\dot{q}''_{wall}\left(t(n+1)\right) + \dot{q}''_{wall}\left(t(n)\right)\right]$.

As mentioned before, the integral equation method is not used in our model; however, this is to show an alternative method, which could have been selected if a different equation solver had been used, to treat the conduction in compartment fire.

5.4.4 Radiation Loss through the Opening

For an enclosure with blackbody surface ($\varepsilon_w = 1$), the heat loss by radiation through the opening of area A_o is given as [2]

$$\dot{q}_{vent} = A_o \varepsilon_g \sigma\left(T^4 - T_o^4\right) + A_o\left(1-\varepsilon_g\right)\sigma\left(T_{w,0}^4 - T_o^4\right). \tag{5.37}$$

5.5 Energy Release Rate Criteria and Flame Extinction

As discussed in section 2.6, the condition for flame extinction can be defined by a flammability line that is based on a critical flame temperature below which the extinction occurs and no energy is generated into the system. The flame temperature T_f is given as

$$c_p\left(T_f - T_l\right) = \frac{\Delta h_c - L + c_p\left(T_v - T_l\right) + \dfrac{\dot{q}''_{Ext,b}}{\dot{m}_b}}{1+\left(r/Y_{ox,l}\right)}. \tag{5.38}$$

where Δh_c is the heat of combustion per unit mass of fuel, L is the heat of gasification of the fuel, r is the stoichiometric oxygen to fuel ratio given by $r = \Delta h_c / \Delta h_{ox}$, $Y_{ox,l}$ and T_l and are the local oxygen level and temperature of the gas that is feeding the flame respectively, and $\dot{m}_b$ is the burning rate. Given $Y_{ox,l}$ and T_l are known, the flame temperature T_f can be solved for.

Referring to section 2.2, the energy release rate is given as

$$\dot{Q} = \dot{m}_b \Delta h_c \tag{5.39}$$

Hence for a critical flame temperature of 1300 ºC, the criteria for the burning rate (or the energy release rate) is given as

$$\dot{m}_b = \begin{cases} \dot{m}_F & ; \quad Y_{ox} > 0 \text{ and } T_f > 1300^{\circ}\text{C} \\ \dfrac{\dot{m}_o Y_{ox,o}}{r} & ; \quad Y_{ox} = 0 \text{ and } T_f > 1300^{\circ}\text{C} \\ 0 & ; \quad T_f \le 1300^{\circ}\text{C} \end{cases} \tag{5.40}$$

Notice that here for the model formulation we use the oxygen fraction (Y_{ox}) as a criterion to determine the ventilation condition while in the theory provided in Chapter 3 a global equivalence ratio (ϕ) is used.

5.6 Fuel Mass Loss Rate

Referring to the detail discussion in section 2.3, the fuel mass loss rate can be given as

$$\dot{m}_F = \dot{m}''_{F,o} A_{F,b} \frac{Y_{ox,l}}{Y_{ox,o}} + \frac{\dot{q}_{External}}{L}, \tag{5.41}$$

where $Y_{ox,l}$ is the oxygen mass fraction feeding the flame, $A_{F,b}$ is the fuel burning area (the burning area in ventilation limited, $Y_{ox} = 0$, has been described in section 2.5), and $\dot{m}''_{F,o}$ is the free burning rate giving for pool fire and crib fire as follow:

$$\dot{m}''_{F,o} = \dot{m}''_{F,\max}\left(1 - e^{-\kappa_f L_f}\right) \quad \text{; for Pool Fire} \tag{5.42}$$

$$\frac{\dot{m}''_{F,o}}{\mathrm{C_w} b^{-1/2}} = 0.968\left(1 - \exp\left(-\frac{(sb)^{1/2} A_{C,o}}{0.02 A_F}\right)\right) \quad \text{; for Crib Fire} \tag{5.43}$$

The external heat feedback is defined as follow:

$$\dot{q}_{External} = \dot{q}_{Ext,b} + \dot{q}_{Ext}, \tag{5.44}$$

$$\dot{q}_{Ext,b} = F_g\left(1-\varepsilon_f\right)\varepsilon_g A_{Fp,b}\left(T^4 - T_o^4\right) + F_w\left(1-\varepsilon_f\right)\left(1-\varepsilon_g\right)A_{Fp,b}\left(T_w^4 - T_o^4\right), \text{ and} \tag{5.45}$$

$$\dot{q}_{Ext} = F_g\varepsilon_g\left(A_{Fp} - A_{Fp,b}\right)\left(T^4 - T_v^4\right) + F_w\left(1-\varepsilon_g\right)\left(A_{Fp} - A_{Fp,b}\right)\left(T_w^4 - T_v^4\right), \tag{5.46}$$

where A_{Fp} and $A_{Fp,b}$ are the flaming and non-flaming projected area defined in Eq. (2.30) respectively, F_g and F_w are the shape factor from the fuel to gas and the fuel to wall respectively.

When the burning becomes ventilation limited ($Y_{ox} = 0$), the burning area reduces accordingly to available air supply. The burning area can be determined in terms of the burning diameter (D_b) for the pool fire or the stick burning length ($L_{s,b}$) for the crib fire. Since the internal burn rate is determined from the air supply rate, the burn area must accordingly adjust. The remainder of the fuel area can only be vaporized by the external heat flux. This is done by iteratively solving the following equations:

$$\frac{\pi D_b^2}{4} = \frac{\dot{m}_o}{s} \Bigg/ \left(\dot{m}''_{F,o}\frac{Y_{ox,l}}{Y_{ox,o}} + \frac{\dot{q}''_{Ext,b}}{L}\right) \quad \text{; for a pool fire} \tag{5.47}$$

$$\frac{\dot{m}_o}{s} = \dot{m}''_{F,o}\left(\frac{nb^2 L_{s,b}}{L_s}\left[(1-\frac{nL_{s,b}}{L_s}+2\frac{L_{s,b}}{b})2N+2\frac{nL_{s,b}}{L_s}-\frac{L_{s,b}}{b}\right]\right)\frac{Y_{ox,l}}{Y_{ox,o}} + \frac{\left(L_{s,b}^2+4L_{s,b}bN\right)\dot{q}''_{Ext,b}}{L} \quad \text{; for a crib fire} \quad (5.48)$$

5.7 Vent Mixing Correlation

In order to predict the fuel mass loss rate, we need to know the local oxygen level, $Y_{ox,l}$, that is feeding the flame. The near vent mixing discussed in Chapter 3 is used as a mechanism to determine $Y_{ox,l}$. It has been shown for a single-zone model where the smoke layer is close to the floor that the mixing ratio ($\dot{m}_e/\dot{m}_o$) approaches its limit value of 1.28. Hence, for simplification and conservative purposes the constant maximum value is used.

$$\frac{\dot{m}_e}{\dot{m}_o} = 1.28 \quad (5.49)$$

The local oxygen feeding the flame can be determined from the control volume shown in Figure 3.10 as

$$Y_{ox,l} = \frac{Y_{ox,o}+\left(\dot{m}_e/\dot{m}_o\right)Y_{ox,u}}{1+\left(\dot{m}_e/\dot{m}_o\right)}. \quad (5.50)$$

Similarly the local gas temperature can be calculated from

$$T_l = \frac{T_o+\left(\dot{m}_e/\dot{m}_o\right)T_u}{1+\left(\dot{m}_e/\dot{m}_o\right)}. \quad (5.51)$$

5.8 Model Summary and Mathematica as an Equation Solver

5.8.1 Model summary

Conservation Equations

$$\rho_o T_o V \frac{d}{dt}\left(1/T\right) + \dot{m} - \dot{m}_o - \dot{m}_F = 0$$

$$\rho_o T_o V \frac{d}{dt}\left(Y_{ox}/T\right) + \dot{m} Y_{ox} - \dot{m}_o Y_{ox,o} = -\dot{Q}/\Delta h_{ox}$$

$$\frac{V}{\gamma - 1}\frac{dP}{dt} + c_p \dot{m} T - c_p \dot{m}_o T_o - c_p \dot{m}_F T_F = \dot{Q} - \dot{Q}_{loss}$$

Energy Release Rate Criteria

$$\dot{Q} = \dot{m}_b \Delta h_c$$

$$\dot{m}_b = \begin{cases} \dot{m}_F & ; \quad Y_{ox} > 0 \text{ and } T_f > 1300^{\circ}\text{C} \\ \dfrac{\dot{m}_o Y_{ox,o}}{r} & ; \quad Y_{ox} = 0 \text{ and } T_f > 1300^{\circ}\text{C} \\ 0 & ; \quad T_f \le 1300^{\circ}\text{C} \end{cases}$$

$$T_f = \frac{\Delta h_c - L + c_p\left(T_v - T_l\right) + \dfrac{\dot{q}_{Ext,b}}{\dot{m}_b}}{c_p\left(1 + \left(r/Y_{ox,l}\right)\right)} + T_l$$

Heat Loss

$$\dot{Q}_{loss} = h_c A_w \left(T - T_{w,0}\right) + \varepsilon_g A_w \sigma\left(T^4 - T_{w,0}^4\right) + \varepsilon_g A_o \sigma\left(T^4 - T_o^4\right) + \left(1 - \varepsilon_g\right) A_o \sigma\left(T_{w,o}^4 - T_o^4\right)$$

Vent Flow

$$\dot{m}_o = \frac{2}{3} \mathrm{C_d} W_o \sqrt{2 g \rho_o \left(\rho_o - \rho\right)} \left(z_2^{3/2} - z_1^{3/2}\right),$$

$$\text{where} \quad z_1 = \begin{cases} 0, & \text{for} \quad \Delta p_B < 0 \;\&\; \Delta p_T > 0 \\ N - (H_o + S), & \text{for} \quad \Delta p_B < 0 \;\&\; \Delta p_T \le 0 \\ 0, & \text{for} \quad \Delta p_B \ge 0 \;\&\; \Delta p_T > 0 \end{cases} \text{, and}$$

$$z_2 = \begin{cases} N - S, & \text{for} \quad \Delta p_B < 0 \;\&\; \Delta p_T > 0 \\ N - S, & \text{for} \quad \Delta p_B < 0 \;\&\; \Delta p_T \le 0 \\ 0, & \text{for} \quad \Delta p_B \ge 0 \;\&\; \Delta p_T > 0 \end{cases}.$$

$$\dot{m} = \frac{2}{3} \mathrm{C_d} W_o \sqrt{2g\rho(\rho_o - \rho)} \left(z_4^{3/2} - z_3^{3/2} \right),$$

$$\text{where} \quad z_3 = \begin{cases} 0, & \text{for} \quad \Delta p_B < 0 \;\&\; \Delta p_T > 0 \\ 0, & \text{for} \quad \Delta p_B < 0 \;\&\; \Delta p_T \le 0 \\ S - N, & \text{for} \quad \Delta p_B \ge 0 \;\&\; \Delta p_T > 0 \end{cases} \text{, and}$$

$$z_4 = \begin{cases} H_o + S - N, & \text{for} \quad \Delta p_B < 0 \;\&\; \Delta p_T > 0 \\ 0, & \text{for} \quad \Delta p_B < 0 \;\&\; \Delta p_T \le 0 \\ H_o + S - N, & \text{for} \quad \Delta p_B \ge 0 \;\&\; \Delta p_T > 0 \end{cases}.$$

$$N = \frac{-P}{(\rho_o - \rho)g}$$

$$\Delta p_B = \Delta p(0) + (\rho_o - \rho) g S$$

$$\Delta p_T = \Delta p(0) + (\rho_o - \rho) g (H_o + S)$$

Fuel Mass Loss Rate

$$\dot{m}_F = \dot{m}''_{F,o} A_{F,b} \frac{Y_{ox,1}}{Y_{ox,o}} + \frac{\dot{q}_{External}}{L}$$

$$\dot{m}''_{F,o} = \dot{m}''_{F,\max} \left(1 - e^{-\kappa_f L_f} \right) \qquad \text{; for Pool Fire}$$

$$\frac{\dot{m}''_{F,o}}{C_w b^{-1/2}} = 0.968 \left(1 - \exp\left(- \frac{(sb)^{1/2} A_{C,o}}{0.02 A_F} \right) \right) \qquad \text{; for Crib Fire}$$

$$\dot{q}_{External} = \dot{q}_{Ext,b} + \dot{q}_{Ext}$$

$$\dot{q}_{Ext,b} = F_g\left(1-\varepsilon_f\right)\varepsilon_g A_{Fp,b}\left(T^4 - T_o^4\right) + F_w\left(1-\varepsilon_f\right)\left(1-\varepsilon_g\right)A_{Fp,b}\left(T_w^4 - T_o^4\right)$$

$$\dot{q}_{Ext} = F_g\varepsilon_g\left(A_{Fp} - A_{Fp,b}\right)\left(T^4 - T_v^4\right) + F_w\left(1-\varepsilon_g\right)\left(A_{Fp} - A_{Fp,b}\right)\left(T_w^4 - T_v^4\right)$$

Burning Area for ventilation limited ($Y_{ox} = 0$)

$$\frac{\pi D_b^2}{4} = \frac{\dot{m}_o}{s}\Bigg/\left(\dot{m}''_{F,o}\frac{Y_{ox,l}}{Y_{ox,o}} + \frac{\dot{q}''_{Ext,b}}{L}\right) \qquad \text{; for pool fire}$$

$$\frac{\dot{m}_o}{s} = \dot{m}''_{F,o}\left(\frac{nb^2L_{s,b}}{L_s}\left[(1-\frac{nL_{s,b}}{L_s}+2\frac{L_{s,b}}{b})2N + 2\frac{nL_{s,b}}{L_s} - \frac{L_{s,b}}{b}\right]\right)\frac{Y_{ox,l}}{Y_{ox,o}} \qquad \text{; for crib fire}$$
$$+ \frac{\left(L_{s,b}^2 + 4L_{s,b}bN\right)\dot{q}''_{Ext,b}}{L}$$

Emissivities

$$\varepsilon_g = 1 - \exp\left(-\kappa_g L_{mg}\right)$$

$$\varepsilon_f = 1 - \exp\left(-\kappa_f L_{mf}\right)$$

$$\frac{\rho_o T_o V}{T\dot{m}}\frac{d}{dt}\left(\kappa_g\right) + \kappa_g = \kappa_f\left(\frac{1+r/Y_{ox}}{\dot{m}/\dot{m}_b}\right)\frac{1573}{T}$$

Convective Heat Transfer

$$\frac{h_c}{\rho_o c_p (gH)^{1/2}} = \begin{cases} 3.5\times10^{-3} & ;\dfrac{T-T_o}{T_o} < 2.2 \\ 16\times10^{-3}\left(\dfrac{T-T_o}{T_o}\right) - 31.7\times10^{-3} & ;\dfrac{T-T_o}{T_o} \geq 2.2 \end{cases}$$

Wall Conduction

$$\begin{pmatrix} \dfrac{dT_{w,1}}{dt} = \dfrac{k_{w,2}\left(T_{w,2}-T_{w,1}\right)-k_{w,1}\left(T_{w,1}-T_{w,0}\right)}{\Delta x^2 \rho_w c_{pw,1}} \\ \dfrac{dT_{w,2}}{dt} = \dfrac{k_{w,3}\left(T_{w,3}-T_{w,2}\right)-k_{w,2}\left(T_{w,2}-T_{w,1}\right)}{\Delta x^2 \rho_w c_{pw,2}} \\ \vdots \\ \dfrac{dT_{w,n}}{dt} = \dfrac{k_{w,n+1}\left(T_{w,n+1}-T_{w,n}\right)-k_{w,n}\left(T_{w,n}-T_{w,n-1}\right)}{\Delta x^2 \rho_w c_{pw,n}} \end{pmatrix}$$

$$\frac{-k_{w,1}\left(T_{w,1}-T_{w,0}\right)}{2\Delta x} = h_c\left(T-T_{w,0}\right)+\varepsilon_g \sigma\left(T^4-T_{w,0}^4\right)$$

$$\frac{-k_{w,n}\left(T_{w,n+1}-T_{w,n-1}\right)}{2\Delta x} = h_{c,ambient}\left(T_{w,n}-T_o\right)$$

Mixing Model

$$\frac{\dot{m}_e}{\dot{m}_o} = 1.28$$

$$Y_{ox,l} = \frac{Y_{ox,o}+\left(\dot{m}_e/\dot{m}_o\right)Y_{ox,u}}{1+\left(\dot{m}_e/\dot{m}_o\right)}.$$

$$T_l = \frac{T_o+\left(\dot{m}_e/\dot{m}_o\right)T_u}{1+\left(\dot{m}_e/\dot{m}_o\right)}.$$

State Variable

T : Compartment gas temperature

Y_{ox} : Oxygen mass fraction

P : Differential pressure at the floor

5.8.2 Time Integration and Equation Solver

As previously shown, our model composes of a system of ordinary differential equations which are the conservation equations, the wall heat equations, and the gas absorption coefficient, and algebraic equations including the flow dynamics and the fuel mass loss rate. The system of ODEs is considered to be a stiff problem because the time constant relative to the pressure variation is much shorter than the time constant of the temperature variation. In other words, dP/dt go to zero much faster than the temperature; also the pressure can lead to a rapid variation in the solution. Hence, it is better to rely on a solver that is specifically designed and capable to treat this type of problem.

The system of ODEs in our model is solved numerically in Mathematica® using a built-in function called **NDSolve** [91-94]. For initial value problems, **NDSolve** uses an Adams-Moulton Predictor-Corrector method (order between 1 and 12) for non-stiff differential equations and backward difference formulas (Gear method, order between 1 and 5) for stiff differential equations. It switches between the two methods using heuristics based on the adaptively selected step size. It starts with the non-stiff method under essentially all conditions, and checks for the advisability of switching methods every 10 or 20 steps. In addition to solving the system of ODEs, another useful built-in function called **FindRoot** is also used to solve for the fuel burning area and the flame temperature at each time step of solving the ODEs. For a nonlinear equation with one specified starting point, **FindRoot** searches for a solution using the Newton-Raphson method.

Chapter 6

Single-Wall-Vent Compartment Fire Experiment and Mathematical Model Application

6.1 Introduction

A single-zone mathematical model featuring important physics such as fuel response to enclosure effects and mixing behavior has been developed to study fully-developed compartment fires. To validate and examine the capability of the model, a well-controlled experimental database is needed. A series of experiments using a small-scale compartment is conducted in which the quantity and configuration of the fuel are varied under natural ventilation condition of various doorway and window widths. This chapter will present the detail of the experimental program along with some analysis and discussion of both transient and average peak properties measured and predicted. Some generalities of the compartment fire behavior will be examined using the experimental results and the model simulations. Fuel type and scale effects will be examined.

6.2 Experimental Design

6.2.1 Compartment and Vent Configuration

The small-scale compartment was built with 2.54 cm (1 inch) thick Type-M Kaowool board. The compartment inner size was measured 40 cm × 40 cm × 120 cm (height × width × depth). Two kinds of the single-wall-vent, doorway-like and window-like, were used. The vent height and the sill height were designed such that they represented the common doorway and widow height in real buildings. The width of the

vent was varied in each test. Figure 6.1a shows the global view of the compartment and vent panels.

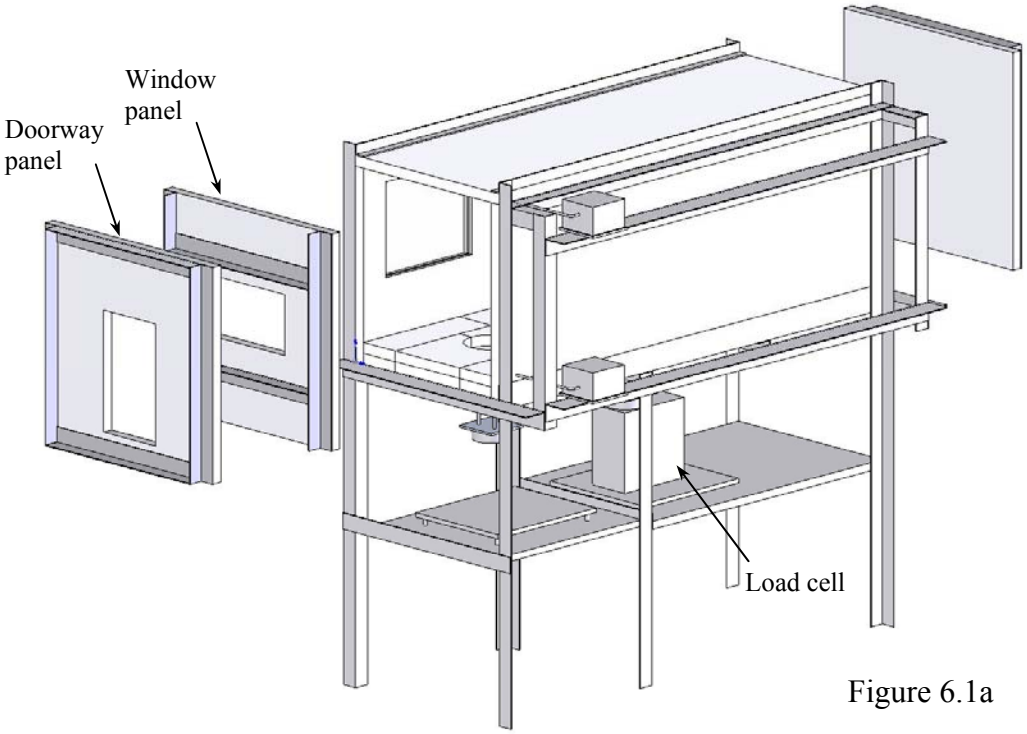

Figure 6.1a

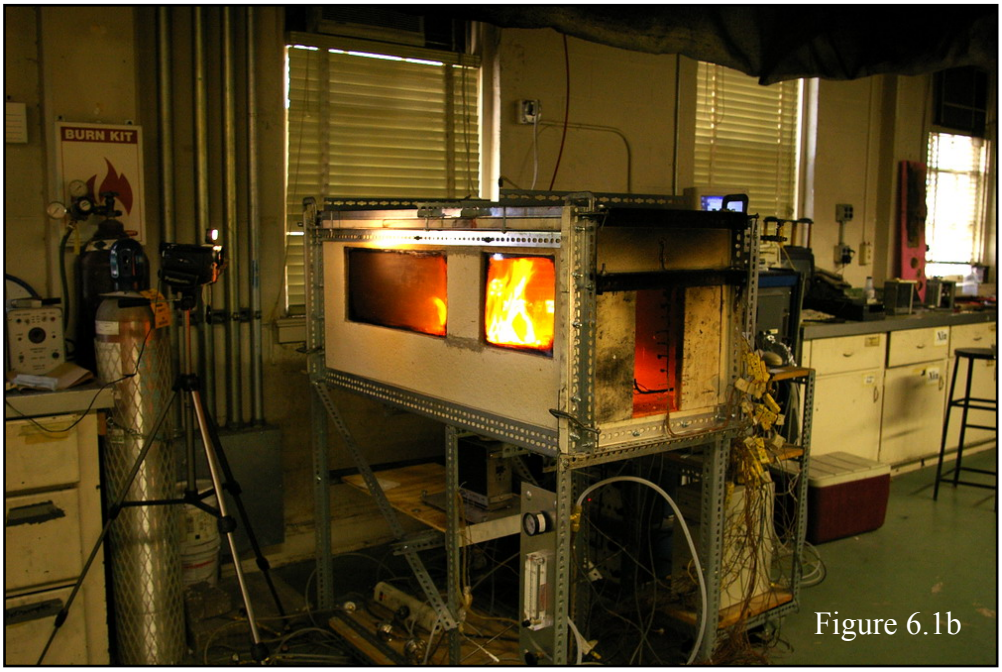

Figure 6.1b

Figure 6.1a Schematic showing the compartment and vent panel; Figure 6.1b Photo of a running test and video recording through the glass window

All joints between the walls and the ceiling were sealed using LCI300 intumescent firestop sealant and RESBOND^{TM} 907GF adhesive sealant to insure no unintended leaks. Steel angles were used to support the compartment walls and the instruments. On the side wall of the compartment, 22 cm × 27 cm and 22 cm × 55 cm transparent glass windows (5 mm thick Robax® Transparent Glass-Ceramic with thermal shock resistance and low thermal expansion) were installed to allow the observation of the compartment fire behavior and video recording. The experiments were conducted at the Fire Dynamics Laboratory (Potomac Laboratory), University of Maryland at College Park.

6.2.2 Fuel Description

The fuel configurations selected here were the *crib* fire and the *pool* fire. The crib fire represents the common furniture-like fire, while the pool fire corresponds to the horizontal or in general flat surface burning. These fuel configurations response differently to the heat feedback from the enclosure and hence raise our interest to investigate them.

6.2.2.1 Crib Fire

Two types of wood, Oak and Pine, were selected as the material for the crib fire. The crib configurations were designed to have surface controlled burning. Both square and rectangular crib footprints were used. The crib description is given in Table 6.1.

Table 6.1Wood crib description

Crib	b (m)	n_i	n_j	L_i (m)	L_j (m)	N	Type
1	0.012	4	7	0.3	0.15	5	Pine
2	0.01905	4	4	0.15	0.15	5	Pine
3	0.012	5	5	0.15	0.15	4	Pine
4	0.011	9	9	0.25	0.25	5	Oak
5	0.022	5	9	0.414	0.207	3	Oak

The crib variables are given as follows: b is thickness dimension of a stick, n_i and n_j are the number of stick i and j per layer respectively, L_i and L_j are the length of stick i and j respectively. (Shown in Figure 6.2)

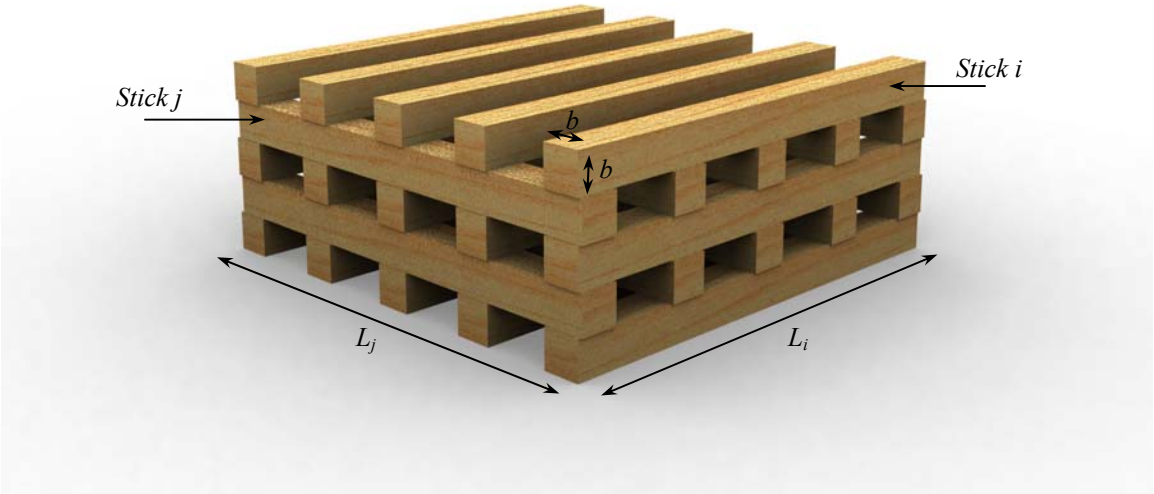

Figure 6.2 Wood crib descriptions

6.2.2.2 Pool Fire

Heptane (C_7H_{16}) was used for the pool fire tests. Two fuel pan configurations were used: a single circular pan with a diameter of 24.5 cm and an array of 10 circular pans with a diameter of 14 - 15 cm. The pool fire description is given in Table 6.2

Table 6.2 Heptane pool description

Pool	Pool size – Diameter (m)	Heptane volume (ml)
1	7x0.138, 3x0.147	300
2	0.245	90 (each pan)

6.3 Instrumentation

The instrumentation was selected to characterize the thermal and flow phenomena of the compartment fire. The fuel mass loss, oxygen concentration, heat flux to wall, temperature, and pressure difference were recorded. The layout of the compartment instrumentation is presented in Figure 6.3.

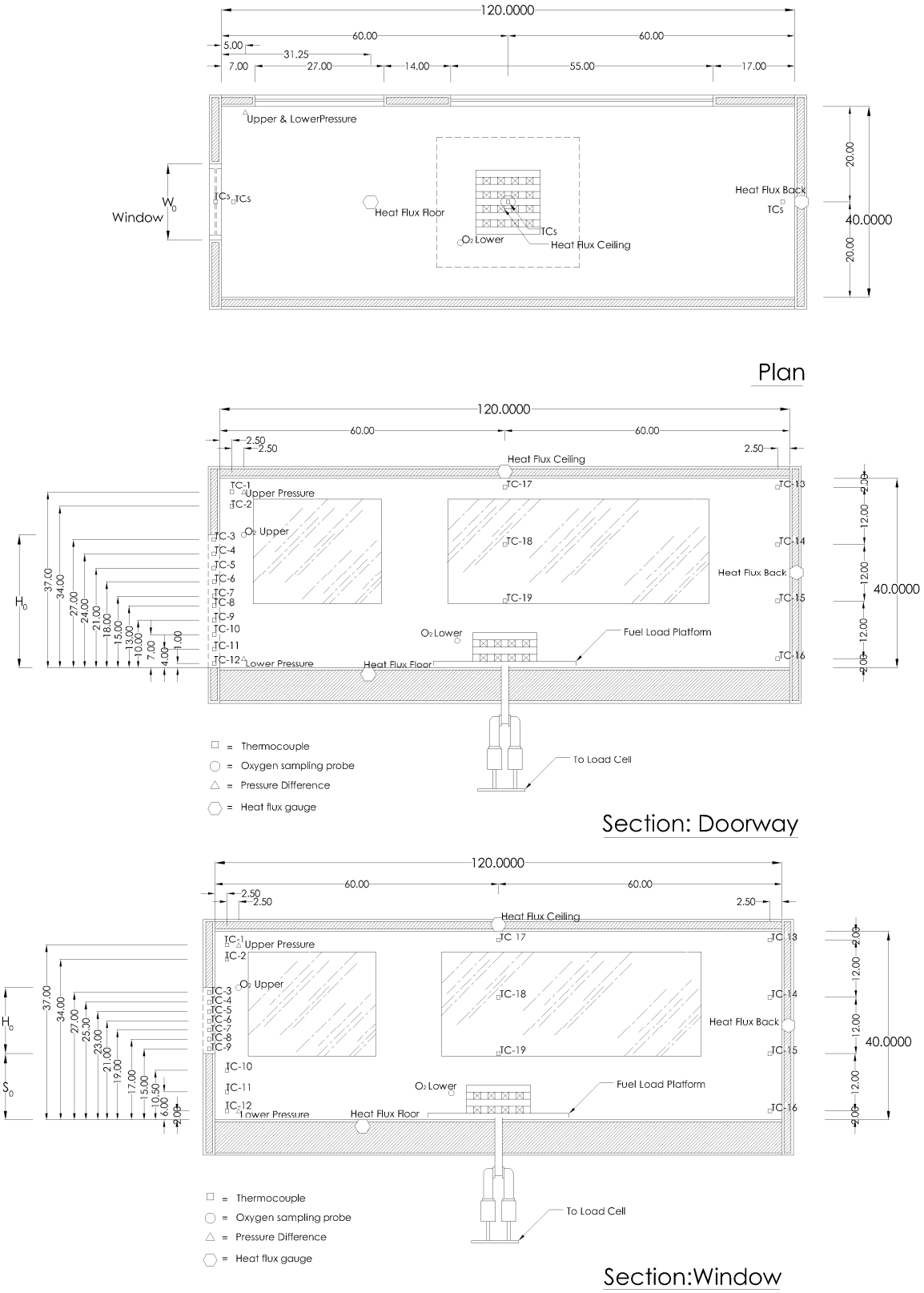

Figure 6.3Plan and section view showing measurement layout

6.3.1 Fuel Mass Loss

Due to the wide range of the fuel mass used in our experiments, three load cells with different load capacities were used to measure the fuel mass loss. (250 g span with 2.0 kg capacity, 600 g span with 4 kg capacity, and 4 kg span with 30 kg capacity) All load cells, manufactured by Automatic Timing and Controls (Model 6005D), provided voltage output 800 millivolts DC. To control the overshoot of the scale and prevent an oscillating signal, damping fluid with a proper viscosity (350 c.s. for the 250 g and 600 g load cell, and 5000 c.s. for the 4 kg load cell) was used in the load cell. Figure 6.1 shows the arrangement of the cell underneath the compartment. Fuel mass loss in the free burning condition (pure air, outside) was also measured for all pool sizes and also for Crib 1, 2, and 3. The free burning of Crib 4 and 5 was estimated using the correlation given in Eq. (2.24).

6.3.2 Oxygen Concentration

Oxygen volume concentration was measured using the automotive oxygen sensor (Teledyn R22A). The upper and lower layer sampling gas were collected at the flow rate of 1.5 SCFH and passed through the soot filters (type-304 Fisher Scientific) with Advantest glass sheet filter (934-AH). A cold trap was also used to cool down the temperature of the sampling gas to approximately 25 ºC before it reached the oxygen sensor. The temperature and the flow rate of the sampling gas for every test were kept consistent with those of the calibration gas. The oxygen sensors were attached to a custom designed chamber allowing the sampling gas to impinge onto the sensing surface. Figure 6.4 shows the oxygen sensor and its setup.

Figure 6.4 Oxygen sensor setup

6.3.3 Heat Flux

Three Gardon gages (Model 40-15-4-36-20-21124 MEDTHERM Corporation) were used to measure heat flux to the back wall panel, the ceiling, and the floor. Cooling water supplied to the three heat flux gauges had a flow rate approximately 11 ml/s and a temperature of 23 ºC.

6.3.4 Temperature

Type K glass-insulated thermocouple wires were used to measure the vertical temperature profile across the vent, at the center of the box, and near the back wall panel. The surface temperatures of the ceiling, back wall, and floor were also monitored. The thermocouple bead diameter was approximately 1.0 -1.5 mm. The surface monitoring thermocouples were inserted from the outside of the wall (Kaowool board) to have half of their bead below the inside surface.

6.3.5 Pressure Difference

To observe the gas flow characteristic coming in and out of the compartment, Two Barocell pressure transducers with 133 Pa range were used to measure pressure

differences near the ceiling and the floor. The transducers were connected to the electric manometer which gave the output signal ranged from 0 to 1 volt.

6.3.6 Data Recording

All the data were taking using data acquisition system from National Instruments. PCI-MIO-16-E-4 DAQ Card, which was installed to 1.0 GHz Pentium III 128 MB memory Dell-PC, was connected to an SCXI-1100 chassis where two SCXI-1300 terminal block modules with 32 analog channels were installed to convert signals from the sensors with high accuracy. To reduce the noise that thermocouples and other transducers inevitably pick up when we were taking data, the negative input of a floating thermocouple was connected to the chassis ground within terminal block SCXI-1300 and then referenced to the building ground. LabVIEW version 5.1 was used to acquire, display and save data from the acquisition system. Data were taken at 0.5 Hz with 100 samples to average and 6,000 scan rate.

6.4 Experimental Procedure and Data Post Processing

All tests were strictly conducted according to the same preparation steps and test running procedures to make data from all cases consistent and comparable. This section presents the routine procedure for the experiment. A post processing method to obtain the fuel mass loss rate will be provided, and the correction for the radiation to the thermocouple signal will be discussed.

6.4.1 Test Preparation and Procedures

Compartment and Vent Size: Before each experiment the compartment and the glass window were cleaned of excess soot deposits. Kaowool board was cut to meet the desired shapes and assembled to the front wall panel to adjust the vent sizes. All connections and gaps were sealed with LCI intumescent sealant.

Oxygen Analyzer: The gas sampling flow rate was adjusted to be at 1.5 SCFH. The cold trap was refilled with ice. The soot filter chambers were cleaned and the glass sheet filters were replaced. The oxygen sensors were calibrated at ambient air (20.9%) before each test; however, every week the zero and 15.3% calibrations were performed with a known concentration gas.

Thermocouples: Location and noise were of concern for the thermocouples. Since we used the flexible wire thermocouples which could move during the experiment, before each test the thermocouple beads were assured to be located at the correct position as in the design drawing. Noise was occasionally picked up by thermocouples (also by other transducers) due to the connector from transducers or the ground reference was not properly connected to the systems. Hence before starting the actual test, it was necessary to pre-run the data acquisition program to see if there were any unusual signals.

Load Cell: Load cell calibration was performed before each test with the standard weights. The fuel platform was checked so that it stayed in place and moved freely without touching the shaft or the compartment floor. The capacity of the load cell was

checked to match the fuel weight. The output signal was assured to not overshoot, oscillate or exhibit noise. The damping adjustment was performed as needed.

Pressure Transducers: The zero adjustment was performed to the pressure transducers before each test. This process was done by using a bypass line to connect the pressure detection side to reference side so that the electric manometer gave a 0 volt output.

Heat Flux Gauges: All heat flux gauges were cleaned of excess soot using a soft bush. The water cooling was adjusted to have a proper flow rate.

Video Recorder: All tests were video taped through the side wall window. A thin film of soap was applied to the cleaned glass by rubbing all around until we could see through the glass clearly. This was to help preventing excessive soot from sticking on the window glass.

Fuel: The wood crib was dried in the oven at the temperature of 80 ºC for at least 12 hours, and kept in a dry tank filled with Drierite at the room temperature. The fuel tray was cleaned and checked for the alignment. The initial weight of the crib and the volume of the heptane were recorded just before starting the test. For the pool fire experiment, unless noticed otherwise, some water was added to the fuel pan to adjust the level of the heptane and prevent the fuel from bulk boiling.

After the instrumentation was prepared, the preparation for ignition commenced. For the crib fire experiment, the wood crib was positioned at the center of the fuel tray and 10 ml of heptane was used as the ignition source. For the pool fire experiment, the recorded amount of heptane was carefully poured into the pan. Then, the front panel was closed and locked tightly with c-clamps. The data and video began recording before ignition.

For most cases, the fuel was ignited by a long match with extended holder. Only for the largest pool fire test (array of 10 fuel pans) the fuel was ignite by an electric spark. While the test was running, the flow rate of the sampling as for oxygen measurement was monitored and always adjusted at the 1.5 SCFH. All measurements were recorded until 5 minutes after the fuel was exhausted.

6.4.2 Data Post Processing

The raw data taken from the oxygen sensors, heat flux gauges, and the pressure transducer were generally in voltage and needed to be converted using the calibration coefficients to the meaningful result. However, for the mass loss signal and the temperature reading, some post processing was performed besides the voltage conversion. This includes differentiating the mass loss signal to obtain the mass loss rate and correcting thermocouple reading in the flow field. The post processing will be described in this section.

6.4.2.1 Fuel mass loss rate

To obtain the fuel mass loss rate it is necessary to differentiate the mass loss signal. However, due to some noises that could occur during the measurement and did not represent any physical phenomena, a smoothing process was applied on the mass loss signal before any of the differentiating process was performed. A 10-point-moving average was usually used as the smoothing method; however, for the cases where the large span load cell (4 kg span) was used, more data points were needed for the moving average. Since the resolution of the load cell was in the order of 0.02% of its range, the larger span load cell would normally give a larger error in mass measurement than the smaller one and hence yield the larger error in the mass loss rate results. The two-point interpolation formula to calculate the derivative of the fuel mass loss is given as [95]

$$\dot{m}_{F,n} = \frac{dm_{F,n}}{dt} = \frac{m_{F,n+1} - m_{F,n}}{\Delta t} \tag{6.1}$$

6.4.2.2 Thermocouple reading correction

Due to the radiation from the flame sheet, enclosure walls, and the hot gas itself, the thermocouple reading might be different than the actual gas temperature. In this section we present a method of correcting the thermocouple reading based on the measured heat flux. The incident radiation heat flux to the Gardon gage can be estimated as

$$\dot{q}''_{inc} = \dot{q}''_{mea} - h_{conv}(T - T_{gage}), \tag{6.2}$$

where $\dot{q}''_{mea}$ is the measured heat flux from the Gardon gage, T_{gauge} is the gage temperature assumed to be at the cooling water temperature (25˚C), T is the gas temperature, and

h_{conv} is the compartment convective heat transfer coefficient given by Veloo [90] in Eq. (5.21). Considering the energy balance at the thermocouple bead, we have

$$\dot{q}''_{inc} A_{TC} = h_{conv,TC} A_{TC} (T_{TC} - T) + \sigma A_{TC} T_{TC}^4 , \tag{6.3}$$

where T_{TC} is the temperature of the thermocouple bead and $h_{conv,TC}$ is the thermocouple convective heat transfer coefficient taken value of 100 W/m^{2}K for the thermocouple at the vent and the back wall and 300 W/m^{2}K for the thermocouple above the fuel plume. The approximation for $h_{conv,TC}$ was based on the characteristic vent flow velocity. Upon substituting Eq. (6.2) into (6.3) and rearranging, the gas temperature is

$$T = \frac{\dot{q}''_{mea} - \sigma T_{TC}^4 + h_{conv} T_{gauge} - h_{conv,TC} T_{TC}}{\left(h_{conv} - h_{conv,TC}\right)} \tag{6.4}$$

By this method, a 10% - 25% correction was found. The correction results from this method are also consistent with the result from the method given by Diné [96], based on an exact calculation using shape factors for the radiation heat transfer to each thermocouple bead.

6.5 Scope of the Experiments

One of the key parameters that was used to present various compartment fire database [17, 20, 33] is $A_o \sqrt{H_o} \rho_o \sqrt{g} / A_F$, here called the *ventilation factor*. This parameter can also be viewed as the ratio of air flow to the fuel flow or the inverse of the global equivalence ratio. A range of opening sizes and the fuel loadings was selected to span over this key parameter to represent the full range of real fire conditions. The ventilation factor is also used to provide the basis for comparing with the experimental

results. There are 14 wood crib and 3 heptane pool fire experiments in our test program and Table 6.3 provides the experiment conditions.

Table 6.3 Experimental Conditions

Test	H_o (m)	W_o (m)	S (m)	A_F	$A_o\sqrt{H_o}\rho_o\sqrt{g}/A_F$
Crib1D28x15	0.28	0.15	0.15	0.234	356.3
Crib1W14x20	0.14	0.20	0.20	0.234	168.0
Crib1W14x32	0.14	0.32	0.32	0.234	268.7
Crib2D28x05	0.28	0.05	0.05	0.185	150.3
Crib2D28x15	0.28	0.15	0.15	0.185	450.9
Crib2D28x30	0.28	0.30	0.30	0.185	901.9
Crib2D28x40	0.28	0.40	0.40	0.185	1202.5
Crib2W14x06	0.14	0.06	0.06	0.185	63.8
Crib2W14x32	0.14	0.32	0.32	0.185	340.1
Crib3D28x30	0.28	0.30	0.30	0.119	1402.0
Crib3D28x40	0.28	0.40	0.40	0.119	1869.3
Crib3W14x32	0.14	0.32	0.32	0.119	528.7
Crib4D28x15	0.28	0.15	0.15	0.403	207.4
Crib5D28x15	0.28	0.15	0.15	0.414	201.8
Pool1D28x15	0.28	0.15	0.00	0.1557	536.6
Pool2D28x15	0.28	0.15	0.00	0.0472	1771.1
Pool2D28x30	0.28	0.30	0.00	0.0472	3542.2

6.6 Average Peak Result Summary

In order to present the experiment results and the model prediction in a global perspective, an average peak value was determined for the significant variables from each test. The variables are the fuel mass loss rate, the upper layer gas temperature, and the oxygen concentrations. The average peak value for both measured and predicted variables was determined in the following manner. The time interval corresponding to the fuel mass changing from 80 to 30 percent of its initial mass was identified. This method is consistent with the averaging method used in the CIB test [7]. All variables were numerically averaged over this time interval to yield the average peak values. Note for

the upper layer temperature peak value, generally the gas temperature measured at the vent is the best representation of the upper layer gas temperature; however, in some cases, the flame extended outside the compartment through the vent and the thermocouple might measure the local flame temperature instead of the average outflow gas temperature. Hence, in addition to the average peak value for the temperature at the vent, the near back wall temperature was also presented. Arbitrarily the averaged gas temperature at the vent was defined as the arithmetic average of thermocouples TC3 and TC4, and for the temperature near back wall, thermocouple TC14 was selected for averaging. Table 6.4 gives the summary of the peak average results.

Table 6.4 Peak Average Summary

Test	$\dot{m}''_F$ [g/m^{2}s] Fuel mass loss rate	T_{vent} [ºC] Vent gas temperature	T_{back} [ºC] Near back wall gas temperature	$X_{ox,u}$ [%] Upper O_2 volume conc.	$X_{ox,l}$ [%] Lower O_2 volume conc.	$\dot{m}''_{F,o}$ [g/m^{2}s] Free burning rate
Crib1D28x15	11.62	543	425	0.86	20.14	17.50
Crib1W14x20	8.50	402	414	1.05	16.09	17.50
Crib1W14x32	9.30	506	423	0.97	19.11	17.50
Crib2D28x05	7.14	338	423	3.92	6.17	10.95
Crib2D28x15	11.62	566	539	0.09	18.48	10.95
Crib2D28x30	12.06	565	470	0.88	19.16	10.95
Crib2D28x40	13.79	533	439	0.79	18.66	10.95
Crib2W14x06	2.75	294	362	5.55	9.44	10.95
Crib2W14x32	10.44	504	549	2.39	16.46	10.95
Crib3D28x30	13.06	565	380	0.88	19.16	16.84
Crib3D28x40	13.52	339	339	10.12	20.06	16.84
Crib3W14x32	10.73	384	409	6.96	15.55	16.84
Crib4D28x15	7.41	650	527	0.24	5.96	12.07
Crib5D28x15	7.11	695	669	0.23	10.22	8.63
Pool1D28x15	12.80	448	357	1.43	2.68	54.66
Pool2D28x15	19.40	576	432	1.36	1.84	22.69
Pool2D28x30	55.59	728	453	1.55	19.67	22.69

All experiments were simulated by the single-zone model and the peak average values from the simulations were also determined by the same process as described for the data. Note that for the model simulation, unless stating otherwise, the measured free burning rate is used as an input for $\dot{m}''_{F,o}$ in Eq. (5.41) instead of using the correlation given in Eq. (5.42) and (5.43) for the corresponding crib and pool. All other inputs and control variables for the wood crib and heptane pool fire simulation are summarized in the Appendix. Figures 6.6 to 6.7 show the comparisons of the peak average values from the experiments and the simulations.

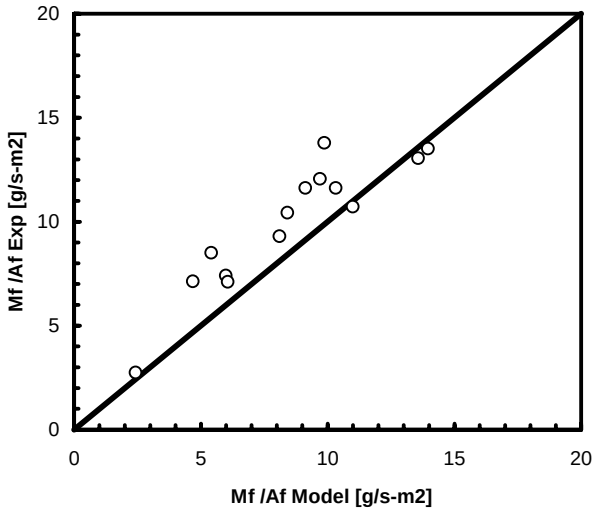

Figure 6.5Comparison of peak average fuel mass loss from experiment and prediction

From the comparison in Figure 6.5, the single-zone model is able to predict the fuel mass loss rate reasonably well, although it slightly underestimates in some cases. In Figure 6.6 the peak average gas temperatures comparison are shown. As mention before, the peak average values are determined for both temperatures measured at the vent and near the back wall. The upper end of the error bar represents the peak average value of the vent temperature and the lower end for the back wall. The plot between each end

signifies the space average temperature from these two locations. The comparison in Figure 6.6, the model is able to predict a reasonable result for the gas temperature.

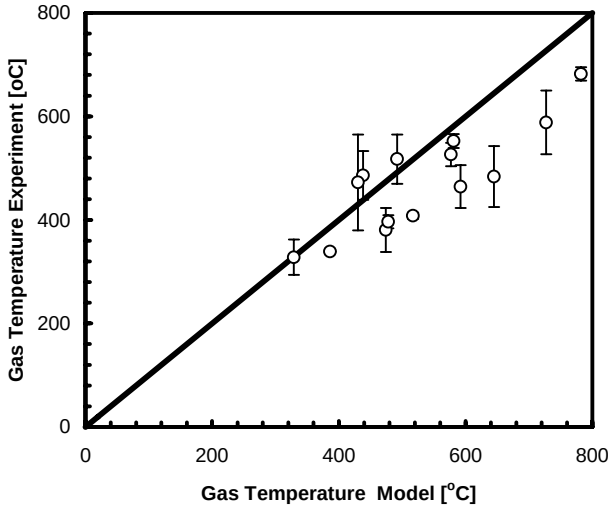

Figure 6.6 Comparison of peak average gas temperature from experiment and prediction

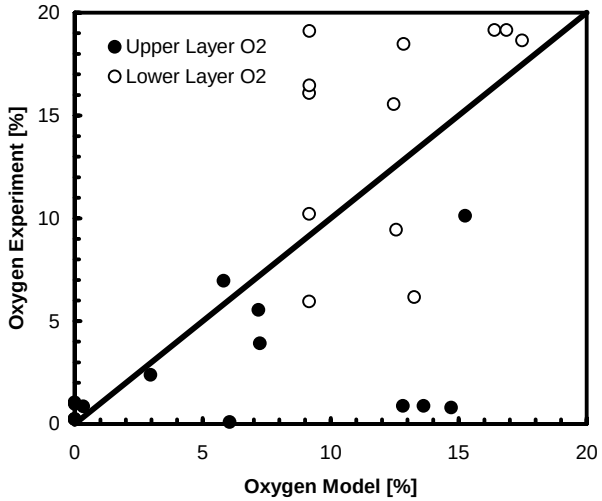

Figure 6.7 Comparison of peak average oxygen fraction from experiment and prediction

As for the oxygen concentration, the prediction seems to exhibit some agreement with the experiment, although it also shows fairly large discrepancy in some cases. We believe this could be due to the interference from the flame in some cases where the

oxygen probe in the upper layer was located inside or at the flame sheet. Another possible reason is the limitation of the mixing model which is based on a well-mixed condition and becomes too strong for the cases where the stratified smoke layer is well above the floor. In addition, the oxygen concentration in the lower layer is usually less uniform then that in the upper layer (shown in Chapter 3), hence a single point measurement of the oxygen may not be a good representation for the "average" concentration for the entire layer.

6.7 Observations and Burning Behavior

The observations were made during the experiment and through the recorded video. For the wood crib fire tests, the flame generally took up to 1 minute to propagate throughout the crib due to the non-uniform ignition. The smoke from the wood crib fire tended to have a lighter color than that of the heptane pool fire. *Clean burn*, the situation where all the soot was completely burned and no soot residual was left on the walls, was observed in the wood crib experiments due to an achievement of the maximum temperature of 890ºC (Crib5D28x15). No complete flame extinction was observed in any experiments. From the observations we found that the burning behavior of both wood crib and heptane fires mainly depend on the room ventilation condition and can be categorized into 3 cases as follows:

1) *Steady well-ventilated burning*: This is the case where the opening is large and the flame behavior is somewhat similar, although not identical, to the free burning since there is plenty of air supply. The flame stabilizes above the fuel package and the oxygen in the upper layer usually is well above zero percent. The global equivalence ratio (GER

is less than one. (Note that the global equivalence ratio is given by $\phi = \dot{m}_F \cdot s / \dot{m}_o$, where the air flow is estimated by $\dot{m}_o = 2/3 \rho_o C_d A_o \sqrt{H_o} \sqrt{2g(1 - T_o/T)} \left[1 + (T/T_o)^{1/3}\right]^{-3/2}$ [2])

2) *Steady under-ventilated burning*: This is the case where the opening size is reduced and the air supply is less than its stoichiometric value. The burning becomes ventilation controlled and a shrinking in burning area is observed. Oxygen concentration in the upper layer in this case is at (or close to) zero since all the incoming air is consumed and the GER is above one.

3) *Unsteady under-ventilated burning*: This is the case where the opening is very small and the flame becomes unsteady due to periodic flame extinction. Both *oscillating flames* and *ghosting flames* were observed. The GER is above unity.

Note that these 3 cases are consistent with the first three burning regimes addressed by Hu et al. [34] using a CFD model to predict for the two-slit-vent compartment fire experiment conducted by Utiskul et al [33].

In order to show dependence of the burning behavior on the room ventilation, the peak average fuel mass loss rates per unit fuel area from all tests are presented in Figure 6.8 with the *ventilation factor*, $A_o \sqrt{H_o} \rho_o \sqrt{g} / A_F$, which is the same parameter used before by Harmathy [17] and Bullen and Thomas [20] to present the fuel mass loss rate data for various fuel types and configurations. This parameter generally shows the effect of room ventilation to the burning behavior. However, as described by Utiskul et al. [33] and Quintiere [87] there are other parameters such as the enclosure heat transfer (wall surface area, heat loss, etc), and the specific fuel properties (heat of gasification and heat of combustion for a specific fuel) that can also influent the burning. Hence, a generality for all types of data may not be achieved by using this parameter alone.

The wood crib and liquid pool data from Harmathy [17] and Bullen and Thomas [20] are also included in this plot. The symbol legend used for presenting the peak average values is given as following. Generally, □ and + signify a wood crib fire; ○ and × represent a liquid pool fire. The open symbols signify – case 1 (steady well-ventilated burning); half-filled symbols – case 2 (steady under-ventilated burning); filled symbols – case 3 (unsteady under-ventilated burning).

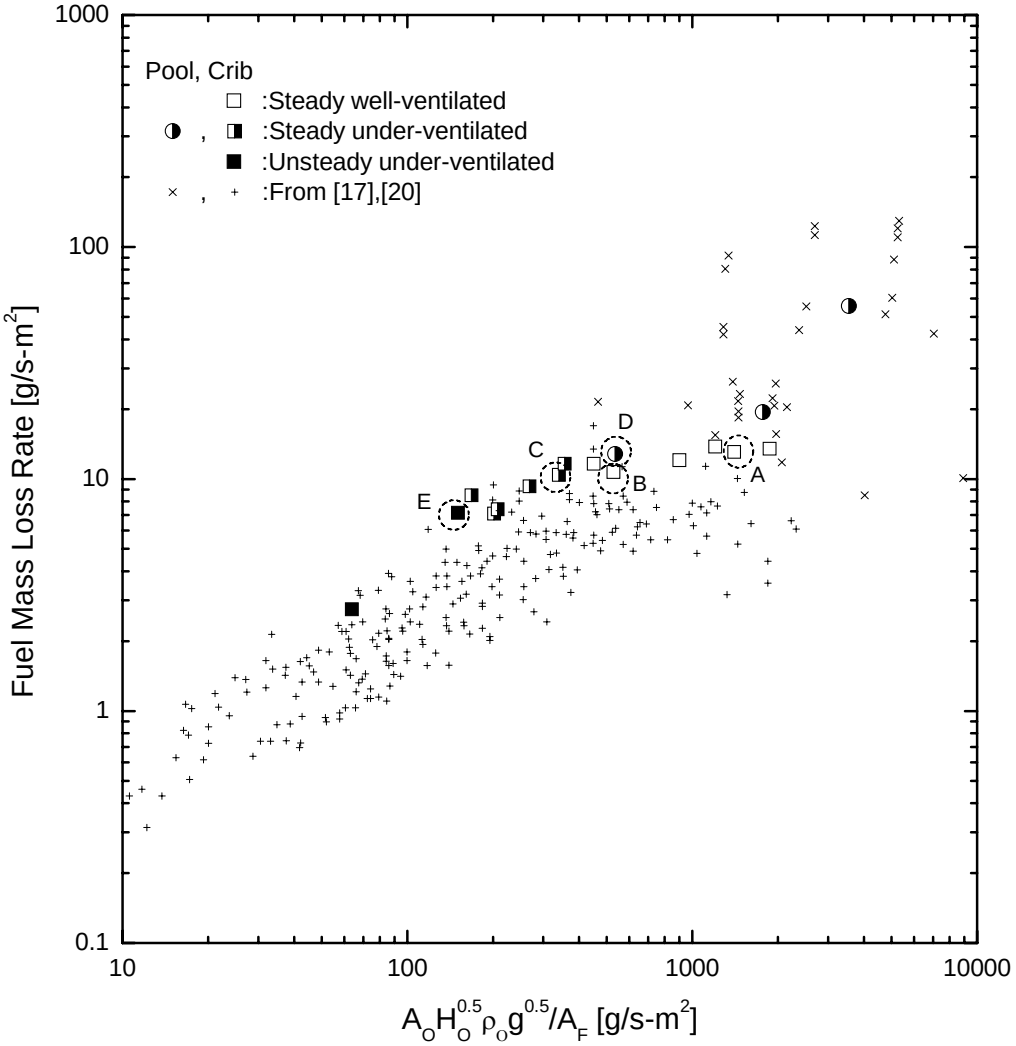

Figure 6.8 Dependence of the peak average fuel mass loss rate from current study and [17, 20] on the ventilation factor

It can be seen from Figure 6.8 that our data are consistent with the existing data from various scale experiments and span over a good range of ventilation. The data also show the regime of each burning category based on the ventilation factor: above the ventilation factor of 400 g/m^{2}s, the burning is steady well-ventilated (case 1); between 150 to 400 g/m^{2}s – steady under-ventilated (case 2); and below 150 g/m^{2}s – unsteady under-ventilated (case 3). Harmathy [17] defined a boundary, for wood crib data, for the *ventilation controlled burning* and the *fuel controlled burning* at the ventilation factor of 260 g/m^{2}s which is lower than what is found in our wood crib data at 400 g/m^{2}s.

We will discuss further on each burning category along with the dynamic results and the model prediction from the selected tests that represent such category. The selected tests are marked by the dash-circles labeled with the letter A to E on Figure 6.8. The complete experimental results and the prediction for all tests are also found in the Appendix.

6.7.1 Case 1: Steady well-ventilated burning

Figure 6.9 shows the dynamics results along with the single-zone model prediction from Test A (Crib2D28x30). Figure 6.10 shows the snapshot photo of this test. The GER is estimated to be 0.45. The free burning rate from the same type of crib (Crib2) is also shown in Figure 6.9 (bottom right), and the solid line on the same chart represents the free burning rate "input" for the simulation. The measured compartment fuel mass loss rate shows a 35% value higher than its free burn value. The lower layer oxygen in this case barely changed from its ambient value. This shows that the *oxygen effect* (or *ventilation effect* in Chapter 2) to the burning is very minimal, and the

contribution on the change of the fuel mass loss rate is mainly from *the thermal feedback* thus enhancing the mass loss rate. Signified by the dark solid lines, the single-zone model predictions are overlaid onto the measured variables. The predicted flame and the thermal feedback effects are also shown. In this case the model seems to underestimate the fuel mass loss rate and slightly for gas temperature. The reason can be that since the smoke layer height in this case is stratified and located well above the floor (as shown in Figure 6.11 to be approximately 50% and estimated by Eq. (4.5) to be 47% of the opening height), the assumption for the single zone may not be well satisfied. The near vent mixing model is then "too strong" for this case and causes the predicted oxygen feeding the flame to be too low, hence the underestimated fuel mass loss rate.

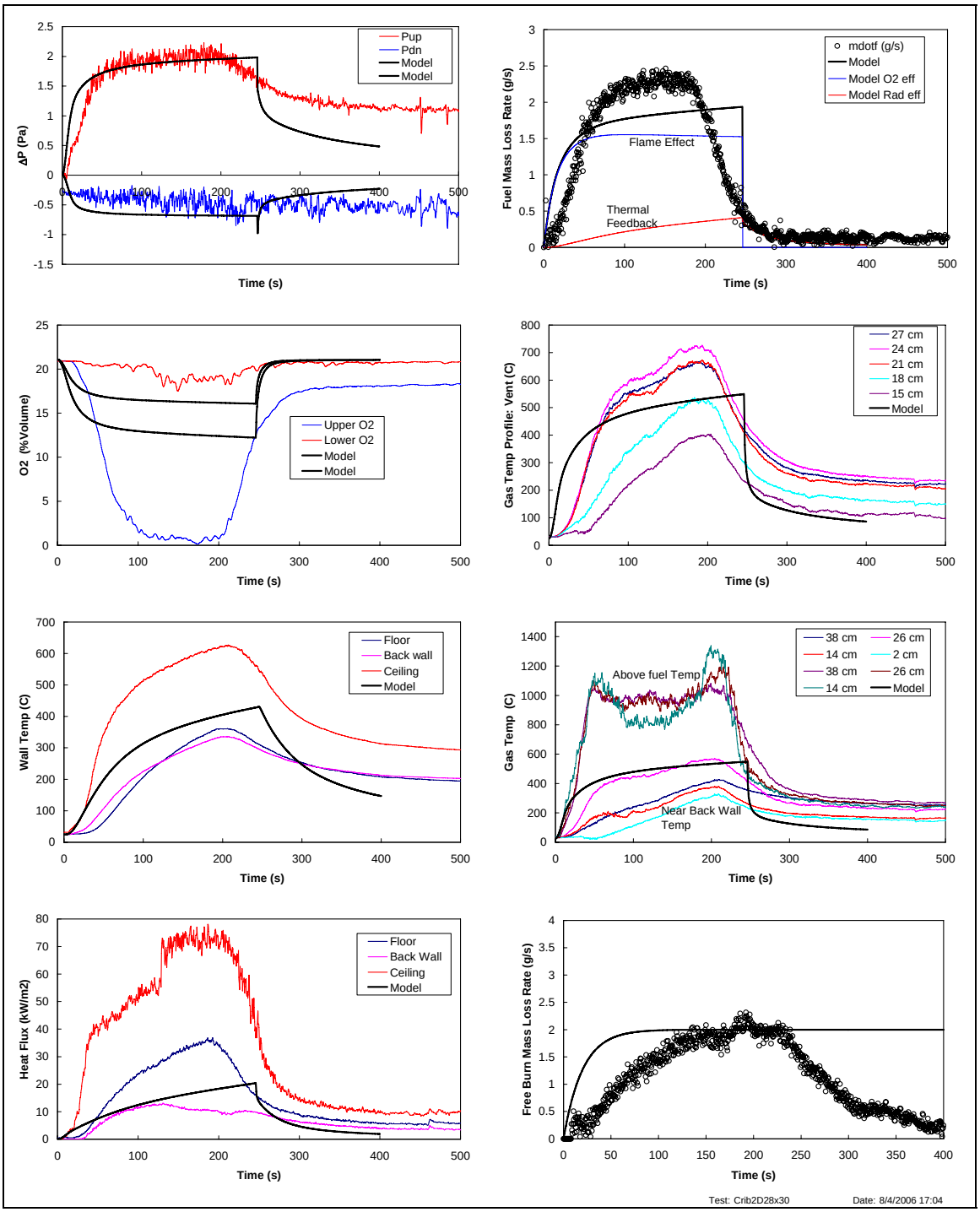

Figure 6.9 Transient result for wood crib fire Case 1 (Test A: Crib2D28x30), GER = 0.45

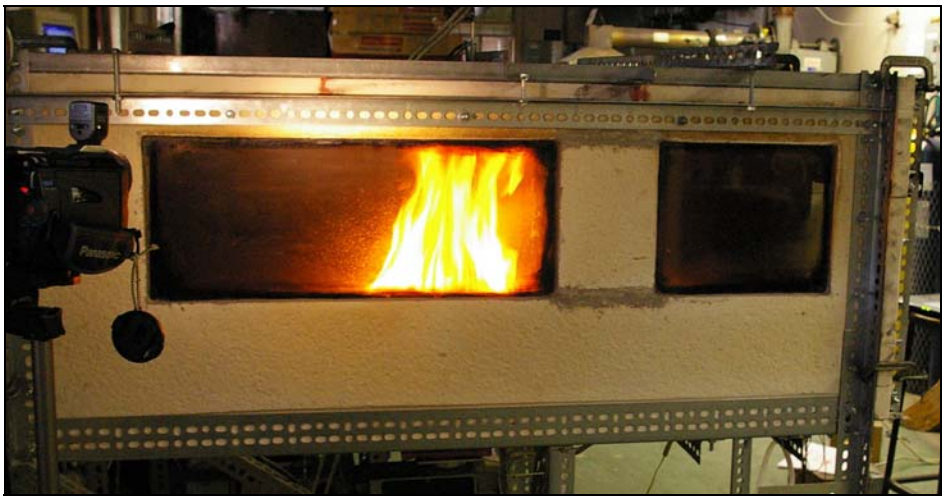

Figure 6.10 Photo snapshot for wood crib burning in case 1 (Test A: Crib2D28x30) showing a steady burn above the fuel package

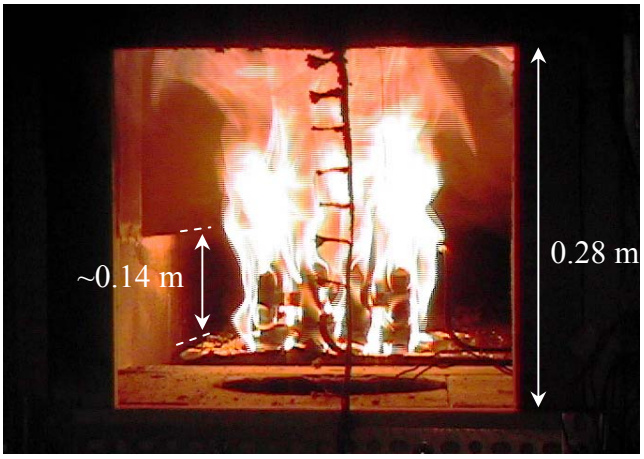

Figure 6.11 Caption showing approximated stratified smoke layer height (Test A: Crib2D28x30)

Figure 6.12 shows the dynamic results from the wood crib experiment Test B (Crib3W14x32). The GER is estimated to be 0.72. The measured compartment fuel mass loss rate is 30% less than its free burning rate value. This reason is due to the oxygen effect on the flame radiation as seen by the oxygen concentration in the lower layer that decreases to 15%. On the other hand, the oxygen volume concentration in the upper layer reaches a minimum of 6% which shows that all oxygen is not completely consumed and

the burning is still well-ventilated. The predicted fuel mass loss rate shows good agreement to the measurement. Except for the gas temperature that is overestimated, in this case the model is able to provide a good prediction for most part.

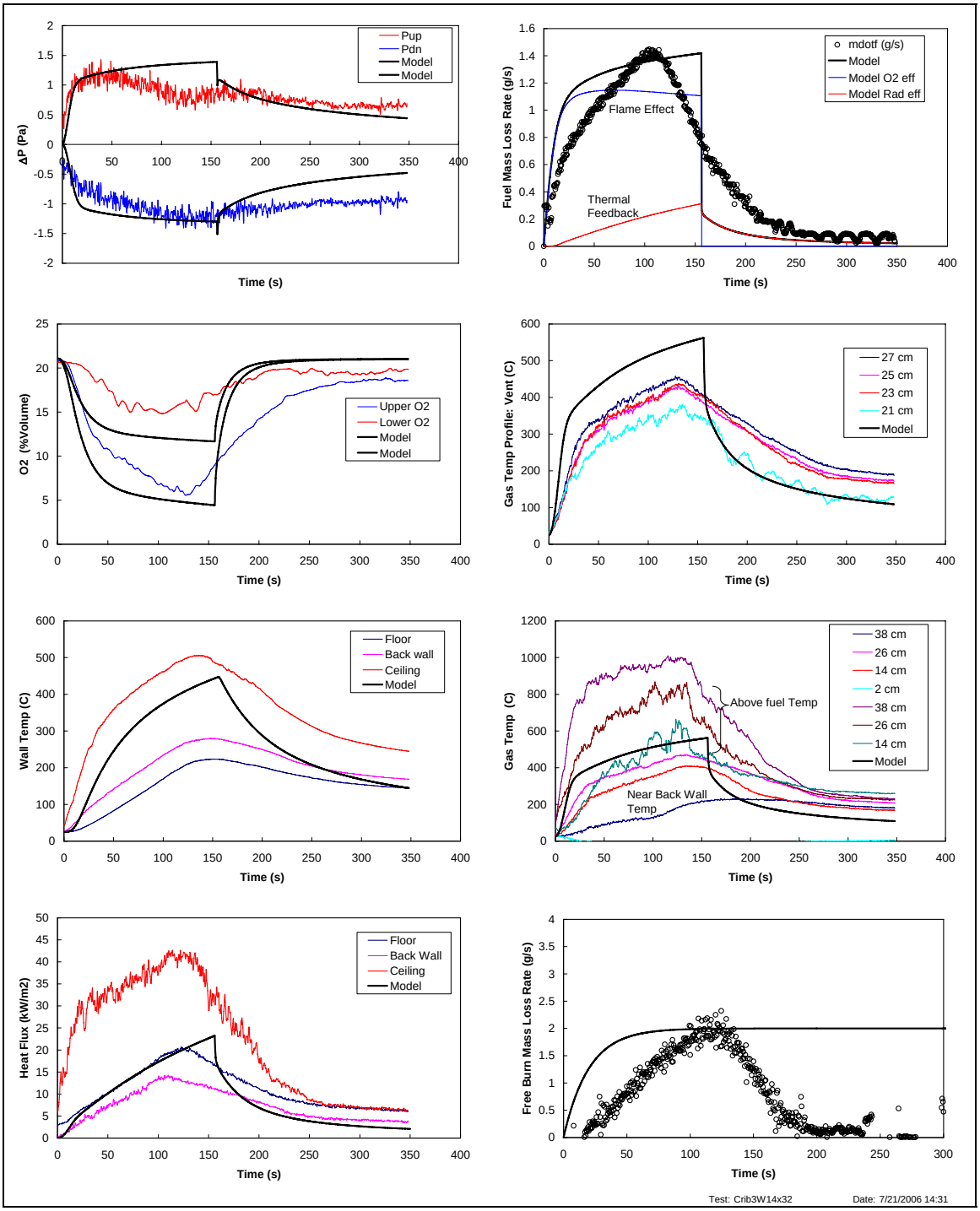

Figure 6.12 Transient result for wood crib fire Case 1(Test B: Crib3W14x32), GER = 0.7

6.7.2 Case 2: Steady under-ventilated burning

For this case, at the growing phase, the fire behaved similarly to Case 1 until the condition became ventilation-limited and the burning is controlled by the available air. The flaming area reduces here and the fire extends out of the vent. Figure 6.13 shows the transient results for Test C (Crib1W14x32). In this case, due to the non-uniform ignition, the flame took almost 60 seconds to spread throughout the crib. The recorded video shows that once the flame uniformly covered the entire crib, the fire grew similarly to free burning for about 50 sec then the flaming area started to shrink (as shown in Figure 6.14c) due to the ventilation limited condition. This corresponds with the measurement for the fuel mass loss rate that shows a drop and the oxygen in the upper layer reaches zero percent at time ~ 110 sec. The prediction is able to show the same shrinking over time consistent with the measurement. In other words, had the fire been ignited uniformly, the prediction would have matched the time at which the burning area shrank and the fuel mass loss dropped. An attempt to estimate the shrinking burning area has been made from video observation as shown in Figure 6.14. This estimation is presented along with the prediction from the model in Figure 6.13.

The model seems to slightly underestimate the fuel mass loss rate, while matching well with the peak gas temperature measured at the vent. In this case the compartment fuel mass loss rate is 50% lower than its free burning value because of two reasons: 1) the oxygen effect is more dominant than the thermal effect and 2) the reduction in burning area due to ventilation limited condition.

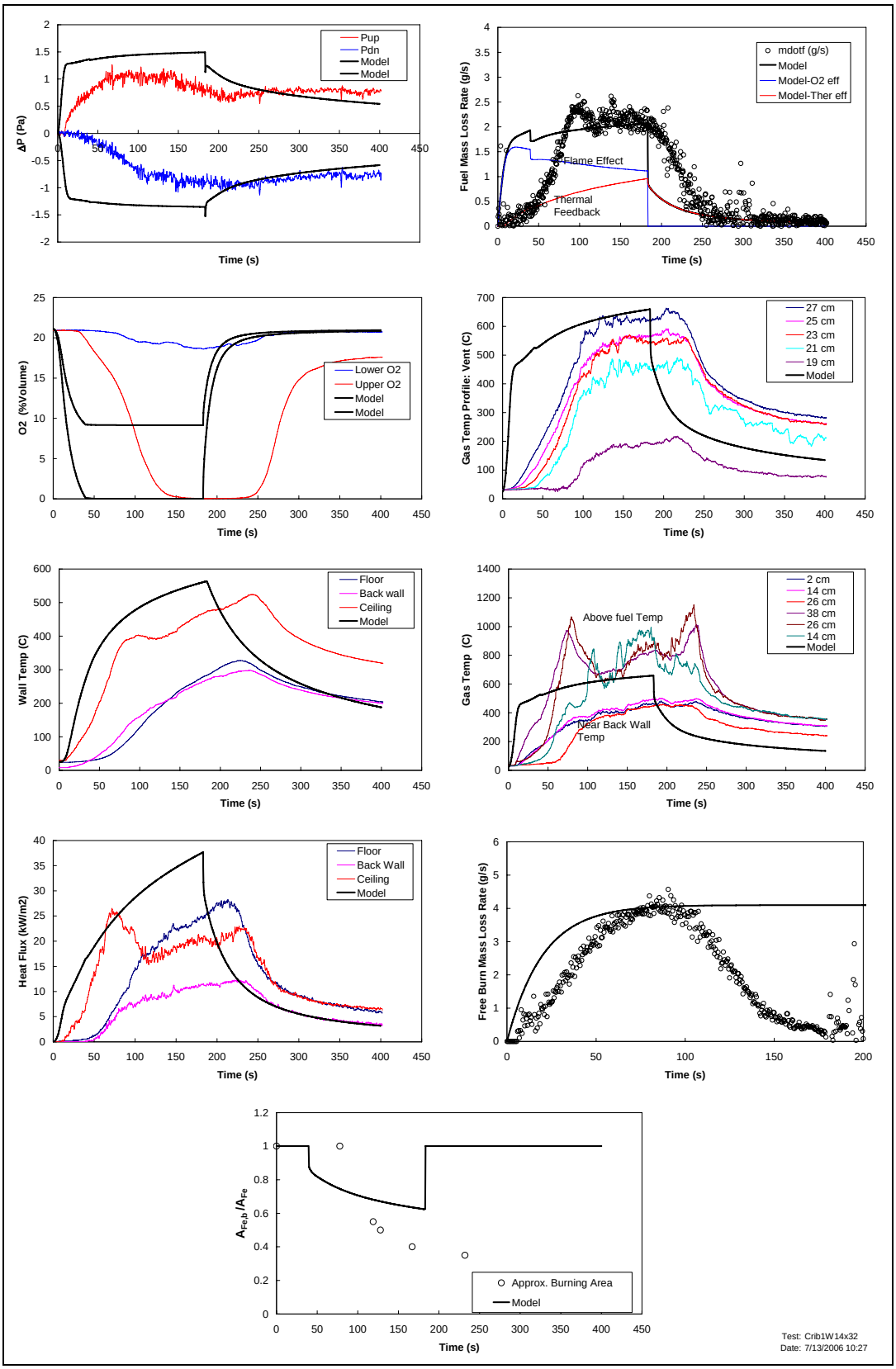

Figure 6.13 Transient result for wood crib fire case 2 (Test C: Crib1W14x32), GER = 1.2

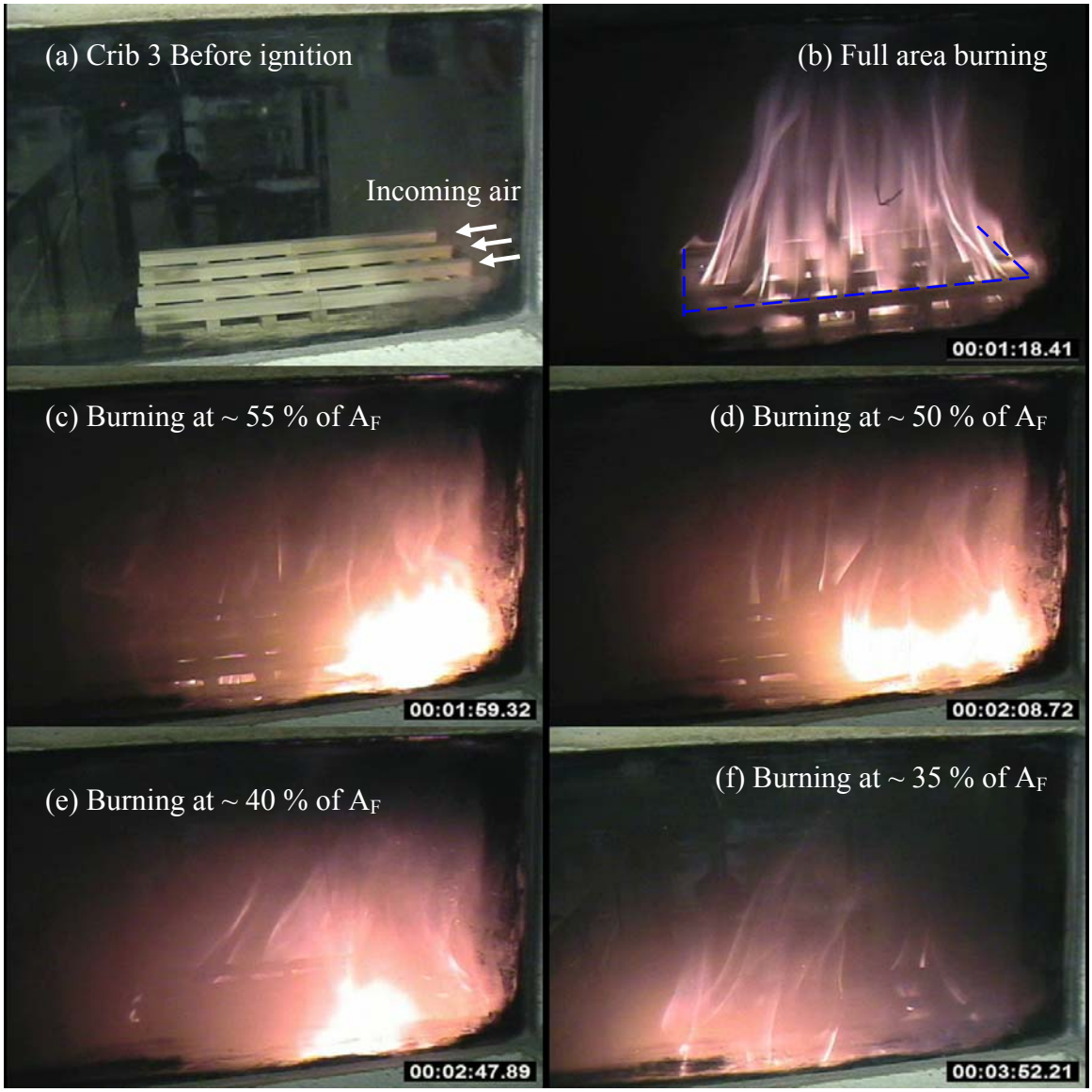

Figure 6.14 Caption showing estimation for the reduced burning area in under-ventilated burning, wood crib experiment Test C (Crib1W14x32)

All heptane pool fire experiments in this study were found to be in the steady under-ventilated burning (Case 2). The dynamics of the flame is similar, but not identical to that of the wood crib fire since the liquid pool fire is more sensitive to the thermal radiation feedback. The heptane pool experiment, Test D (Pool1D28x15) is shown in Figure 6.15 and some explanations are given as follows. In this test a series of 10 heptane

pans were distributed over the load platform. The ignition was started at the fuel pan located closest to the vent and the flame propagated through all other pans almost immediately. Since the heptane fuel exposing area was large and the gasified fuel was more than a stoichiometric need, the burning condition reached the ventilation-limited condition quickly. This is shown by the measured oxygen approaching near zero percent at about 20 s after ignition. Shrinking in burning area was observed and the flame was then stabilized near the vent. This case is an example of the classical ventilation-limited burning where the most of the flame burns outside of the vent (shown in Figure 6.16f). Note that the gas temperature measured across the vent in this case is basically the flame temperature. Despite the enhancement from enclosure thermal feedback, the measured fuel mass loss rate is much lower than the free burning rate because of the reduction in the burning area and the change of the flame location. As for the model prediction in this case, the model shows a sharp peak in the fuel mass loss rate about 5 s, then a sharp decrease due to the ensuing ventilation-limited condition. The shrinking in burning area predicted by the model is consistent to the estimation made from the video observations. Overall, the model did a reasonable job for this case; it slightly over-predicts the mass loss rate but underestimates the gas temperature. However, the reduction in mass loss rate due to area shrinking is well captured.

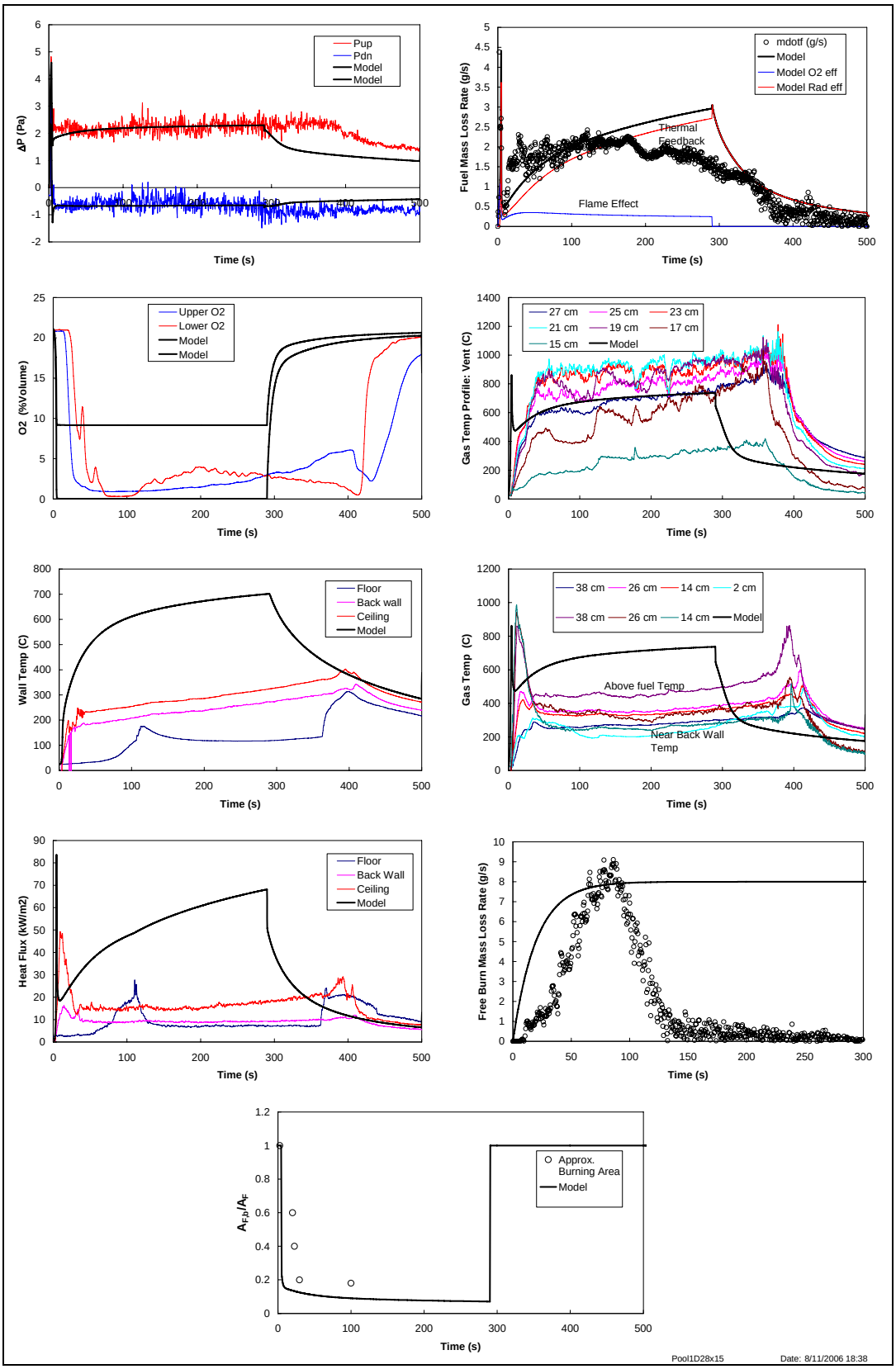

Figure 6.15 Transient result for pool fire Case 2 (Test D: Pool1D28x15), GER = 3

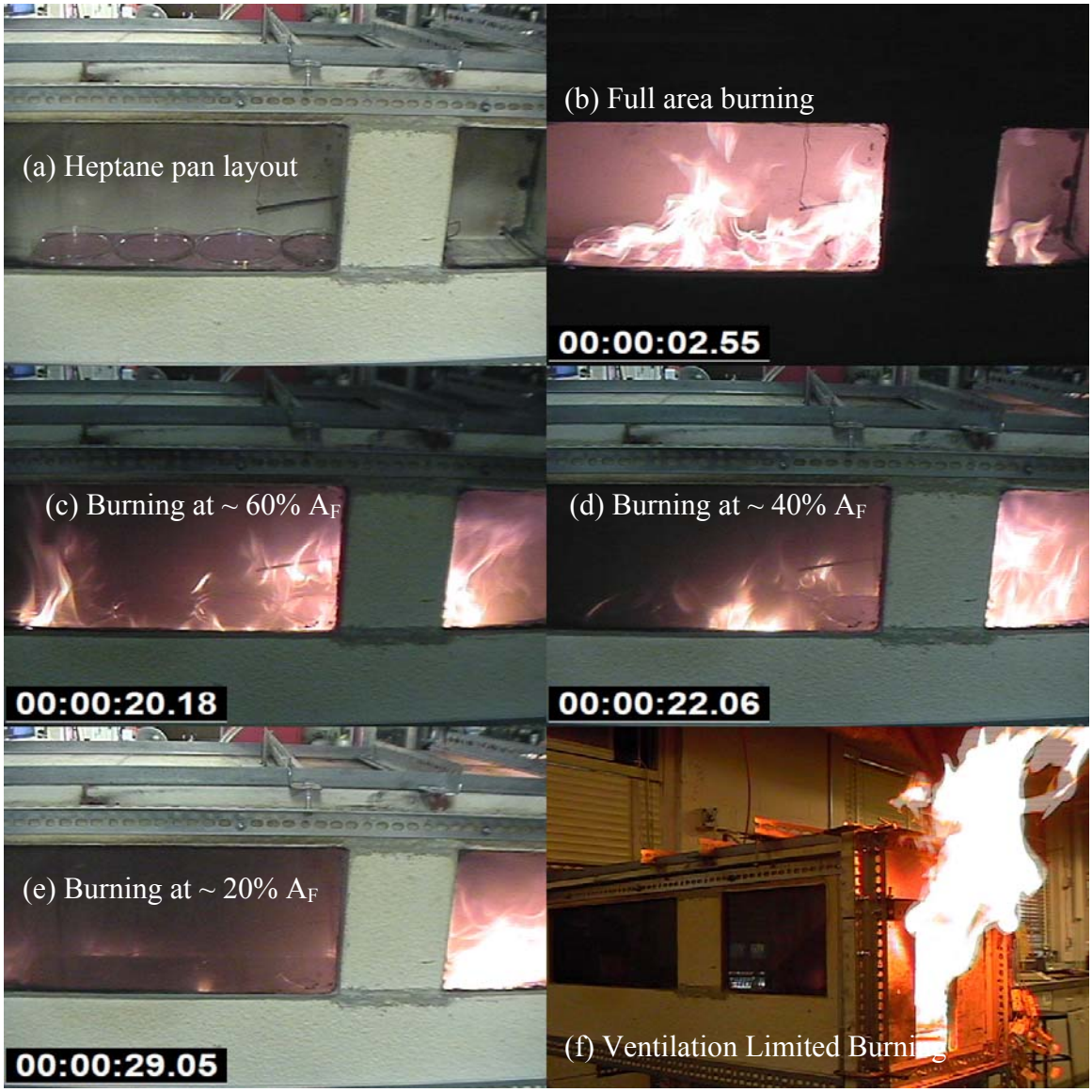

Figure 6.16 Caption showing estimation for the reduced burning area in under-ventilated burning, heptane pool fire experiment Test D (Pool1D28x15)

6.7.3 Case 3: Unsteady under-ventilated burning

Unsteady flames usually occur in a very low ventilation condition and can appear in several forms such as a periodically *oscillating flame* stabilizing above the fuel bed, and a *ghosting flame* that drifts away from the fuel bed with temporally extinction. Takeda and Akita [12] have observed the unstable oscillation flames of methanol and

PMMA pool in their compartment fire experiments, and identified the ventilation regime that these behaviors were seen. The recent study by Utiskul et al. [33] also showed both oscillating and ghosting flame phenomena of a heptane pool in a two-slid-vent small-scale compartment fire. Chamchine et al. [97] have also seen this type of unsteadiness flame in their experiments using a hydrocarbon gas fuel.

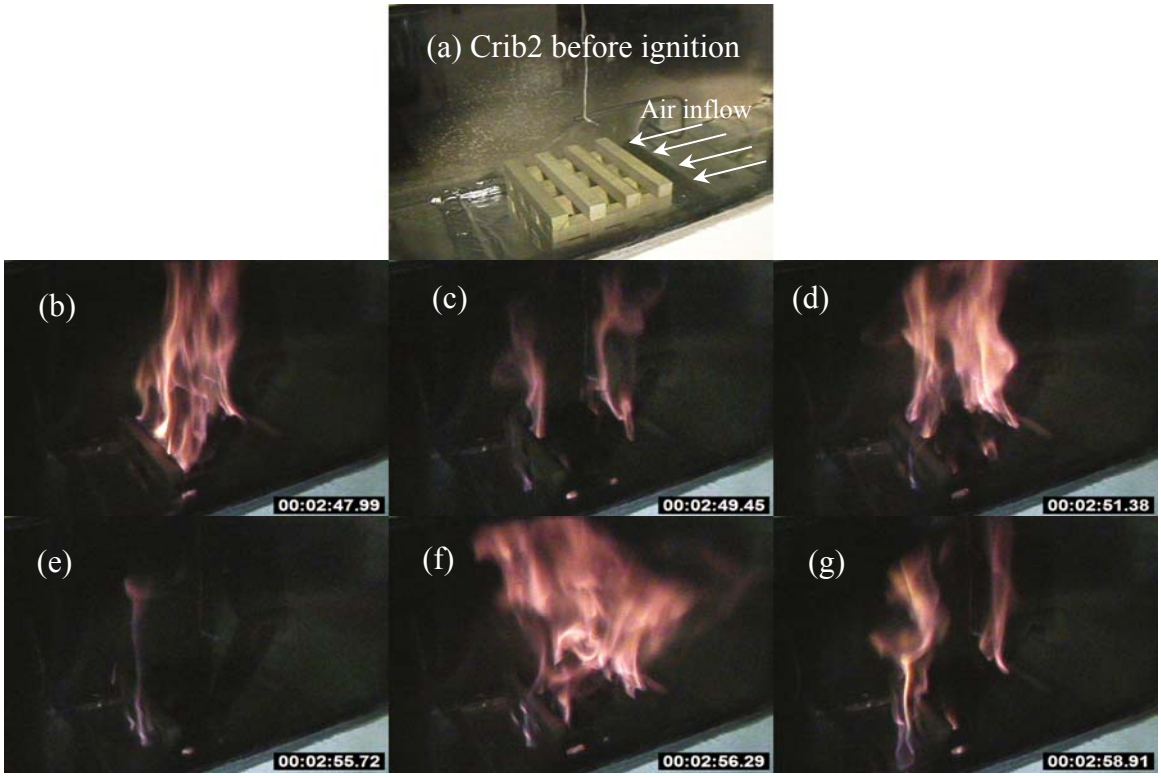

Figure 6.17 Photo sequence capturing the wood crib oscillating flame in unsteady under-ventilated burning Test D (Crib2D28x5)

In this study, we also observed the unsteady flame in our wood crib experiments as well. Figure 6.17 shows the photo sequence capturing the oscillating flame from Test E (Crib2D28x5). The GER is ~ 1.8. The dynamic results for this test area shown in Figure 6.18. The fuel mass loss rate was significantly lower than the free burning rate due to the reduction in oxygen feeding the flame, and hence resulted in much longer burning

time. In this test, we observed a slow frequency (approximately 0.3 - 0.5 Hz) for the oscillating flame clearly seen after 1 min. and lasted until the fuel was exhausted.

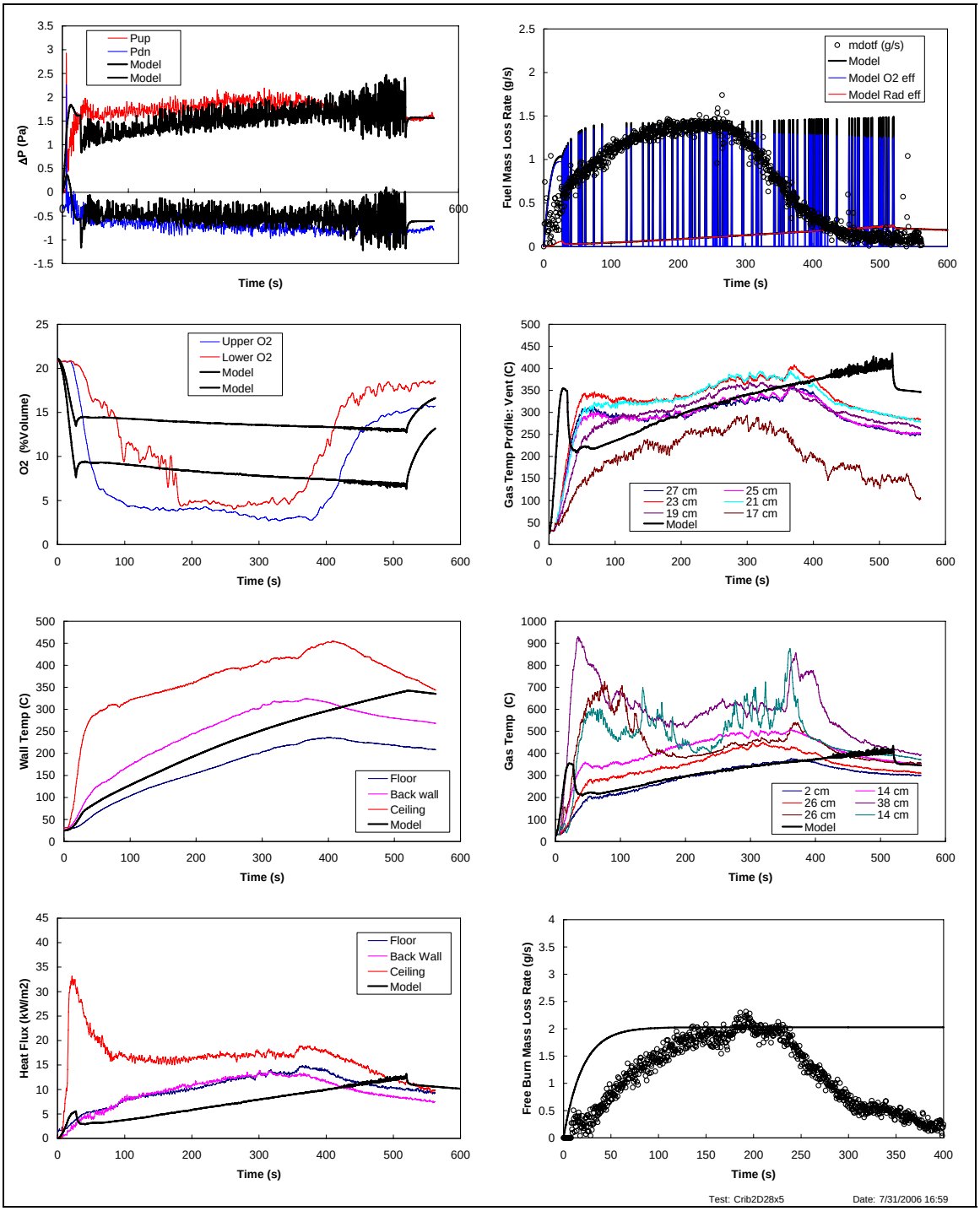

Figure 6.18 Transient result for pool fire Case 3 (Test E: Crib2D28x5), GER = 1.8

The oscillating, or on-off flame phenomena, were also evident from the measurements of the pressure difference and the gas temperatures at the vent. We offer an explanation for this flame behavior as follows: As the oxygen concentration feeding the flame decreases the flame becomes weak [22] and is almost extinguished, the compartment temperature also reduces. The sudden change in temperature causes the change in the differential pressure and induces the fresh air into the compartment. This fresh air then revitalizes the flame which later causes the sudden increase in temperature and again consumes most oxygen; hence the process repeats. As for the prediction in this case, the model gives a reasonably good simulation for both effects. It is able to capture the oscillating phenomenon as shown in the predicted mass loss rate and the pressure differences. Nevertheless, it is worth mentioning that although the oscillating flame phenomena involves the extinction and re-ignition events, the current single zone model uses the critical flame extinction criteria, Eq. (5.38), for both events; a true ignition model has not been included in the current work.

In this case, although the global equivalence ratio is more than one, the oxygen in the upper layer from both measurement and prediction shows more than zero percent. This means that all oxygen is not consumed due to the temporary flame extinction. In other words, the flame reaches its extinction criteria before the ventilation limited condition prevails.

6.8 Generality of the Results

Previously in section 6.7 (Figure 6.8), a global perspective of the fuel mass loss rate dependence on the ventilation factor ($A_o\sqrt{H_o}\rho_o\sqrt{g}/A_F$) has been presented for the data from this study and the large scale database. However, the ventilation factor alone may not be sufficient to show the generality of the compartment fire data. Dimensionless analysis by Utiskul et al. [33] shows that besides the ventilation factor, other variables such as the compartment wall heat loss, specific fuel properties, and length scale can also influent the compartment fire burning behavior. The wall heat loss is expressed in terms of the total heat loss to the fuel flow as $h_{total}A_s/\dot{m}''_{F,o}A_Fc_p$, where h_{total} is the total heat transfer coefficient (convection and radiation). In this section, the effect of the ventilation ($A_o\sqrt{H_o}\rho_o\sqrt{g}/A_F$), wall heat loss (A_s/A_F), length scale, and fuel type and configuration will be examined using the experimental results and the single-zone model prediction to potentially show the generality of the compartment fire model.

The peak average results presented in section 6.6 will be used here. The model was run for a wide range of ventilation for three wood crib configurations (Crib 1 to 3) and one heptane pool (Pool 1). The peak average value for the prediction was also determined similarly to the experiment. The symbol legend used for presenting the peak average values is given as following. Generally, □ and solid line signify – a wood crib fire; ○ and dash line – a liquid pool fire; the open symbols – case 1 (steady well-ventilated burning); half-filled symbols – case 2 (steady under-ventilated burning); filled symbols – case 3 (unsteady under-ventilated burning). Each experiment plot and

simulation line is marked with the ratio A_s / A_F. Crib 1, 2, 3, and Pool 1 corresponds to A_s / A_F of 9, 12, 18, and 48 respectively.

6.8.1 Fuel Mass Loss Rate

Figure 6.19 shows the fuel mass loss rate per unit fuel area with the ventilation factor. The free burning rate is also presented on the right-vertical axis for each crib. The trend predicted by the model generally agrees well with the experiment for both wood crib and heptane fires. The regimes of burning (case 1 to case 3) based on the observation in the simulation are illustrated on the plot using the horizontal arrow-head line. The number marked on each regime corresponds to the case 1 to case 3 and the abbreviation "Ext" designates the complete flame extinction. As shown by the experiments and simulations on the figure, the burning behavior regime of the heptane pool and wood crib fire do not coincide with each other. For instance, at the same ventilation factor ($A_o \sqrt{H_o} \rho_o \sqrt{g} / A_F$) of 1000 g/m^{2}s, the pool fire is already in its ventilation-limited range while the crib fire is still in the well-ventilation regime.

The prediction of the crib shows that in the well-ventilated regime (case 1), the thermal feedback enhancement does not exhibit a strong effect on the mass loss rate and the flame (or oxygen) effect is more dominant as seen by the less value of the crib mass loss rate than its free burning rate. This is also consistent with the experimental result. In addition, no trend is observed for the area ratio, A_s / A_F, in the well-ventilated regime because the thermal effect is small and the crib mainly burns according to its free

burning. In other words, for non-porosity-controlled cribs, the stick size is responsible for the mass loss rate of the different crib configuration in the well-ventilated regime.

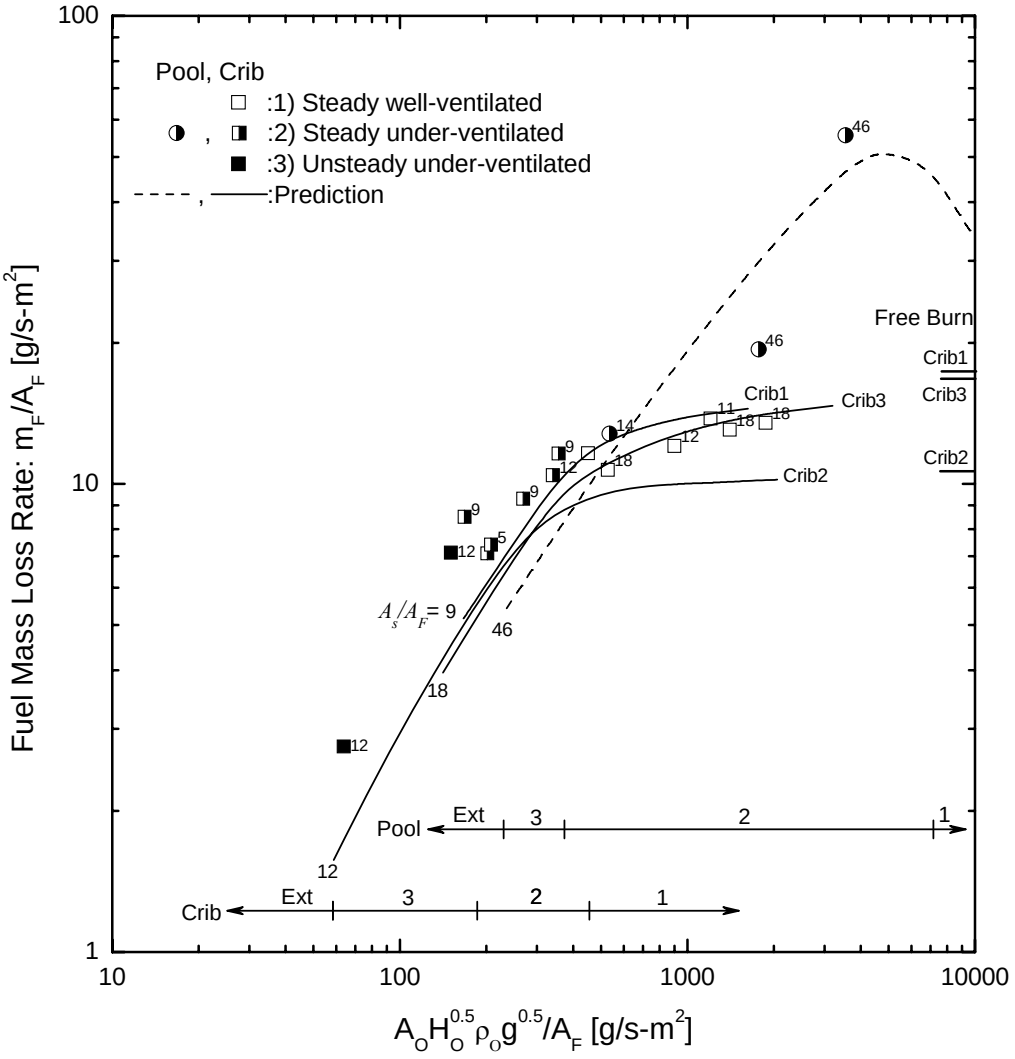

Figure 6.19 Dependence of the peak average fuel mass loss rate on ventilation and enclosure wall heat loss

In the under-ventilated regime (case 2 and 3), a general observation from the model and the experiment is that the mass loss rate decreases as the ventilation decreases. However, the wood crib burning dependence on A_s / A_F becomes clearer from the

simulation as the burning is now controlled by the air inflow, oxygen reduction in the lower layer and higher gas temperatures as the amount of fuel (A_F) is increased. Hence, without the scale differences, for ventilation-limited fires, the smaller the ratio A_s / A_F, the higher the mass loss rate.

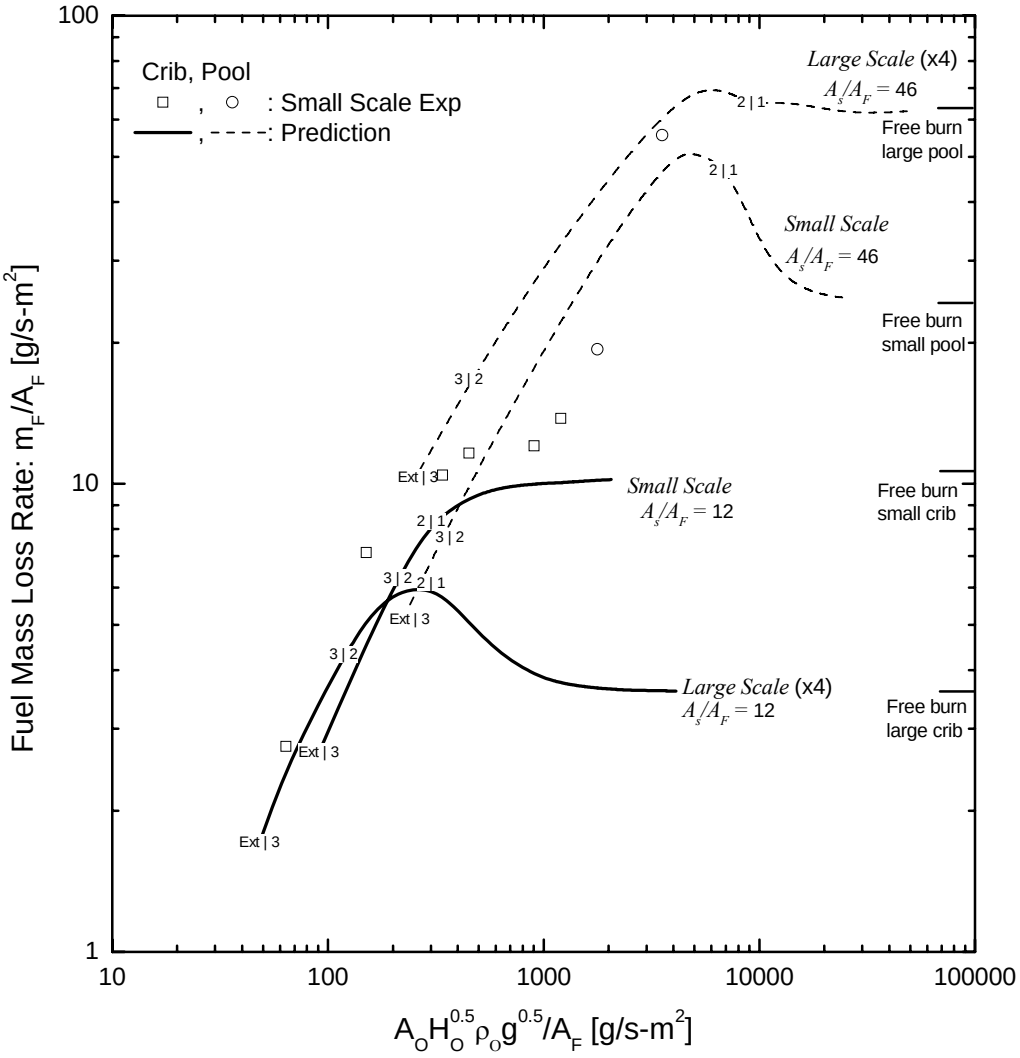

Figure 6.20 Scale and fuel type effects on the compartment fuel mass loss rate

The simulation from the mathematical model is used to investigate the effect of the scale on the burning. The compartment used in the large-scale simulation is geometrically scaled up 4 times from the compartment size used in the experiment. This gives a compartment height of 1.6 m. Crib 2 and Pool 1 are also scaled up similarly to preserve the A_s / A_F ratio. Note that the number of the sticks and layers of the crib does not change; only the stick length and thickness increase by 4. The mass of the fuel is consistent with the increased volume. The free burning rates for the large-scale heptane pool and wood crib are determined by Eq. (2.23) and (2.24) respectively. The results are presented in Figure 6.20. The experimental data from Crib 2 and Pool 1 are also included. Similarly to Figure 6.19, the free burning rates are also indicated on the right-vertical axis. On each prediction line, the marked number signifies the boundary of the burning regime. For instance, "2 | 1" indicates the boundary between case 1 and case 2 (the steady well-ventilated and the under-ventilated regime).

Note that the free burning rate per unit area of the large scale crib is less than the small scale crib because of the larger thickness (b) as defined in the Eq. (2.24), while the free burning rate per unit area of the large pool fire is larger then the small-scale one. The simulation shows for the small-scale pool that at the near ventilation limited (moving Case 1 to Case 2) the thermal effect is dominating as evident from the increase of the mass loss rate to a higher than its free burning value. In the large-scale pool case the thermal effect is less significant. This is reasonable because the larger-scale heptane pool fire has a higher flame emissivity than the small-scale ($\varepsilon_{f,pool}$ = 0.68 vs. 0.22); hence, the external heat feedback is "blocked" more by the sootier large-scale flame. However, the

wood crib fires exhibit an opposite behavior. In the small-scale crib, at the near ventilation limited, the oxygen effect is more dominated while in the large-scale crib the mass loss is enhanced more by the thermal feedback. This could be due to the nature of the heptane pool flame that is much sootier than the wood crib fire. In other words, the emissivities of both large-scale and small-scale wood crib are generally small ($\varepsilon_{f,\text{wood crib}}$ = 0.18 vs. 0.05); the higher thermal feedback in the large-scale case can penetrate through the wood crib flame and enhance the burning more than the small-scale case.

In the ventilation limited regime (Case 2 and Case 3) the large-scale configuration shows a higher mass loss rate in both wood crib and the heptane pool fire. Moreover, the flame oscillation in the large-scale simulation seems to take place at a lower ventilation condition than that in the small-scale. The flame extinction regime of the large-scale is also changed to a lower ventilation condition.

6.8.2 Gas Temperature

Figure 6.21 shows the peak average gas temperature from experiment and the simulation with the ventilation factor. The peak average values in the experiment are determined for both temperatures measured at the vent and near the back wall. The upper end of the error bar represents the peak average value of the vent temperature and the lower end for the back wall. The plot between each end signifies the space average temperature from these two locations. Similar to the previous shown fuel mass loss rate (Figure 6.19), the corresponding ratio A_s / A_F is presented on the plot and the prediction line. The trend mapped by the simulation follows the experiment data reasonably well.

The highest temperature from the simulation for both wood crib and heptane pool fire is found to be at the boundary of well-ventilated and under-ventilated regime, or at the point where the global equivalence ratio is unity. The effect of the wall heat loss to the temperature is quite obvious that the gas temperature increases as the ratio A_s / A_F decreases.

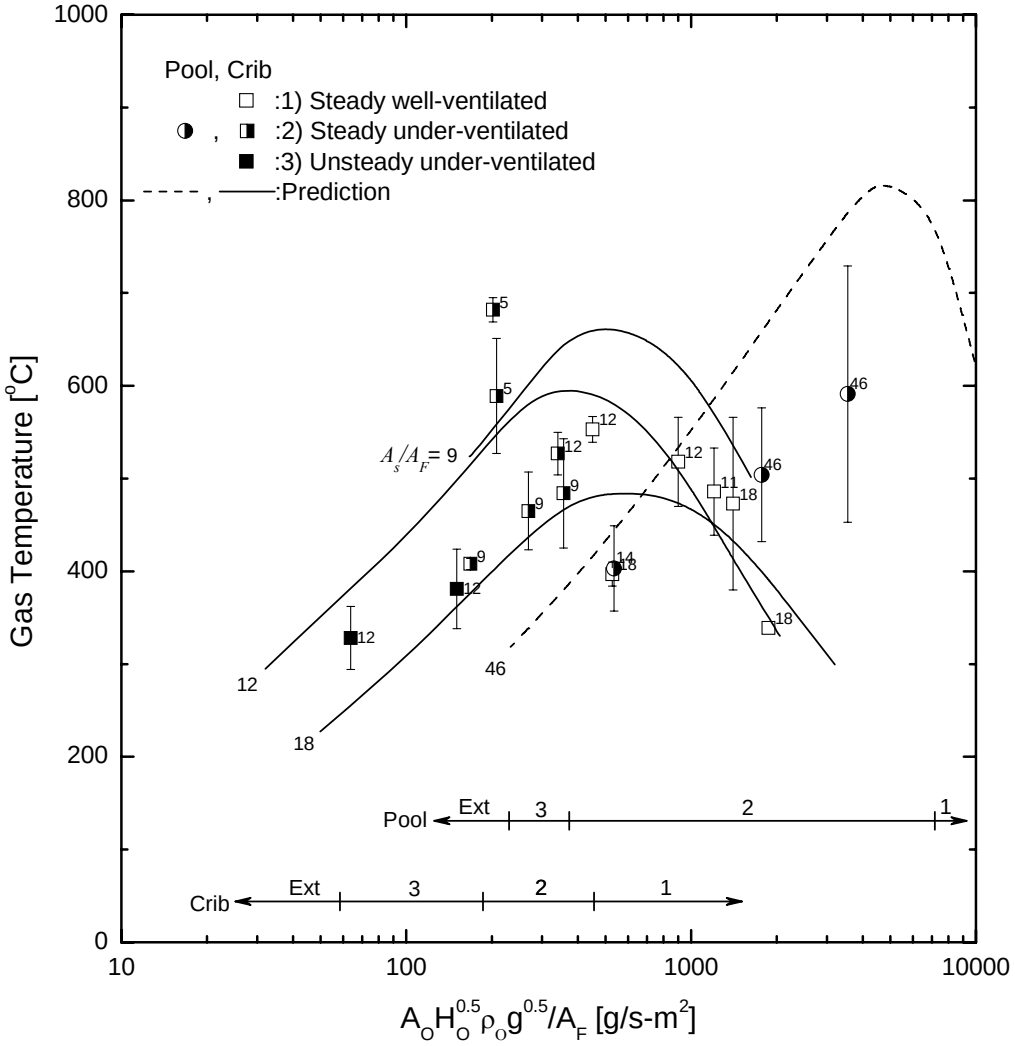

Figure 6.21 Dependence of the peak average gas temperature on ventilation and enclosure wall heat loss

The scale effect on the gas temperature is presented in Figure 6.22. The symbol legend and burning regime indication are similar to the description provided for Figure 6.20. For the liquid pool fire, the temperature predicted in the large-scale is higher than the small-scale throughout the range of the ventilation. As for the wood crib the large-scale only shows higher temperature than the small-scale in the ventilation limited regime. The temperature from the large-scale simulation exceeds the small-scale temperature at the boundary of the well-ventilated to under-ventilated regime; this confirms a strong thermal feedback from the hot gas layer to the fuel mass loss rate increasing significantly at this location as described in Figure 6.20.

Note that the temperature presented here is the average peak temperature, which does not represent the maximum temperature recorded in the experiments and the simulations. The maximum peak temperature measured from the largest wood crib experiment in our study is found to be at 890 ºC (from Crib5D28x15) and the prediction for this test yield a maximum temperature of 840 ºC. The dynamic results for this test can be found in the Appendix.

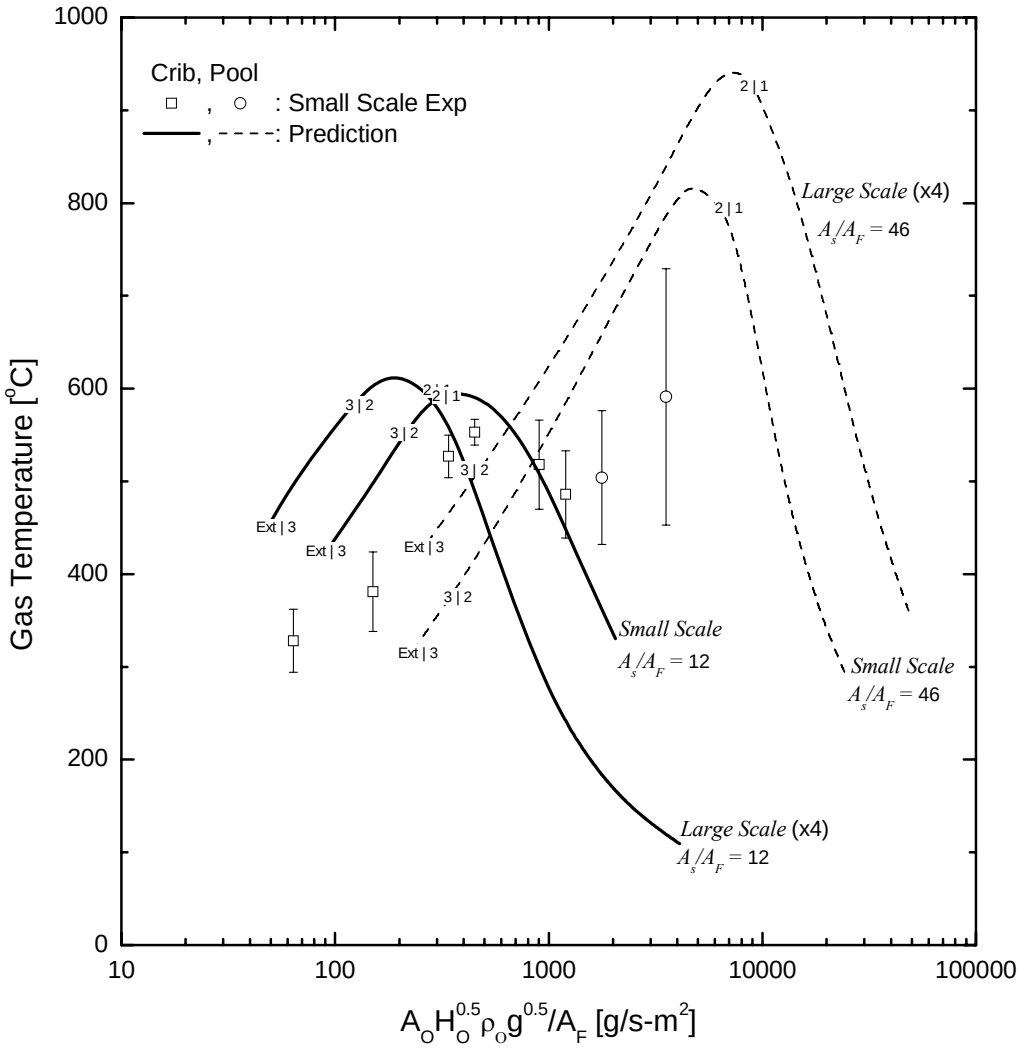

Figure 6.22 Scale and fuel type effects on the compartment fuel mass loss rate

6.8.3 Oxygen Concentration

Figure 6.23 shows the peak average upper layer oxygen volume concentration with the ventilation factor. The prediction and the experiment from wood crib and heptane pool fires show that the upper layer oxygen reaches near zero percent in the under-ventilated regime (case 2) which is consistent with the definition of the ventilation limited where all available oxygen is consumed by the flame. However, some peak

average upper oxygen data from the well-ventilated burning (Case 1) are also at near zero percent and we believe this is an error in the measurement as the oxygen probe is located in the flame sheet in some cases where the tip of the flame extends through the vent. It is interesting to see that in the unsteady regime (Case 3) where oscillating flame occurs, both measured and predicted upper layer oxygen is well above zero percent. (Noted by a sudden jump of oxygen at the border between Case 2 and Case 3) This is because the flame extinction condition is reached before all the oxygen is used up in the compartment, hence the some oxygen still remain in the layer. Note that in the model the extinction condition is defined by a local temperature and oxygen level associated with a critical flame temperature of 1300 ºC. Nevertheless, if the oscillation persists and the fuel mass is sufficient, the temperature of the compartment may increase to the point where the flame condition is above the flammability limit and no longer exhibits the temporary extinction. Then, the oxygen may be used up and the flame reaches the steady under-ventilated condition. In other words, the oscillation can be viewed as a transient behavior before reaching the steady ventilation-limited condition. This phenomenon was observed in the previous study by Utiskul[98] utilizing the slit-vent compartment where the oscillating flame was observed before and the flame later became ventilation-limited and burned steadily at the vent.

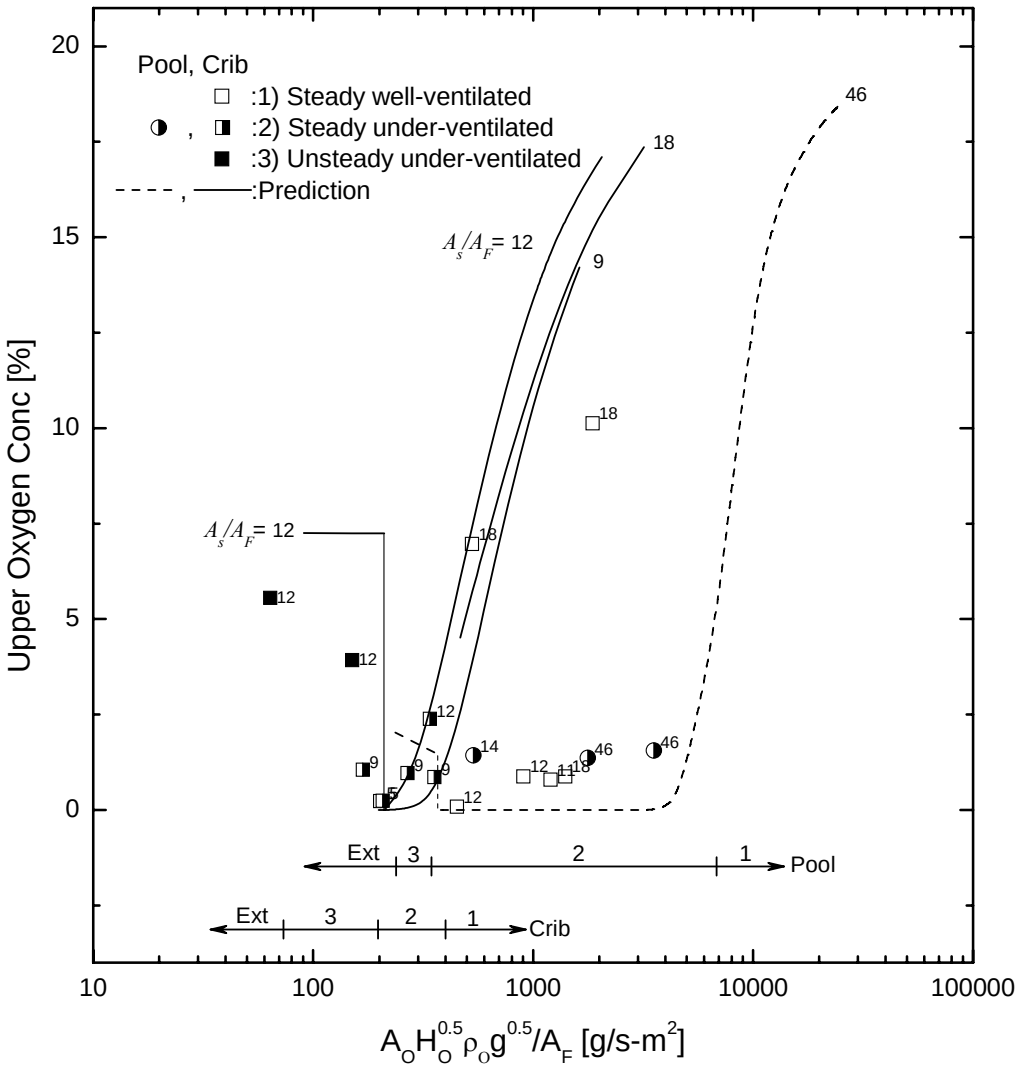

Figure 6.23 Dependence of the peak average upper layer oxygen volume concentration on ventilation and enclosure wall heat loss

Figure 6.24 shows the effect of the scale to the upper layer oxygen. For the wood crib, the large-scale shows less oxygen concentration than that of the small-scale at the same ventilation factor, while the opposite trend is found in the heptane pool fire. This is consistent with the results for the fuel mass loss rate and the temperature that the opposite

trend of the large-scale and small-scale in wood crib and heptane pool fire in the well-ventilated condition.

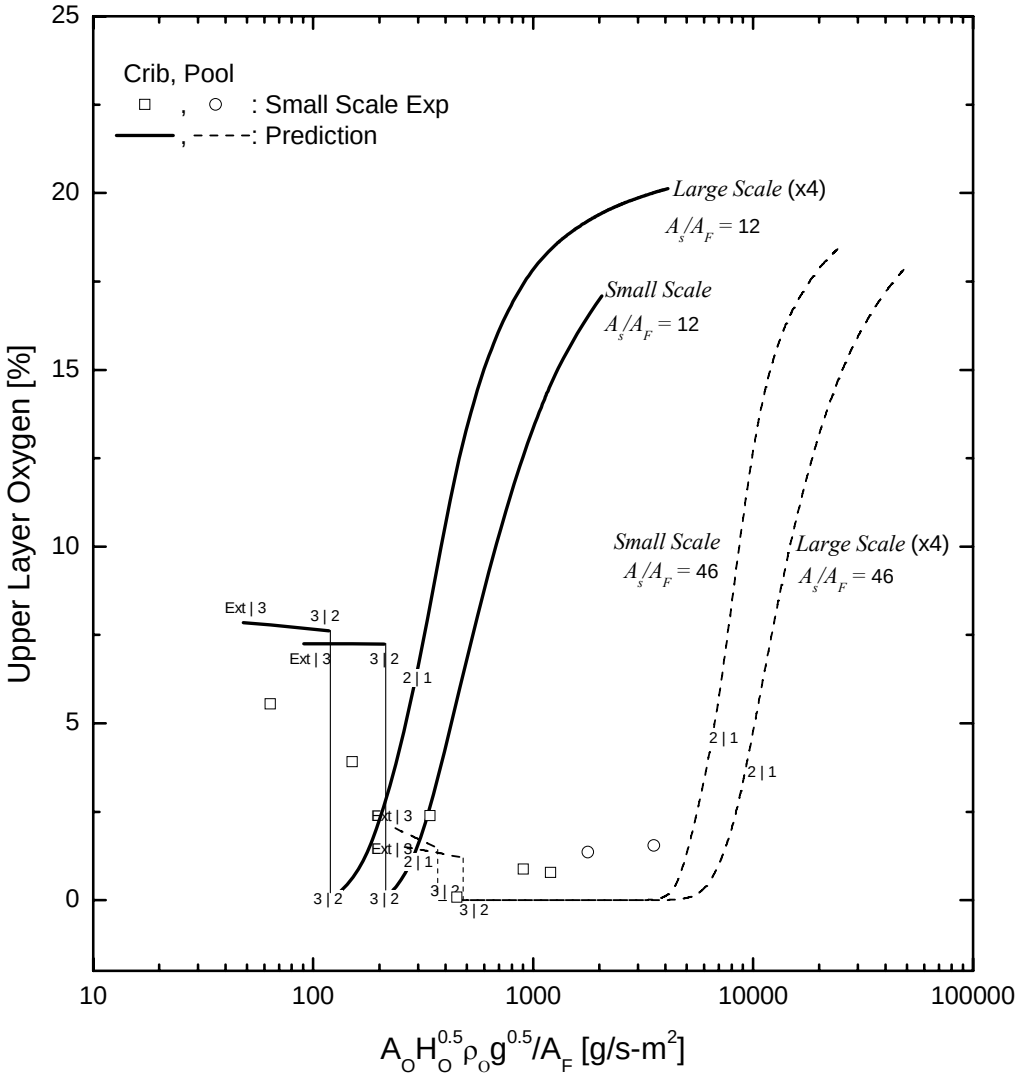

Figure 6.24 Scale and fuel type effects on the compartment upper layer oxygen

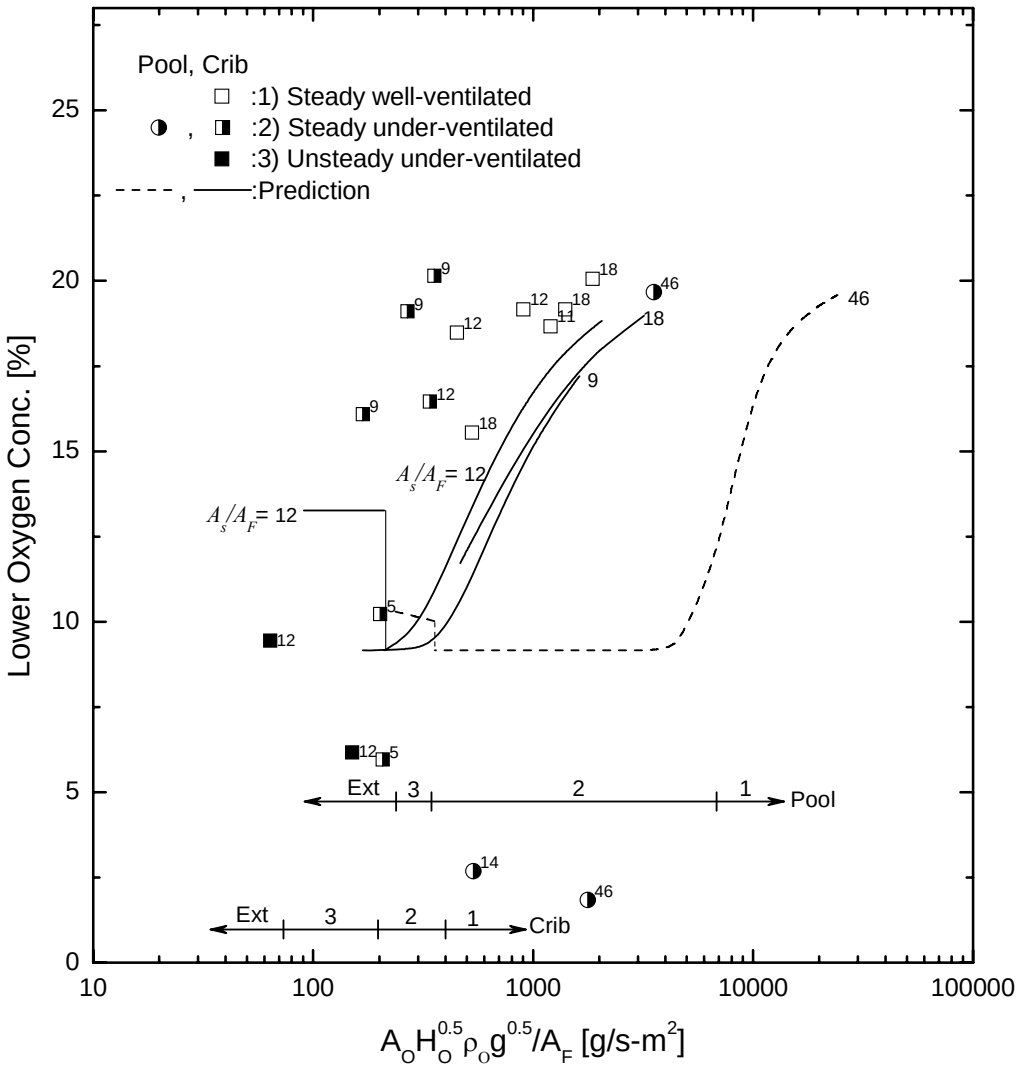

Figure 6.25 Dependence of the peak average lower layer oxygen volume concentration on ventilation and enclosure wall heat loss

The lower layer oxygen is shown in Figure 6.25 and with the scale effect in Figure 6.26. The prediction is less good than the upper layer oxygen but remain reasonable agreement with the experiment. As seen from the prediction line the lower layer oxygen reaches the minimum level of 9 % which corresponds to when the upper reaches zero level. As shown in Chapter 3, the gradient of the oxygen in the lower layer

is much steeper that that in the upper layer which is more uniform, hence the measurement at a fix point may not represent the oxygen in the lower layer well for all experiment since the layer height and the neutral plane are different for each experiment. The scale effect for the lower layer oxygen is similar to that for the upper layer. For the heptane pool fire the larger-scale has less oxygen concentration then the small-scale, and the opposite trend of the scale effect shows for the wood crib fire.

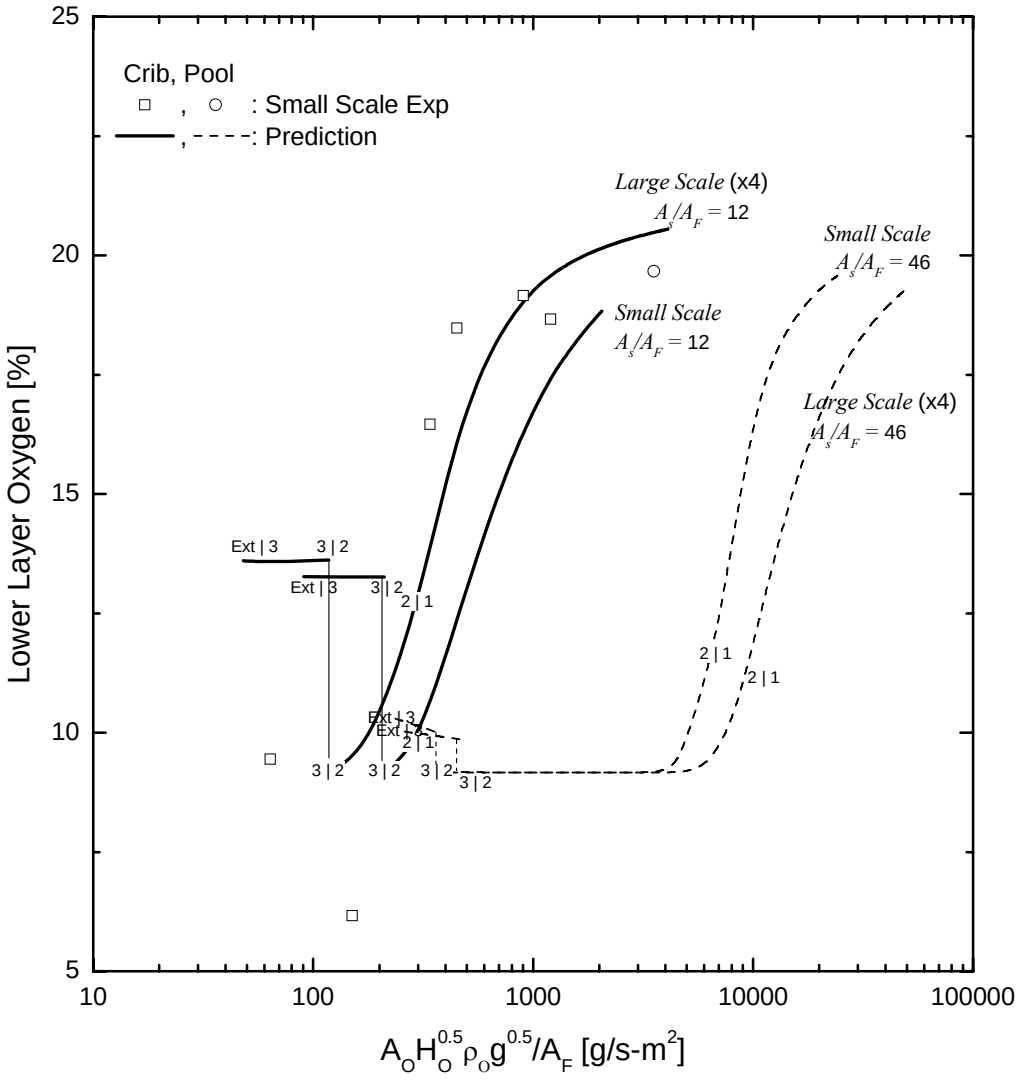

Figure 6.26 Scale and fuel type effects on the compartment lower layer oxygen

6.8.4 Fuel Burning Area

In ventilation limited fire, the burning is controlled by the available air supply and the shrinkage in flaming area may occur as described previously in Chapter 2 and observed in the experiment (Figure 6.14 and 6.16). An attempt to estimate the area shrinkage using by the video observation is made and compared with the area shrinkage predicted from the model. We are aware that there is a high uncertainty associated with the method used for estimation of the area shrinkage; however, the purpose is to qualitatively demonstrate the existing of the phenomena that is also observed in the model, not to precisely evaluate the model. This is shown in Figure 6.27. The estimation for the area shrinkage is mainly from the small-scale case using Crib 1 where $A_s / A_F = 9$ and the prediction for this case is also included. The results show that as the ventilation decreases, the burning area shrinks more. From the simulation, the effect of the scale to the area shrinkage for wood crib is very minimal as shown by the overlap results from the small-scale and large-scale. On the other hands, for the heptane pool fire, the burning area shrinkage is more in the large-scale simulation.

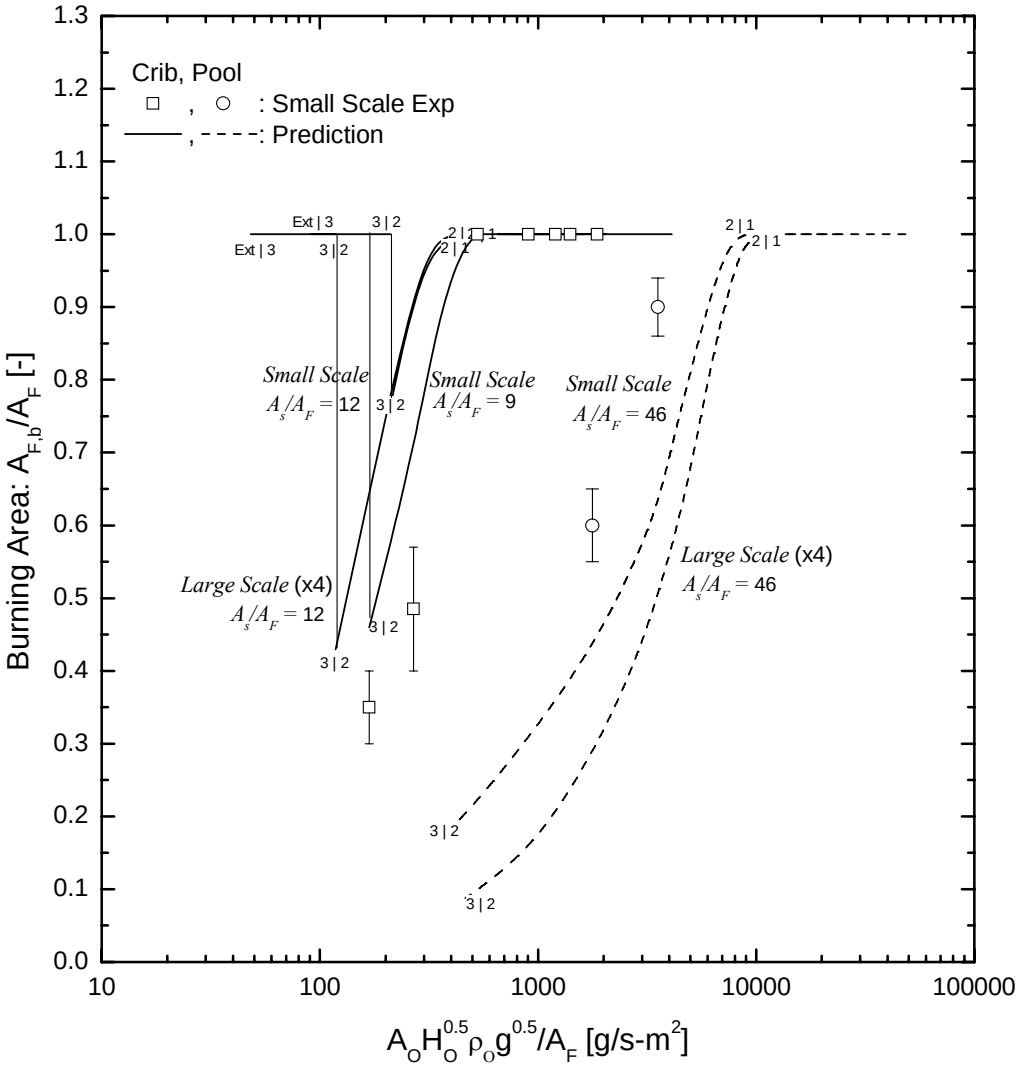

Figure 6.27 Burning area shrinkage in ventilation limited fires

Since the shrinkage in burning area is evident in the ventilation-limited fire as shown by our result, this phenomenon can be responsible for the reduction of the fuel mass loss rate in the ventilation-limited condition (Figure 6.8, 6.18, and 6.19) and can explain why the fuel mass loss rate follows the same trend as the "burning rate" in ventilation-limited fires.

6.9 Conclusions

The experimental program burning wood crib and heptane pool in a single-wall-vent compartment has been conducted and presented in detail. Some observations have been given and the burning has been categorized into 3 cases based on the observed behavior and the ventilation parameter ($A_o\sqrt{H_o}\rho_o\sqrt{g}/A_F$). The 3 cases are:

1) Case 1: Steady well-ventilated burning. This is the case where vent is large and the global equivalence ratio is less than one. The flame stabilized above the fuel, and the oxygen in the upper layer is above zero.
2) Case 2: Steady under-ventilated burning. This case the opening size is reduced and the global equivalence ratio is less than one. The burning is ventilation-limited and the fire area shrinkage occurs. Oxygen in the upper layer is at or near zero. The oscillating flame may take place if the extinction criterion, depending on the local temperature and oxygen, is reached. But the oscillation is only a transient stage for this case and the flame eventually reaches the steady stage where no oscillation occurs and become under-ventilated.
3) Case 3: Unsteady under-ventilated burning. In this case the opening size is the smallest among all cases. Periodic oscillating flame is observed. The global equivalence ratio is less than one; however, the oxygen in the upper layer is above zero. In this case the extinction criterion is reached and the oscillating flame occurs until the fuel is exhausted. Throughout the burning, the flame does not consume all the oxygen available.

The transient and peak-average results have been systematically presented along with the predictions from the single-zone model. The model is able to predict the fuel mass loss rate with good agreement to the measurements and can reveal the important mechanisms: the oxygen effect and the thermal feedback effect. The prediction for the temperature has a qualitatively good agreement with the experiment. In the largest wood crib experiment (Crib 5) the maximum gas temperature is achieved at 890 ºC and the prediction yields 840 ºC.

From a global perspective, the model is sufficient to predict the trend and follow the data from the larger scale experiment. Some generalities of the results have been presented. The effect of the ventilation compartment wall heat loss (A_s / A_F), fuel type and configuration, and scale has been demonstrated using the peak average data from the experiments and the single-zone model simulations. For ventilation-limited fires, the higher the A_s / A_F ratio, the higher the fuel mass loss rate and gas temperature. The peak temperature is achieved at the boundary between well-ventilated and under-ventilated regime or at the near stoichiometry global equivalence ratio. The large-scale simulation achieves a higher peak temperature than the small-scale. In the large-scale heptane pool fires, the thermal feedback is not as significant as in the small-scale pool fires due the scale effect on the flame emissivity. The less scale effect, however, is found on the crib fire due to the low flame emissivity of the wood.

Chapter 7

Conclusion

7.1 Conclusions

The following conclusions can be drawn from this dissertation.

- A theoretical model for the compartment fuel mass loss rate that accounts for the enhancement by the thermal feedback and the diminishment by the vitiated oxygen in the incoming stream has been presented and validated with wood crib and heptane pool experiments. The comparison shows good agreement and confirms the application of the model to the common fuel configurations.

- An empirical correlation for the near-vent mixing of oxygen into the lower layer floor layer has been developed for the first time. Two approaches, *entering-jet* and *point-source plume*, were examined and the entering-jet method was in a better agreement with the experimental data. This correlation is essential to for predicting the oxygen effect on the fuel mass loss rate modeling. A constant maximum value of 1.3 for the mixing ratio in well-mixed compartment fires with single-wall-vent has been suggested for use in a single-zone model.

- A criterion for a single-zone model to be valid in fully-developed fires has been established based on the smoke layer interface at 20% of the opening height. A theoretical method to determine the layer interface has been described in dimensionless form and validated with experiments. Some generalities of the layer interface as a function of vent geometry and fire size were presented. An

approximation from the complete result suggests that any floor fire with diameter, $D > 3/2\sqrt{A_o}$ yields a layer interface close to the floor less than 20% of the doorway height.

- A single-zone fully-developed compartment fire model that accounts for the fuel type and configuration has been established. The model is capable of predicting the gas temperature and the fuel mass loss rate that can relate to the burn time in a fire for any fuel, scale and ventilation.

- Single-wall-vent small-scale compartment fire experiments have been carried out for wood cribs and heptane pools. From observations, the burning is categorized into 3 cases: Case 1: Steady well-ventilated burning where $\phi < 1$, and the flame stabilizes above the fuel, Case 2: Steady under-ventilated burning where $\phi > 1$, the fire burning area shrinks, the flame burning steadily at the vent is observed, and the oscillation may occur in transient stage, and Case 3: Unsteady under-ventilated burning where $\phi > 1$, the oscillation is observed and all oxygen is not used due to unsteadiness burning.

- The single-zone model is able to reveal the full range of phenomena associated with fully developed fires as observed in the experiment: response of fuel to thermal and oxygen effects, fire area shrinkage, oscillation, and extinction. The model also shows good agreement with the experimental measurements.

- Fuel type, scale, and heat loss (A_s / A_F) effects have been demonstrated with the model simulations and the experiments. Generally, the higher temperature and mass loss rate are achieved with the bigger scale and the lower ratio of A_s / A_F .

The maximum temperature and mass loss rate is achieved when $\phi \approx 1$ or at the border between the burning Case 1 and Case 2. The scale effect on the flame emissivity of the heptane pool fires is more than that of the wood crib fires. The fire area shrinkage can be the reason for the *fuel mass loss rate* to follow the same trend as the *burning rate* in ventilation-limited fires.

7.2 Suggestion on Future Work

- Although the single-zone model has been compared with the small-scale experiment and shows satisfying results, a comparison with the large-scale has not been carried out. This could be done in the future work to demonstrate the capability of the model for predicting the large-scale data available in the literature.
- The model can be used as a tool to strategically obtain the key dimensionless variables that can improve the correlation of the large body of literature data.
- The fuel mass loss rate model can be implemented into the more general two-layer-zone model along with the mixing correlation developed in this study to give better prediction of fires in buildings that are essential to the structural fire safety design.

Appendix A

Experimental Result and Model Prediction

Single-Wall-Vent Compartment Fire

Wood Crib

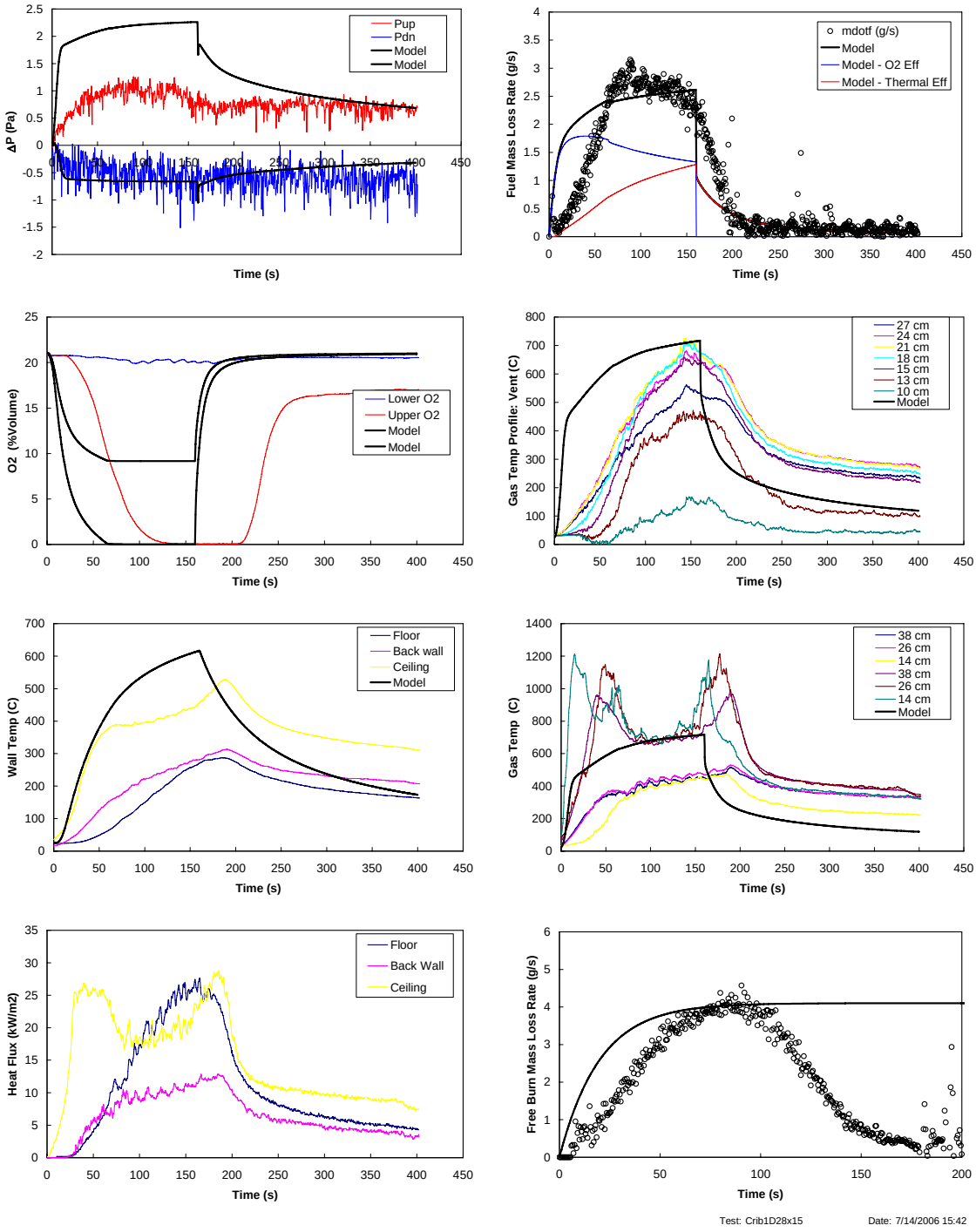

Figure A.1 Experiment and Prediction: Crib 1 – Doorway – 28 cm x 15 cm ($H_o x W_o$) (Crib1D28x15)

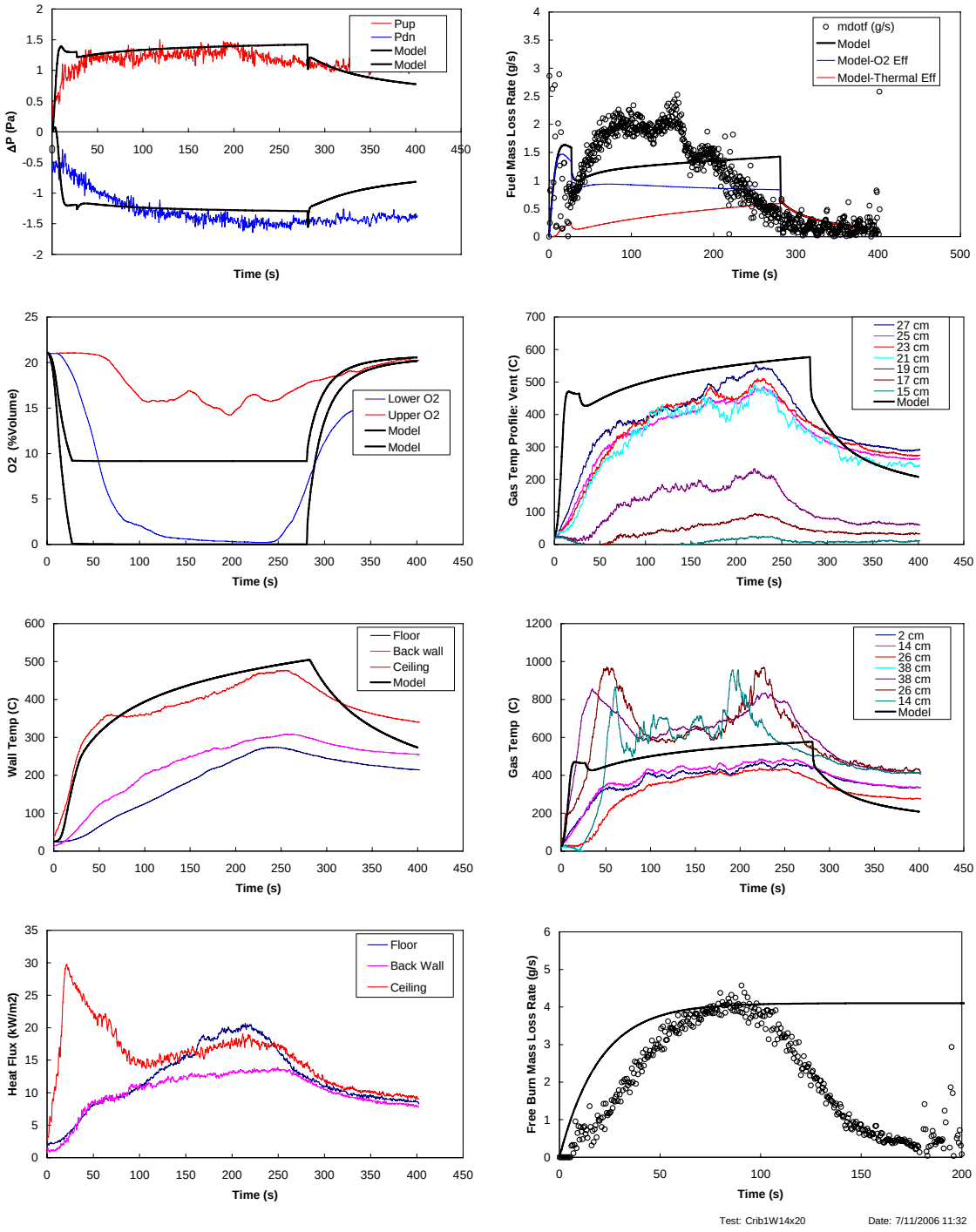

Figure A.2 Experiment and Prediction: Crib 1 – Window – 14 cm x 20 cm ($H_o x W_o$), S = 14 cm (Crib1W14x20)

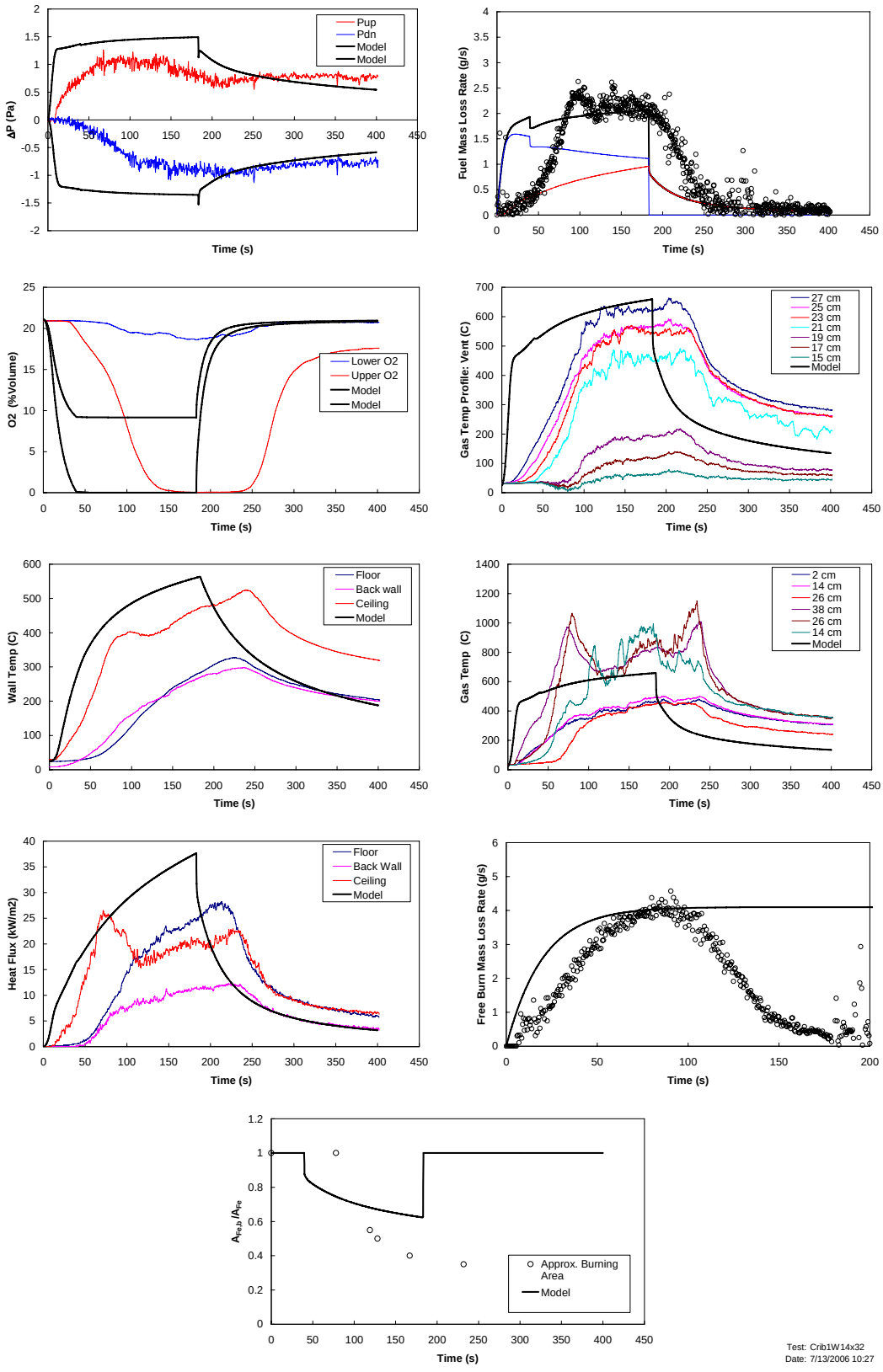

Figure A.3 Experiment and Prediction: Crib 1 – Window – 14 cm x 32 cm ($H_o x W_o$), S = 14 cm (Crib1W14x32)

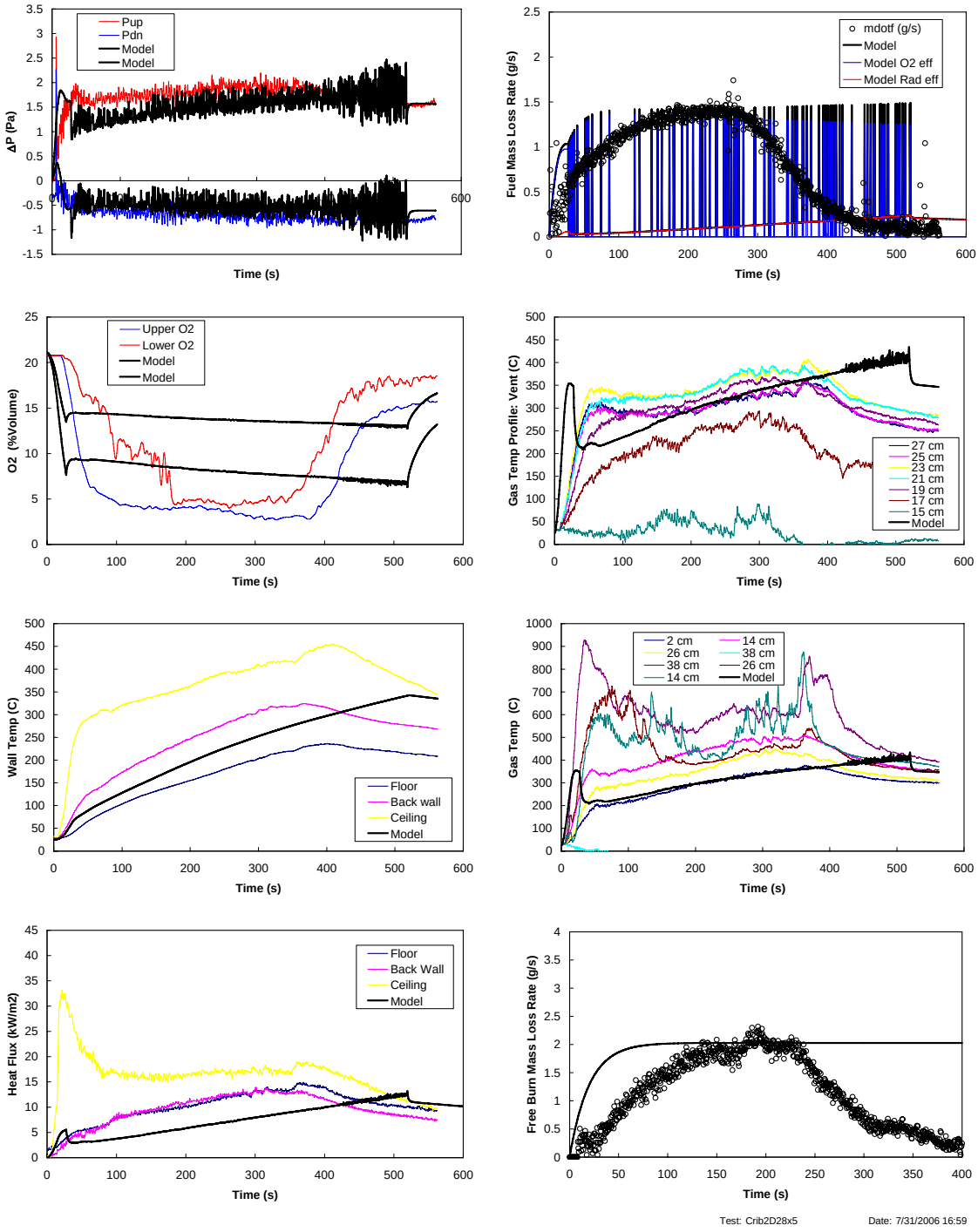

Figure A.4 Experiment and Prediction: Crib 2 – Doorway – 28 cm x 5 cm ($H_o x W_o$) (Crib2D28x5)

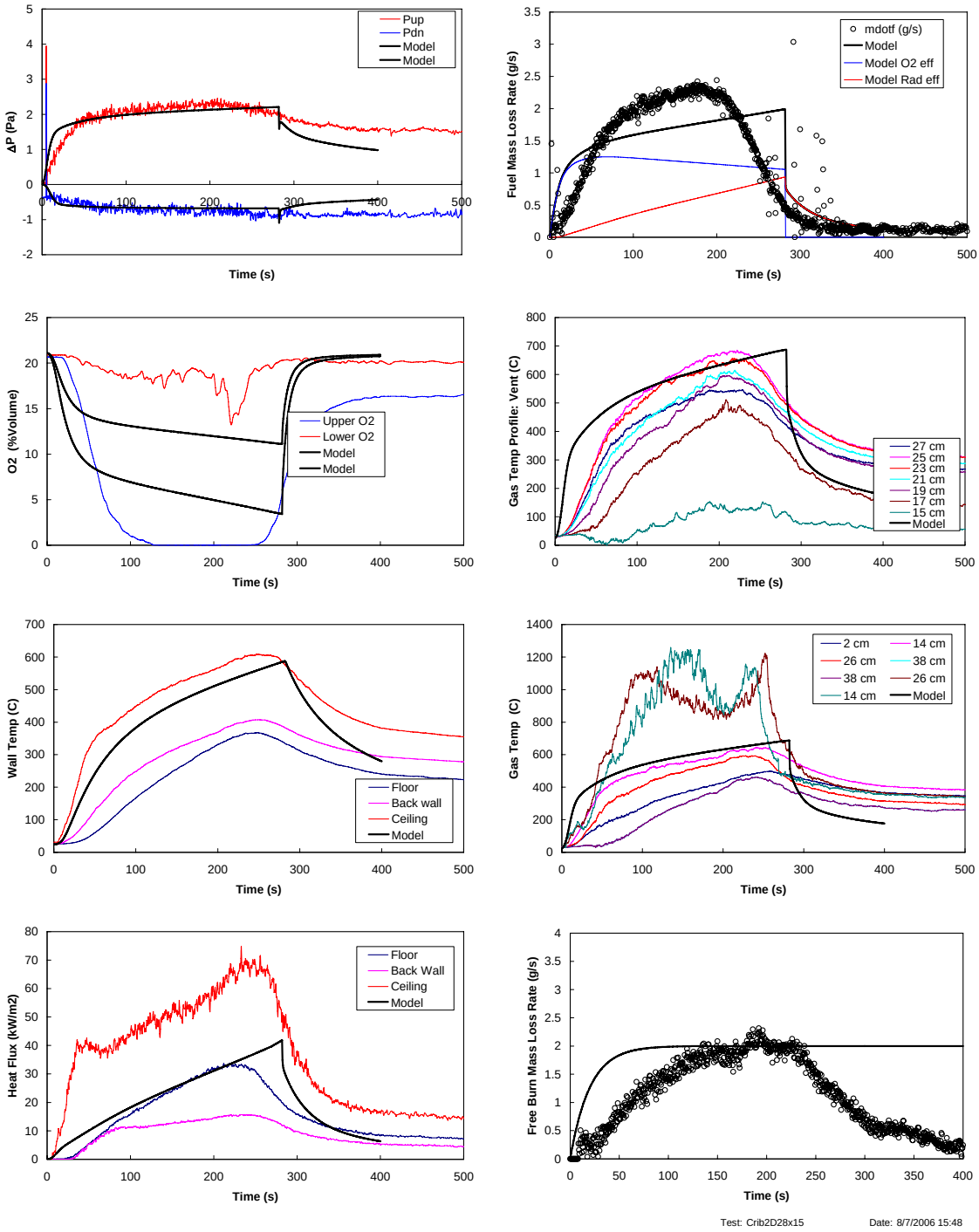

Figure A.5 Experiment and Prediction: Crib 2 – Doorway – 28 cm x 15 cm ($H_o x W_o$) (Crib2D28x15)

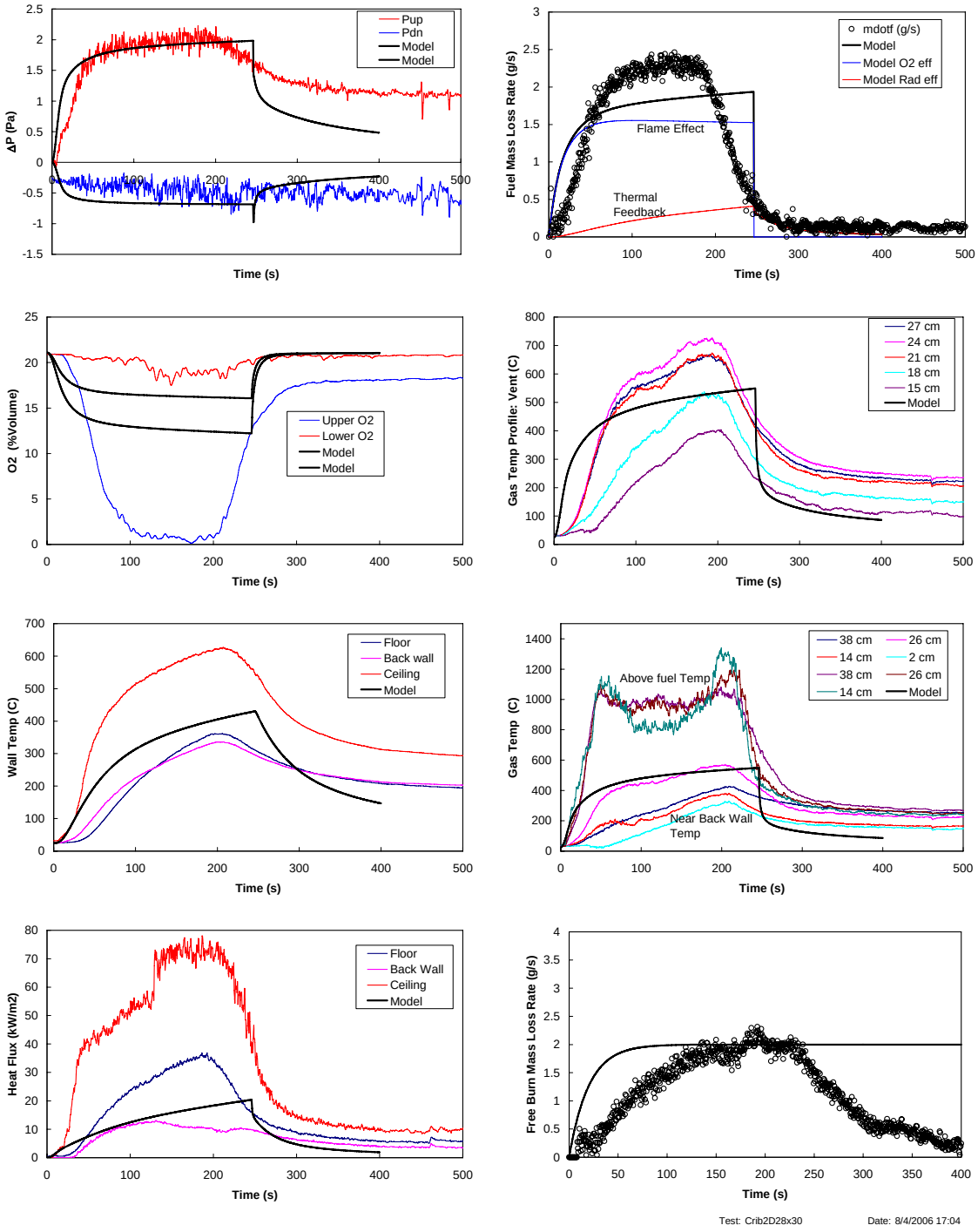

Figure A.6 Experiment and Prediction: Crib 2 – Doorway – 28 cm x 30 cm ($H_o x W_o$) (Crib2D28x30)

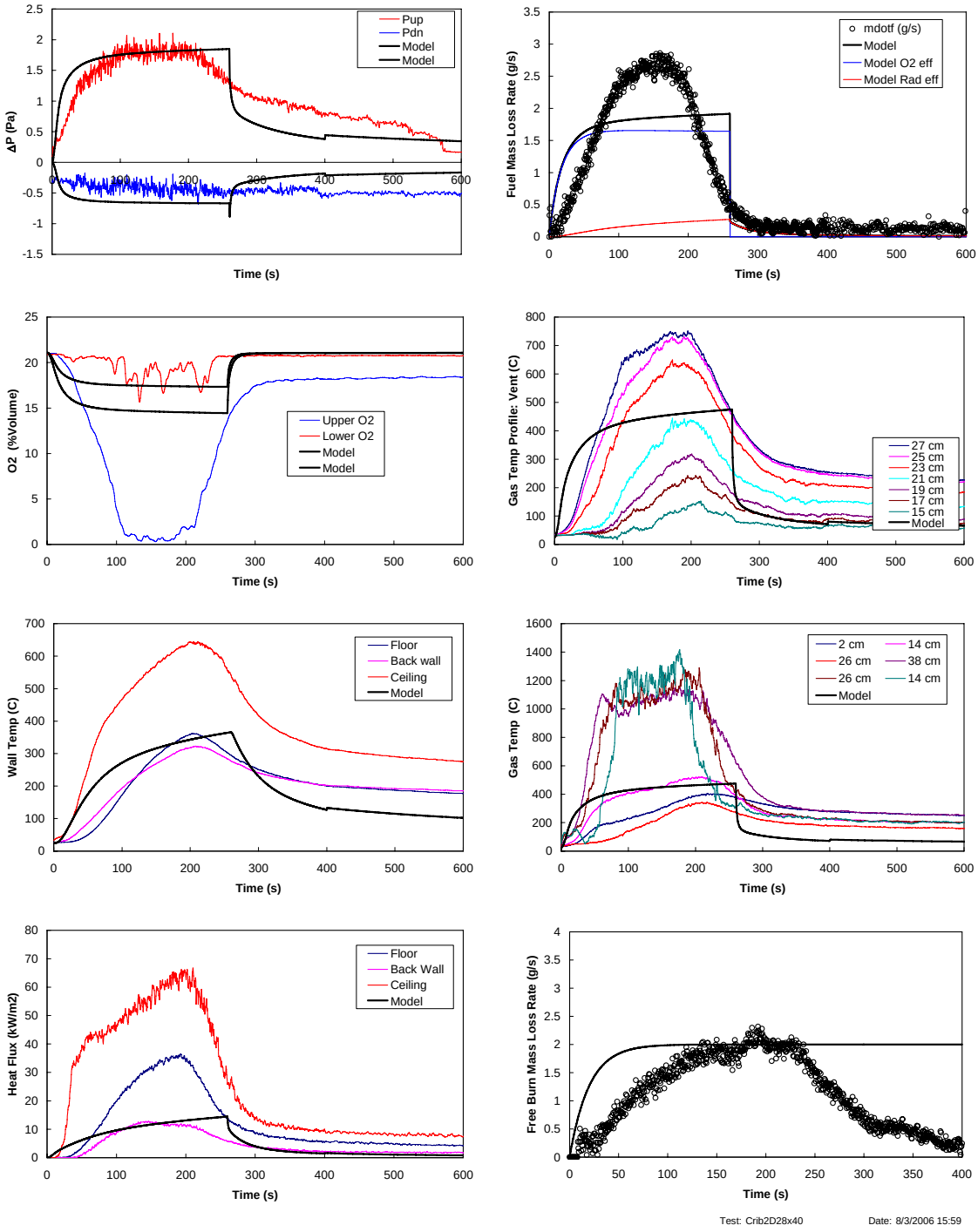

Figure A.7 Experiment and Prediction: Crib 2 – Doorway – 28 cm x 40 cm ($H_o x W_o$) (Crib2D28x40)

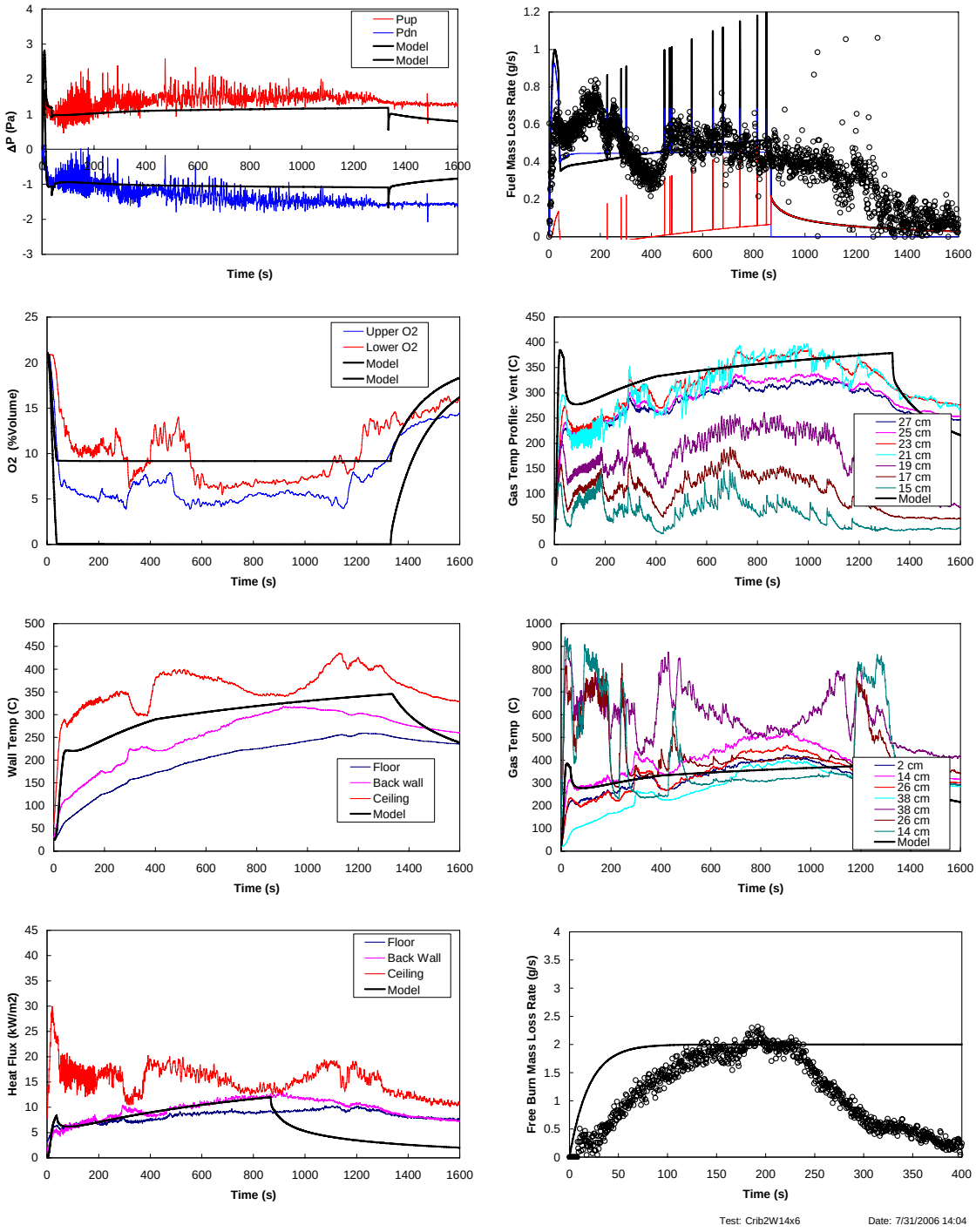

Figure A.8 Experiment and Prediction: Crib 2 – Window – 14 cm x 6 cm ($H_o x W_o$), S = 14 cm (Crib2W14x6)

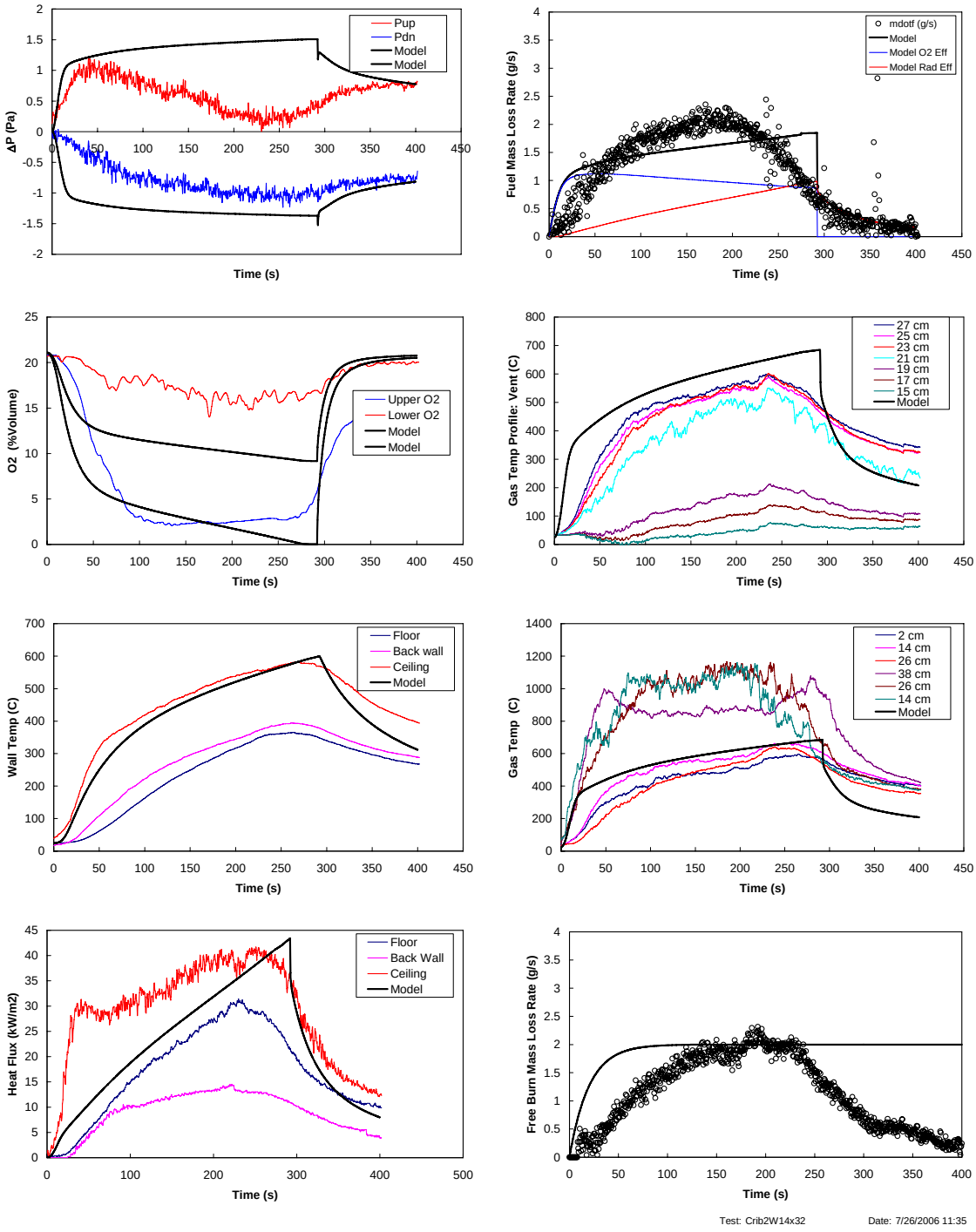

Figure A.9 Experiment and Prediction: Crib 2 – Window – 14 cm x 32 cm ($H_o x W_o$), S = 14 cm (Crib2W14x32)

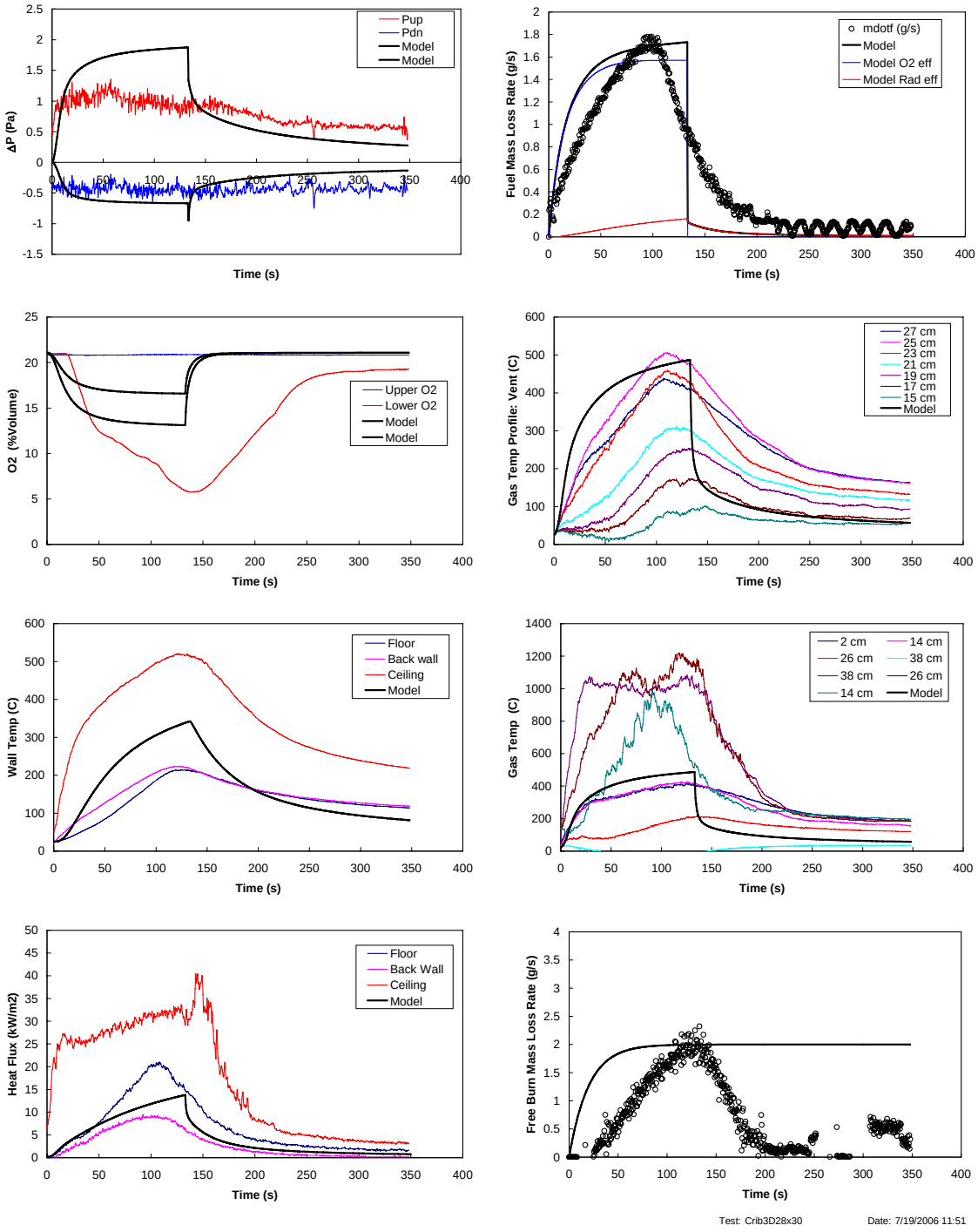

Figure A.10 Experiment and Prediction: Crib 3 – Doorway – 28 cm x 30 cm ($H_o x W_o$) (Crib3W28x30)

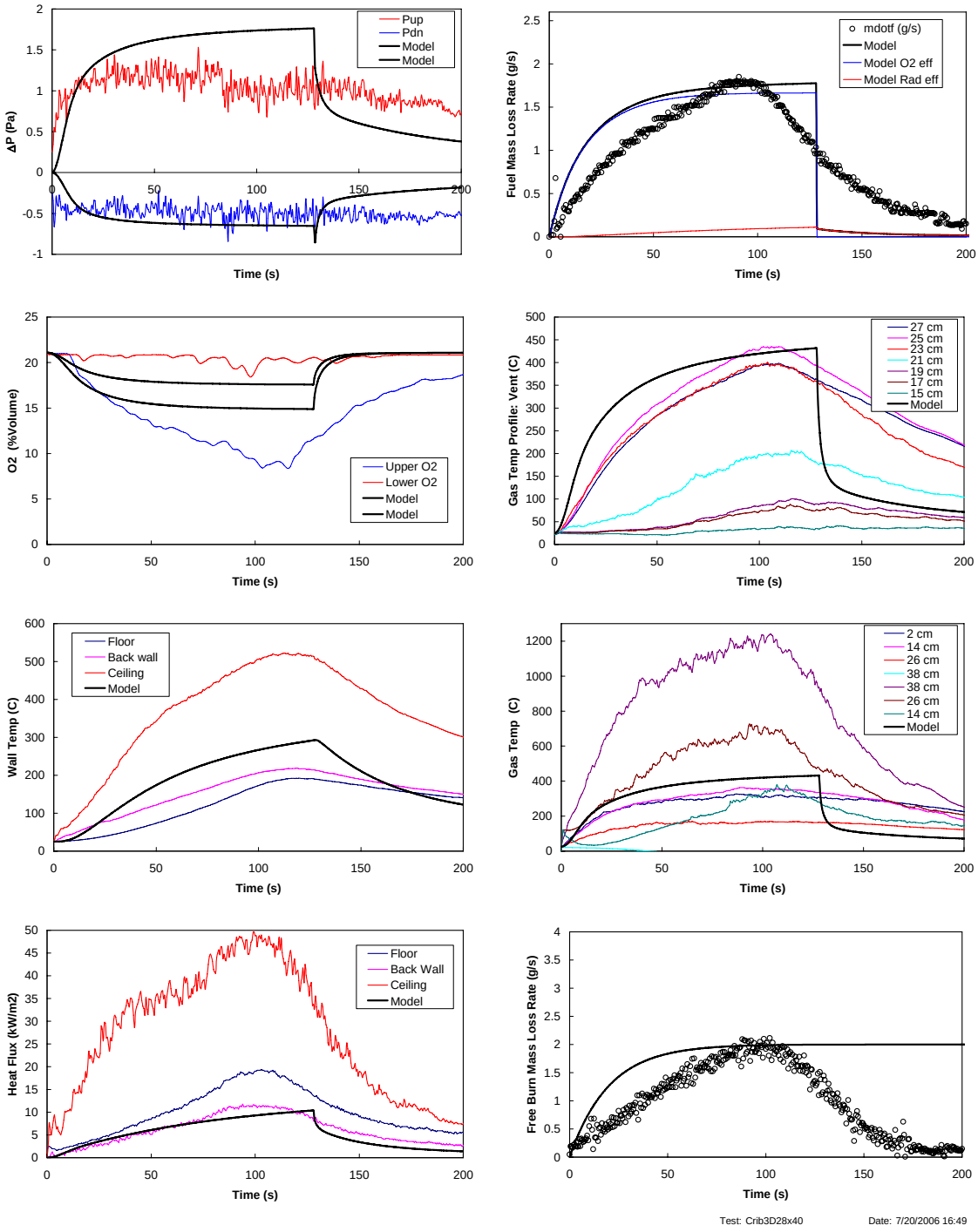

Figure A.11 Experiment and Prediction: Crib 3 – Doorway – 28 cm x 40 cm ($H_o x W_o$) (Crib3W28x40)

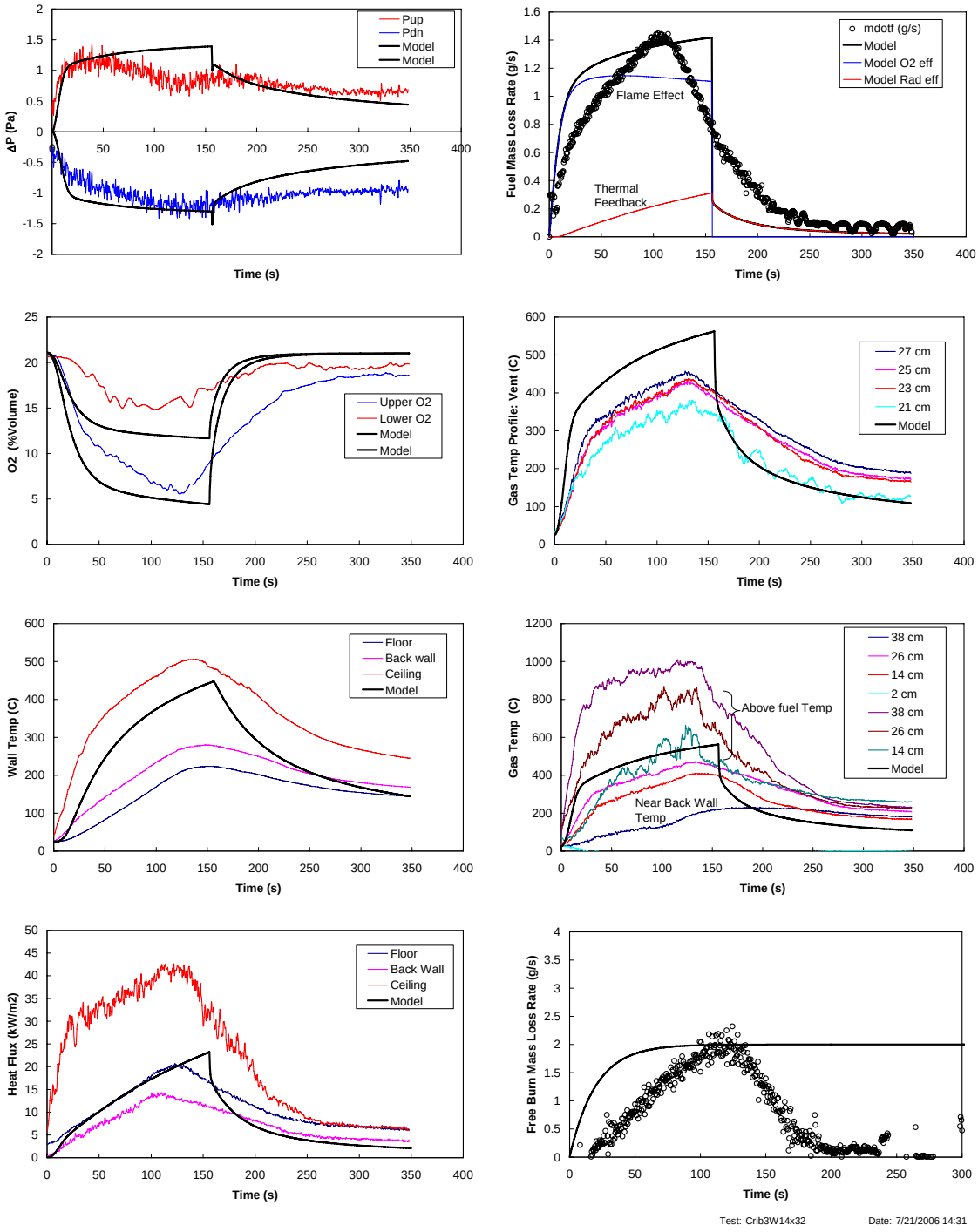

Figure A.12 Experiment and Prediction: Crib 3 – Window – 14 cm x 32 cm ($H_o x W_o$), S = 14 cm (Crib3W14x32)

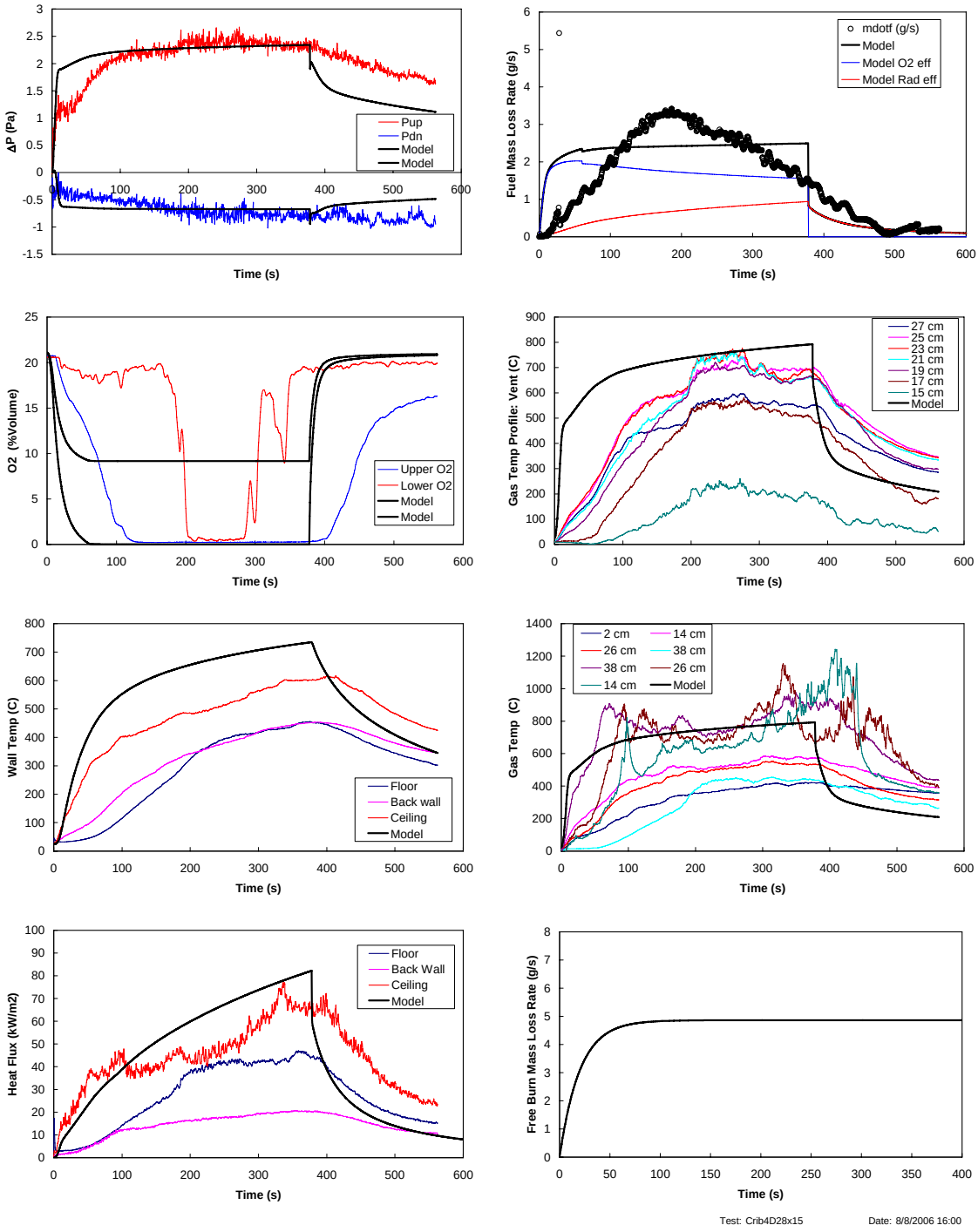

Figure A.13 Experiment and Prediction: Crib 4 – Doorway – 28 cm x 15 cm ($H_o x W_o$) (Crib4D28x15)

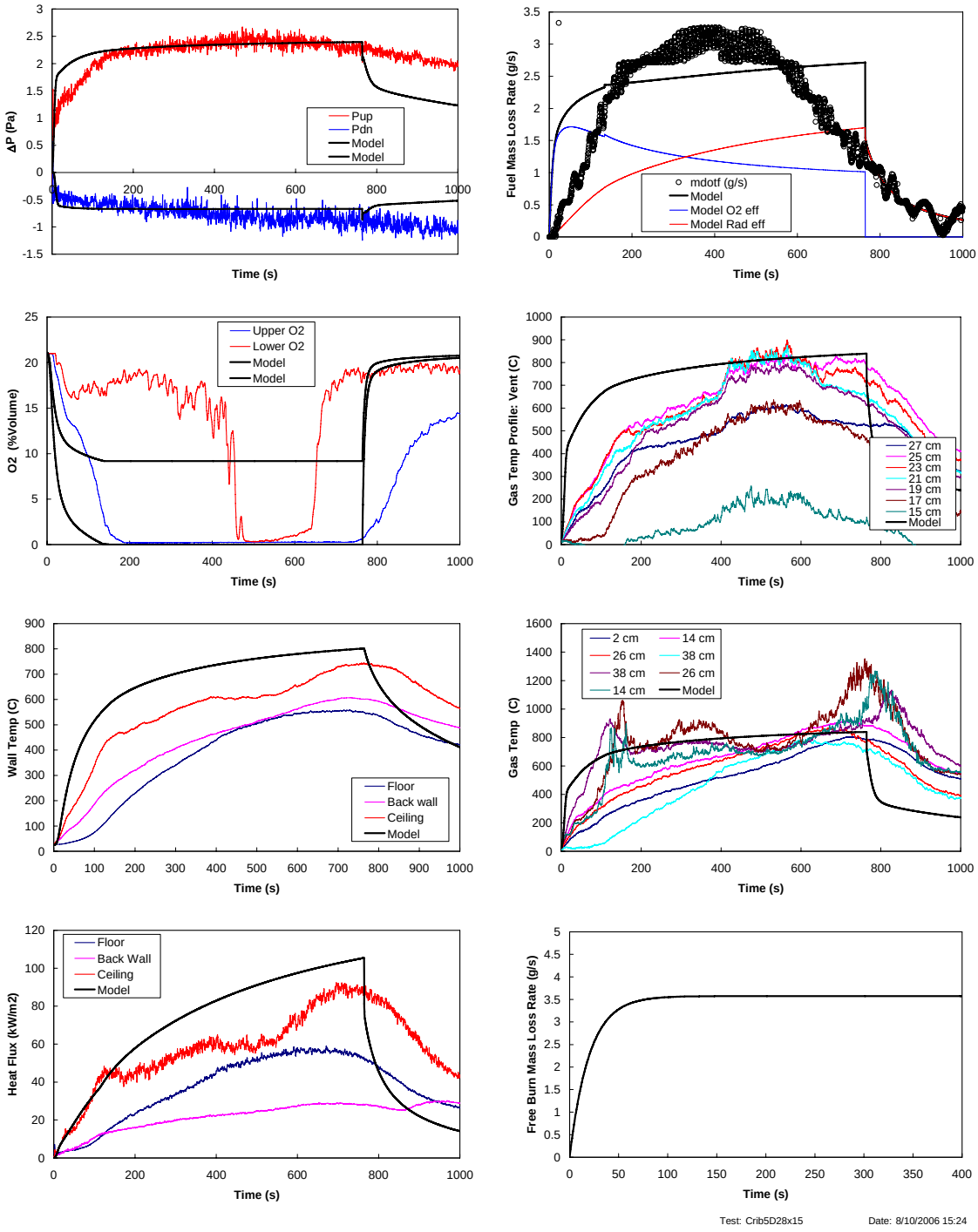

Figure A.14 Experiment and Prediction: Crib 5 – Doorway – 28 cm x 15 cm ($H_o x W_o$) (Crib5D28x15)

Appendix B

Experimental Result and Model Prediction

Single-Wall-Vent Compartment Fire

Heptane Pool

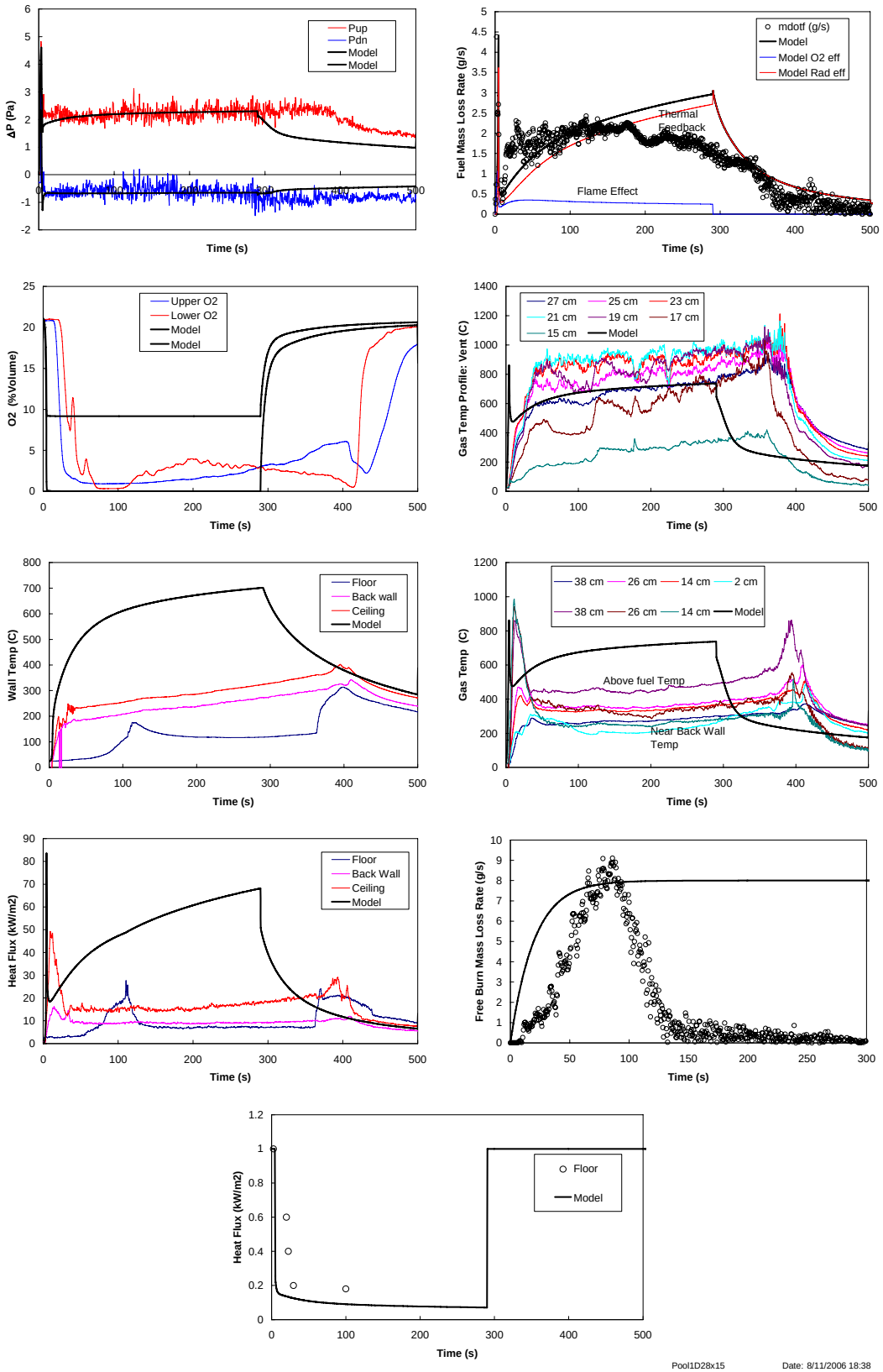

Figure A.15 Experiment and Prediction: Pool 1 – Doorway – 28 cm x 15 cm ($H_o x W_o$) (Pool1D28x15)

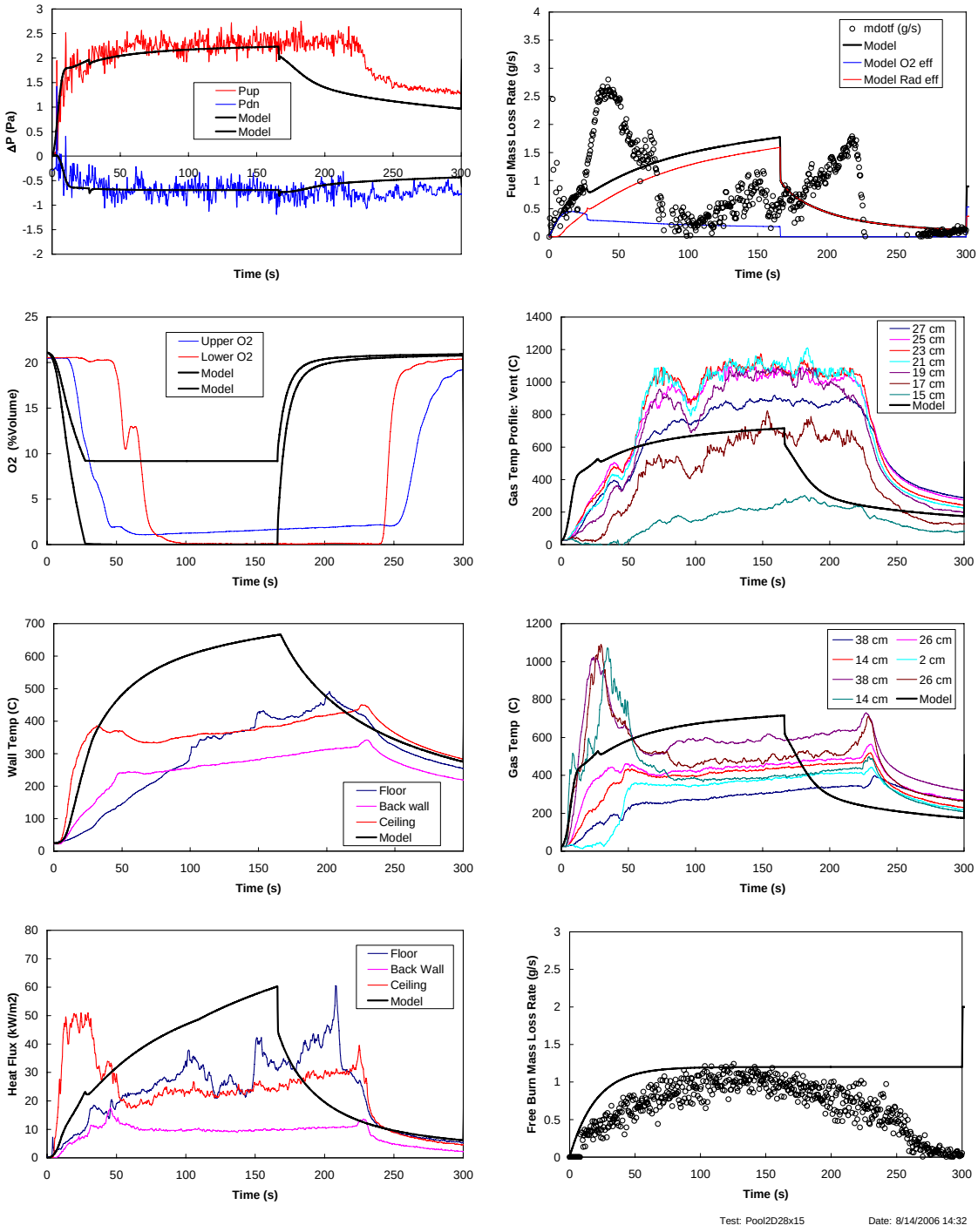

Figure A.16 Experiment and Prediction: Pool 2 – Doorway – 28 cm x 15 cm ($H_o x W_o$) (Pool2D28x15)

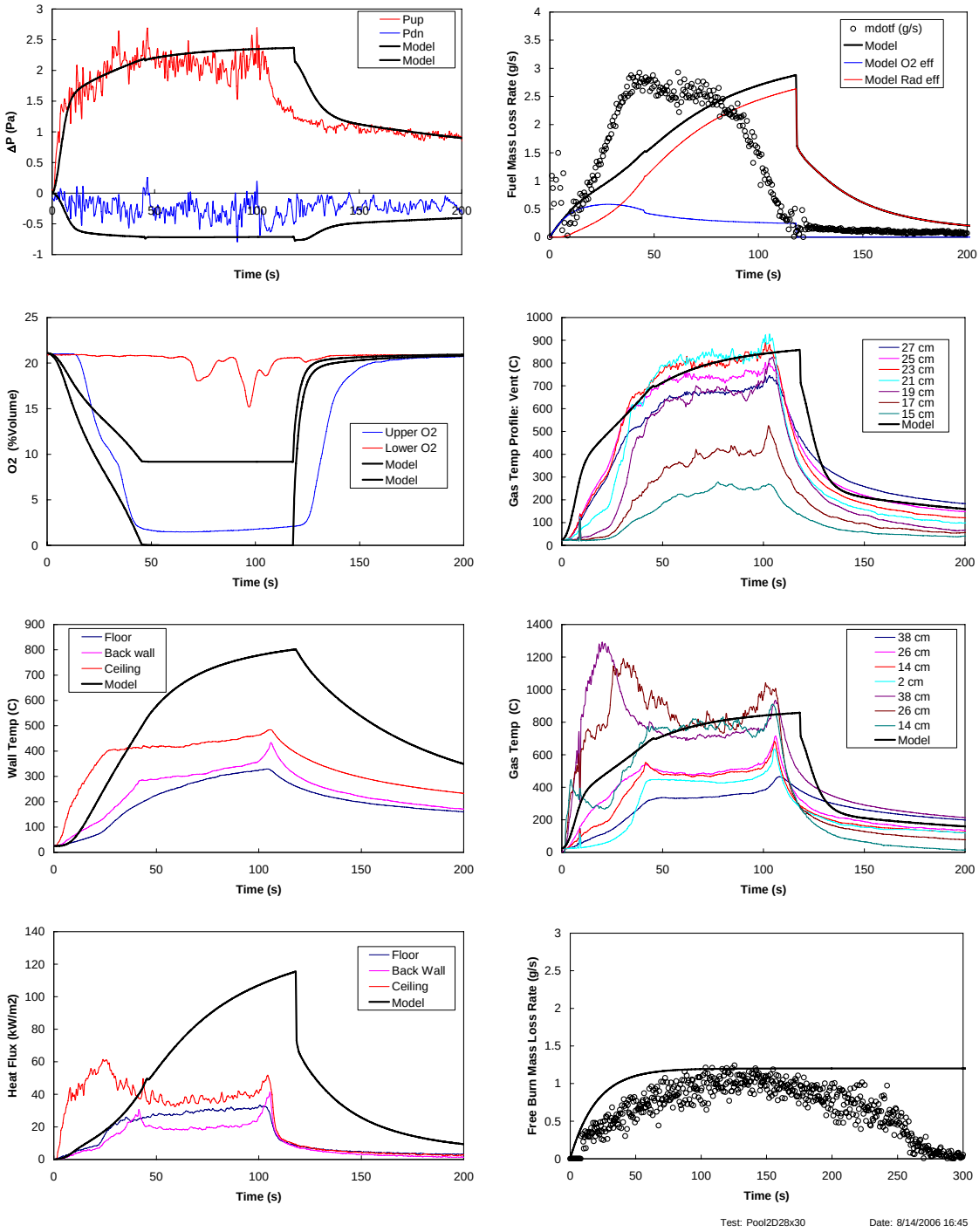

Figure A.17 Experiment and Prediction: Pool 2 – Doorway – 28 cm x 30 cm ($H_o x W_o$) (Pool2D28x30)

Appendix C

Wood Crib Exposed Area Calculation

Square Crib

Geometry

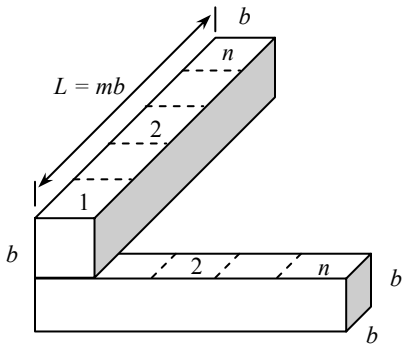

N = Number of stick layers

n = Number of stick per layer

b = Side dimension of square stick

L = Stick length

s = Stick spacing

and define $m = L/b$

Top Layer

$$A_{stick} = 2b^2 + 4b(mb) - nb^2$$

Bottom Layer

$$A_{stick} = 2b^2 + 3b(mb) - nb^2$$

Middle Layer

$$A_{stick} = 2b^2 + 4b(mb) - 2nb^2$$

Total exposed area for square crib

$$A_F = \left(2b^2 + 4b(mb) - 2nb^2\right)(N-2)n + \left(2b^2 + 4b(mb) - nb^2\right)n + \left(2b^2 + 3b(mb) - nb^2\right)n$$

$$A_F = nb^2\left[(1-n+2m)2N + 2n - m\right]$$

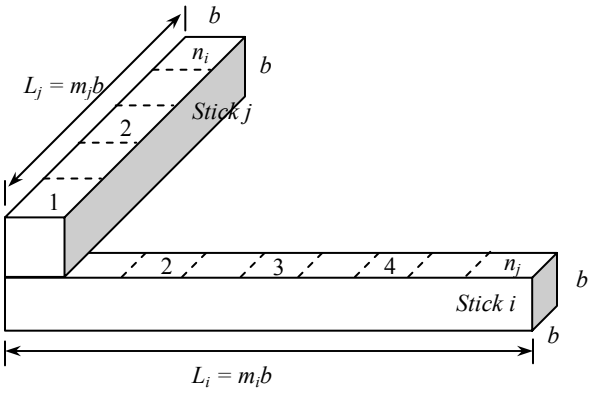

Rectangular Crib

Geometry

N = Number of stick layers

n_i = Number of stick i per layer

n_j = Number of stick j per layer

b = Side dimension of square stick

L_i = Stick i length

L_j = Stick j length

s = Stick spacing

$m_i = L_i / b$

$m_j = L_j / b$

For <u>even *N*</u> (let bottom layer be stick <u>*i*</u>)

Bottom Layers

$$A_{stick,i} = 2b^2 + 3b(m_i b) - n_j b^2$$

Top Layers

$$A_{stick,j} = 2b^2 + 4b(m_j b) - n_i b^2$$

Middle Layers

$$A_{stick,i} = 2b^2 + 4b(m_i b) - 2n_j b^2$$

$$A_{stick,j} = 2b^2 + 4b(m_j b) - 2n_i b^2$$

$$A_F = \left(\frac{N}{2} - 1\right)\left\{n_i\left(2b^2 + 4b^2 m_i - 2n_j b^2\right) + n_j\left(2b^2 + 4b^2 m_j - 2n_i b^2\right)\right.$$
$$\left. + n_i\left(2b^2 + 3b^2 m_i - n_j b^2\right) + n_j\left(2b^2 + 4b^2 m_j - n_i b^2\right)\right\}$$

$$A_F = b^2\left\{m_i n_i(2N-1) + N(n_i + n_j + 2m_j n_j - 2n_i n_j) + n_j(3n_i - n_j)\right\}$$

For <u>Odd *N*</u> (Let bottom and top layers be stick *i*)

N $\neq 1$, and $m_i > m_j$ or $L_i > L_j$

Bottom Layers

$$A_{stick,i} = 2b^2 + 3b(m_i b) - n_j b^2$$

Top Layers

$$A_{stick,i} = 2b^2 + 4b(m_i b) - n_j b^2$$

Middle Layers

$$A_{stick,i} = 2b^2 + 4b(m_i b) - 2n_j b^2$$

$$A_{stick,j} = 2b^2 + 4b(m_j b) - 2n_i b^2$$

$$A_F = \left(\frac{N-2}{2} - \frac{1}{2}\right)\left[n_i\left(2b^2 + 4b^2 m_i - 2n_j b^2\right)\right] + \left(\frac{N-2}{2} + \frac{1}{2}\right)\left[n_j\left(2b^2 + 4b^2 m_j - 2n_i b^2\right)\right] + n_i\left(2b^2 + 3b^2 m_i - n_j b^2\right) + n_i\left(2b^2 + 4b^2 m_i - n_j b^2\right)$$

$$A_F = b^2\left[(N-1)\left(2m_j + 1\right)n_j + n_i(1 + m_i + 2n_j + N + 2N(m_i - n_j))\right]$$

Appendix D

Effective Heat of Gasification for Heptane

The effective heat of gasification, L_{eff}, was experimentally approximated. By using the cone calorimeter, the mass loss rate was measured for a given incident heat flux. Two heptane pool configurations were examined: heptane with added water and heptane without water. A Pyrex® pan with diameter of 9.5 cm was used as a fuel pan and placed on the Kaowool® M-Type board. The results are as follows:

Fuel Area = 0.0071 m2

Test	Mass Loss Rate (g/s)	Heat Flux (kW/m2)	Heat (kJ)	Mass Loss Rate (g/s-m2)	L
Heptane1 with water	0.0170	3.4500	0.0245	2.3903	1.4433
Heptane2 with water	0.0371	7.0000	0.0496	5.2319	1.3379
Heptane 1	0.0280	3.4000	0.0241	3.9486	0.8611
Heptane 2	0.0285	3.5000	0.0248	4.0191	0.8708
Heptane 3	0.0580	7.2000	0.0511	8.1793	0.8803
Heptane 4	0.0840	10.3000	0.0730	11.8459	0.8695

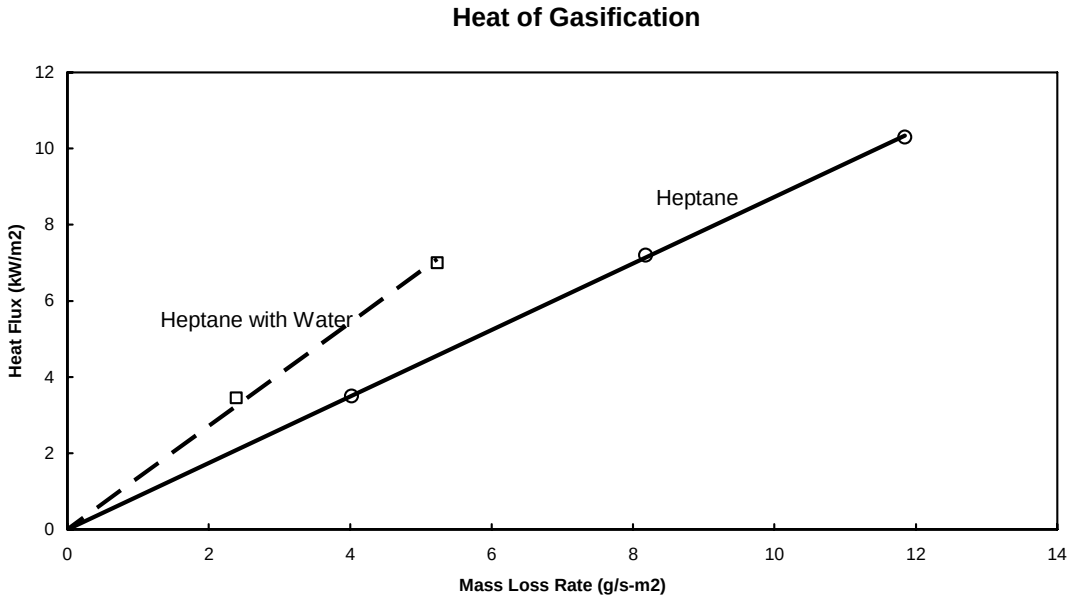

The result shows that for the heptane-with-water setup L_{eff} is approximately 1.4 kJ/g.

Bibliography

[1] Quintiere, J.G., *Principles of Fire Behavior*. 1998, New York: Delmar publishers.

[2] Karlsson, B. and Quintiere, J.G., *Enclosure Fire Dynamics*. 1999, Florida: CRS Press.

[3] Ingburg, S.H., *Tests of Severity of Building Fires.* Quarterly, 1928. **22**: p. 43.

[4] Kawagoe, K., *Fire Behavior in Rooms,* 27, Building Research Institute of Japan, 1958.

[5] Kawagoe, K. and Sekine, T., *Estimation of Fire Temperature-Time Curves in Rooms,* 11, Building Research Institute of Japan, 1963.

[6] Gross, D. and Robertson, A.F., *Experimental Fires in Enclosures*. in *Tenth Symposium (International) on Combustion*. 1965: Combustion Institute.

[7] Thomas, P.H. and Heselden, J.M., *C.I.B. International Co-operative Programme on Fully-Developed Fires in Single Compartments: Comprehensive Analysis of Results,* Internal Note No. 374, Fire Research Station, 1970.

[8] Thomas, P.H., Heselden, J. M., *Fully Developed Fires in Single Compartments, A Co-operative Research Program of the Conseil International du batiment (CIB Report No. 20),* Fire Research Station Note No. 923, Fire Research Station, 1972.

[9] Heselden, A.J., Thomas, P.H., and Law, M., *Burning Rate of Ventilation Controlled Fires in Compartments.* Fire Technology, 1970. **6**: p. 123.

[10] Tewarson, A., *Some Observations on Experimental Fires in Enclosures, Part I - Cellulosic Materials.* Combustion and Flame, 1972. **19**(n 3): p. 101-111.

[11] Tewarson, A., *Some Observations on Experimental Fires in Enclosures, Part II - Ethyl Alcohol and Paraffin Oil.* Combustion and Flame, 1972. **19**(n 3): p. 363-371.

[12] Takeda, H., Akita, K., *Critical Phenomenon in Compartment Fires with Liquid Fuels*. in *Symp Int Combust 18th*. 1981. Waterloo, Ont, USA: Combustion Institute.

[13] Kim, I.K., Ohtani, H., and Uehara, Y., *Experimental Study on Oscillating Behaviour in a Small-Scale Compartment Fire.* Fire Safety Journal, 1993. **20**(4): p. 377-384.

[14] Sugawa, O., Kawagoe, K., Oka, Y., and Ogahara, I., *Burning Behavior in a Pooly Ventilated Compartment Fire-Ghosting Fire.* Fire Science and Technology, 1989. **9**(2): p. 5-14.

[15] Audouin, L., Such, J.M., Malet, J.C., and Casselman, C., *A Real Scenario for a Ghosting Flame*. in *Fifth International Symposium on Fire Safety Science*. 1997. Melbourne.

[16] Harmathy, T.Z., *A New Look at Compartment Fires, Part I.* Fire Technology, 1972. **8**(3): p. 196-217.

[17] Harmathy, T.Z., *A New Look at Compartment Fires, Part II.* Fire Technology, 1972. **8**(3): p. 326-351.

[18] Harmathy, T.Z., *Mechanism of Burning of Fully-Developed Compartment Fires.* Combustion and Flame, 1978. **31**: p. 265-273.

[19] Harmathy, T.Z., *Experimental Study on the Effect of Ventilation on the Burning of Piles of Solid Fuels.* Combustion and Flame, 1978. **31**: p. 259-264.

[20] Bullen, M.L. and Thomas, P.H., *Compartment Fires with Non-Cellulosic Fuels*. in *Symp Int Combust 17th*. 1979. Leeds, England: Combusion Institute.

[21] Santo, G. and Delichatsios, M.A., *Effects of Vitiated Air on Radiation and Completeness of Combustion in Propane Pool Fires,* FMRC J.I. 0F0N4.BU, Factory Mutual Research, 1982.

[22] Tewarson, A., Lee, J.L., and Pion, R.F., *The Influence of Oxygen Concentration on Fuel Parameters for Fire Modeling*. in *Symp Int Combust 18th*. 1981. Waterloo, Ont, USA: Combustion Institute.

[23] Peatross, M.J. and Beyler, C.G., *Ventilation Effects on Compartment Fire Characterization*. in *Fifth International Symposium Fire Safty Science*. 1997. Melbourn.

[24] Fleischmann, C.M. and Parkes, A.R., *Effects of Ventilation on the Compartment Enhanced Mass Loss Rate*. in *Intl. Assoc. Fire Safety Science 5th*. 1997. Melbourne, Australia: Fire Safety Science.

[25] Babrauskas, V., *A Closed-form Approximation for Post-flashover Compartment Fire Temperature.* Fire Safety Journal, 1981. **4**: p. 63-73.

[26] Delichatsios, M.A., Silcock, G.W.H., Lui, X., Delichatsios, M., and Lee, Y.P., *Mass Pyrolysis Rates and Excess Pyrolysate in Fully Developed Enclosure Fires.* Fire Safety Journal, 2004. **39**(1): p. 1-21.

[27] Delichatsios, M. and Silcock, G.W.H., *Fully Involved Enclosure Fires: Effects of Fuel Type, Fuel Area, and Geometry*. in *Seventh International Symposium Fire Safety Science*. 2002. Worcester, Massachusetts, USA.

[28] Ohmiya, Y., Tanaka, T., and Wakamatsu, T., *A Room Fire Model for Predicting Fire Spread by External Flames.* Fire Science and Technology, 1998. **18**(1): p. 11-21.

[29] Kumar, R., M., N., and Sharma, S.K., *Compartment Fires: CALTREE and Cross Ventilation,* CST 06-04-12, Central Building Research Institute, 2006.

[30] Wakatsuki, K., *Low Ventilation Small-Scale Compartment Fire Phenomena: Ceiling Vents*, in *Fire Protection Engineering*. 2001, University of Maryland: College Park, MD.

[31] Ringwelski, B.A., *Low Ventilation Small-Scale Compartment Fire Phenomena: Wall Vents*, in *Fire Protection Engineering*. 2001, University of Maryland: College Park, MD.

[32] Rangwala, A.S., *Mathematical Modelling of Low Ventilation Small-Scale Compartment Fires*, in *Fire Protection Engineering*. 2002, University of Maryland: College Park, MD.

[33] Utiskul, Y., Quintiere, J.G., Rangwala, A.S., Ringwelski, B.A., Wakatsuki, K., and Naruse, T., *Compartment Fire Phenomena under Limited Ventilation.* Fire Safety Journal, 2005. **40**(4): p. 367-390.

[34] Hu, Z., Utiskul, Y., Quintiere, J.G., and Trouve, A., *A Comparison between Observed and Simulated Flame Structures in Poorly Ventilated Compartmnet Fires*. in *Eighth IAFSS Symposium*. 2005. Beijing, China.

[35] Hu, Z., Utiskul, Y., Quintiere, J.G., and Trouve, A., *Towards Large Eddy Simulations of Flame Extinction and Carbon Monoxide Emission in Compartment Fires*. in *31st International Symposium on Combustion*. 2006. Heidelberg: Combustion Institute.

[36] Williamson, J., Marshall, A., and Trouve, A., *Extincton of Vitiated Flame Sheets*. in *Poster and Abstract in 31st International Symposium on Combustion*. 2006. Heidelberg.

[37] Hostikka, S., Kokkala, M., and Vaari, J., *Experimental Study of the Localized Room Fires, NFDC2 Test Series,* VTT Research Note 2104, 2001.

[38] Hamins, A., Maranghides, A., Jhonsson, E., Donnelly, M., Yang, J., Mulholland, G., and Anleitner, R., *Report of Experimental Results for the International Fire Model Benchmarking and Validation Exercise #3,* NIST Special Publication 1013-1, National Institute of Standards and Technology, 2005.

[39] Klein-Hebling, W. and Rowenkamp, M., *Evaluation of Fire Models for Nuclear Power Plant Applications: Fuel Pool Fire inside a Compartment,* 2005.

[40] Hosser, D., Riese, O., and Klingenberg, M., *Performing of Recent Real Scale Cable Fire Experiments and Presentation of the Results in the Frame of the International Collaborative Fire Modeling Project ICFMP*. 2004.

[41] Lie, T., *Fire Temperature-tiem Relationships*, in *SFPE Handbook of Fire Protection Engineering*. 1995, National Fire Protection Association. p. 167-173.

[42] McCaffrey, B.J., Quintiere, J.G., and Harkleroad, M.F., *Estimating Room Fire Temperatures and the Likelyhood of Flashover Using Fire Test Data Correlations.* Fire Technology, 1981. **17**(2): p. 98-119.

[43] Eurocode1, *Basis of design and actions on Structures Part 2.2 Actions on Structures-Actions on Structures exposed to fire, ENV 1991-2-2:1995, CEN.*

[44] Tanaka, T., *Simple Formula for Ventilation Controlled Fire Temperatures*. in *13 th Joint Panel Metting*. 1996. Gaithersburg, MD: U.S./Japan Government Cooperative Program on Natural Resources (UJNR). Fire Research and Safety.

[45] Magnusson, S.E. and Thelandersson, S., *Temperature-Time Curves of Complete Process of Fire Development,* No. 65, ACTA, Polytechnica Scandinavica, 1970.

[46] Law, M., *A Basis for the Design of Fire Protection of Building Structures.* The Structural Engineer, 1983. **61A**(No. 5).

[47] SFPE, *Engineering Guide to Fire Exposures to Structural Elements*. 2003: Society of Fire Protection Engineers.

[48] Friedman, R., *An International Survey of Computer Models for Fire and Smoke.* Journal of Fire Protection Engineering, 1992. **4**(3): p. 81-92.

[49] Olenick, S.M. and Carpenter, D.J., *An Updated International Survey of Computer Models for Fire and Smoke.* Journal of Fire Protection Engineering, 2003. **13**(2): p. 87-110.

[50] Cadorin, J.F., *Compartment Fire Models for Structural Engineering*, in *Department of Mechanics of Materials and Structures*. 2003, University of Liege: Liege, Belgium. p. 189.

[51] *BRANZFIRE Technical Reference Guide,* Building Research Association of New Zealand, 2000.

[52] Wade, C.A., *A Theoretical Model for Fire Spread in a Room Corridor Configuration*. in *3rd International Conference on Performance Based Codes and Fire Safety Design Methods*. 2000. Lund, Sweden.

[53] Tanaka, T. and Yamada, S., *BRI2002: Two Layer Zone Smoke Transport Model.* Fire Science and Technology, 2004. **23**(Special Issue).

[54] *A Technical Reference for CFAST: An Engineering Tools for Estimating Fire Growth and Smoke Transport,* NIST Technical Note 1431, National Institute of Standards and Technology, 2000.

[55] *Competitive Steel Buildings through Natural Fire Safety Concept. Part 2: Natural Fire Models,* Final Report, Profil ARBED, 1999.

[56] Gautier, B., Pages, O., and Thibert, E., *MAGIC: Global Modelling for Fire into Compartments*. in *8th Interflam Conference*. 1999. Edinburgh, Scotland.

[57] Mitler, H.E. and Rockett, J.A., *User's Guide to FIRST, A Comprehensive Single-Room Fire Model,* NBSIR 87-3595, National Bureau of Standards, 1987.

[58] Rockett, J.A., *Using the Harvard/National Institute of Standards and Technology Mark VI Fire Simulation,* NISTIR 4464, National Institute of Standards and Technology, 1990.

[59] Babrauskas, V., *COMPF2- A Program for CAlculating Post-Flashover Fire Temperatures,* Technical Note 991, National Bureau of Standards, 1979.

[60] Quintiere, J.G., *Fundamentals of Fire Phenomena*. 2006, Chichester: John Wiley. 439.

[61] Babrauskas, V., *Estimating Large Pool Fire Burning Rates.* Fire Technology, 1983(19): p. 251.

[62] Babrauskas, V., *Burning Rates*, in *SFPE Handbook of Fire Protection Engineering*. 1995, National Fire Protection Association: Quincy, MA.

[63] Heskestad, G., *Modeling of Enclosure Fires*. in *Symp Int Combust 14th*. 1972. PA, USA: The Combustion Institute.

[64] Block, J.A., *A Theoretical can Experimental Study of Nonpropagating Free-Buring Fires*. in *13th Symposium (International) on Combustion*. 1970. Salt Lake City, Utah: Combustion Institute.

[65] Quintiere, J.G., *Compartment Fire Modeling*, in *SFPE Handbook of Fire Protection Engineering*. 1995, National Fire Protection Association. p. 3.125 - 3.133.

[66] Harmathy, T.Z., *The Role of Thermal Feedback in Compartment Fires.* Fire Technology, 1975. **11**(1): p. 48-54.

[67] Thomas, I.R. and Bennetts, I.D., *Fires in Enclosures with Single Ventilation Openings - Comparison of Long and Wide Enclosure*. in *Fire Safety Science-Proceedings of the Sixth International Symposium*. 1999. France.

[68] Quintiere, J.G., McCaffrey, B.J., *The Burning of Wood and Plastic Cribs in an Enclosure: Volume I,* NBSIR 80-2054, National Bureau of Standards, 1980.

[69] Drysdale, D., *An Introductionto Fire Dynamics*. 1992: Wiley-Interscience.

[70] Hagglund, B. and Persson, L.E., *An Experiment Study of Radiation from wood flames,* FOA 4 Report, C4589D6, Forsvarets Forskningsanstalt, 1974.

[71] Beyreis, J.R., Monsen, H.W., and Abbasi, A.F., *Properties of Wood Crib Flames.* Fire Technology, 1971. **7**: p. 145-155.

[72] Siegel, R., Howell, John, *The Engineering Treatment of Gas Radiation in Enclosures*, in *Thermal radiation Heat Transfer*, 4th, Editor. 2002, Taylor & Francis: New York. p. 612-619.

[73] Modak, A.T., *Radiation from Products of Combustion,* Rept. 22361-8, Factory Mutual Research Corp., 1978.

[74] Utiskul, Y., Qunitiere, J. G., *Generalizations on Compartment Fires from Small-Scale Experiments for Low Ventilation Conditions*. in *Eighth IAFSS Symposium*. 2005. Beijing, China.

[75] Quintiere, J.G. and Rangwala, A.S., *A Theory of Flame Extinction Based on Flame Temperature.* Fire and Materials, 2003. **28**: p. 387-402.

[76] Williams, F.A., *A Review of Flame Extinction.* Fire Safety Journal, 1981. **3**: p. 163 - 175.

[77] Jaluria, Y., *Natural Convection Wall Flows*, in *SFPE Handbook of Fire Protection Engineering*. 1995, National Fire Protection Association. p. 2.50-2.63.

[78] Quintiere, J.G., McCaffrey, B.J., Rinkinen, W., *Visualization of Room Fire Induced Smoke Movement and Flow in a Corridor.* Fire and Materials, 1978. **2**(1): p. 18-24.

[79] McCaffrey, B.J., and Quintiere, J. G., *Buoyancy-Driven Counter-current Flows Generated by a Fire Source.* Heat Transfer and Turbulent Buoyant Convection, 1977. **2**: p. 457-472.

[80] Zukoski, E.E., *Experimental Study of Environment and Heat Transfer in a Room Fire,* NBS Grant No. G8-9014, California Institute of Technology, 1978.

[81] Lim, C.S., Zukoski, E. E., and Kubota, T., *Mixing in Doorway Flows and Entrainment in Fire Flames,* NBS Grant No. NB82NADA3033, California Institute of Technology, 1984.

[82] Rockett, J.A., *Fire Induced Gas Flow in an Enclosure.* Combustion Science and Technology, 1976. **12**: p. 165-175.

[83] Quintiere, J.G. and Grove, B.S., *A Unified Analysis for FIre Plumes*. in *27th Symposium (International) on Combustion*. 1998: Conbustion Institute.

[84] Emmons, H.W., *Vent Flows*, in *SFPE Handbook of Fire Protection Engineering*. 1995, National Fire Protection Association. p. 2.40-2.49.

[85] Panton, R.L., *Incompressible Flow*. 2nd ed. 1996, New York: A Wiley-Interscience publication.

[86] Quintiere, J.G., *Fundamentals of Enclosure Fire "Zone" Models.* Journal of Fire Protection Engineering, 1989. **1**(3): p. 99-119.

[87] Quintiere, J.G., *Fire Behavior in Building Compartments*. in *Twenty-Ninth International Symposium on Combustion*. 2002. Sapporo, Japan: Combustion Institute.

[88] Tanaka, T. and Yamada, S., *Reduced Scale Experiments for Convective Heat Transfer in the Early Stage of Fires.* International Journal on Engineering Performanced-based Fire Codes, 1999. **1**(3): p. 196-203.

[89] Zukoski, E.E. and Kubota, T., *An Experimental Investigation of the Heat Transfer from a Buoyant Gas Plume to a Horizontal Ceiling - Part 2 Effect of Ceiling Layer,* NBS-GCR-77-98, National Bureau of Standards, 1975.

[90] Veloo, P., *Scale Modeling of the Transient Behavior of Heat Flux in Enclosure Fires*, in *Fire Protection Engineering*. 2006, University of Maryland: College Park. p. 127.

[91] Wolfram, S., *The Mathematica Book*. 5th ed. 2003: Wolfram Research, Inc. 1200.

[92] Marasco, A. and Romano, A., *Scientific Computing with Mathematica: Mathematical Problems for Ordinary Differential Equations*. 2001: Edwards Brothers, Inc.

[93] Gray, A., Mezzino, M., and Pinsky, M.A., *Introduction to Ordinary Differential Equations with Mathematica*. 1997, Santa Clara: Springer-Verlag.

[94] Abell, M.L. and Braselton, J.P., *Differential Equations with Mathematica*. 2nd ed. 1997, New York: Academic Press.

[95] Kreyszig, E., *Advance Engineering Mathematics*. 8th ed. 1999: John Wiley & Son, Inc.

[96] Dine, N., *Experimental Study of Ventilated Fire Enclosures*. 2006, ECOLE NATIONALE SUPERIEURE DE MECANIQUE ET D'AEROTECHNIQUE: Poitiers. p. 105.

[97] Chamchine, A.V., Makhviladze, G.M., Snegirev, A., and Graham, T.L., *Interpretation of small and medium scale experiments with an enclosed burner fire*. in *Interflam2004*. 2004. Edinburgh, UK.

[98] Utiskul, Y., Quintiere, J.G., and Naruse, T., *Wall-Vent Compartment Fire Behavior under Limited Ventilation*. in *InterFlam2004*. 2004. Edinburgh, UK.